PNL--8000-Pt.4

DE92 015995

Pacific Northwest Laboratory Annual Report for 1991 to the DOE Office of Energy Research

Part 4 Physical Sciences

L. H. Toburen and members of
the Physical and Technological
Programs Staff

April 1992

Prepared for
the U.S. Department of Energy
under Contract DE-AC06-76RLO 1830

Pacific Northwest Laboratory
Richland, Washington 99352

Preface

This 1991 Annual Report from Pacific Northwest Laboratory (PNL) to the U.S. Department of Energy (DOE) describes research in environment, and health conducted during fiscal year 1991. This year the report consists of four parts, each in a separate volume.

The four parts of the report are oriented to particular segments of the PNL program, describing research performed for the DOE Office of Health and Environmental Research in the Office of Energy Research. In some instances, the volumes report on research funded by other DOE components or by other governmental entities under interagency agreements. Each part consists of project reports authored by scientists from several PNL research departments, reflecting the multidisciplinary nature of the research effort.

The parts of the 1991 Annual Report are:

Part 1: Biomedical Sciences			
	Program Manager:	J. F. Park	J. F. Park, Report Coordinator S. A. Kreml, Editor
Part 2: Environmental Sciences			
	Program Manager:	R. E. Wildung	D. A. Perez, Editor
Part 3: Atmospheric Sciences			
	Program Manager:	W. R. Barchet	L. K. Grove, Editor
Part 4: Physical Sciences			
	Program Manager:	L. H. Toburen	L. H. Toburen, Report Coordinator R. C. Pedersen, Editor

Activities of the scientists whose work is described in this annual report are broader in scope than the articles indicate. PNL staff have responded to numerous requests from DOE during the year for planning, for service on various task groups, and for special assistance.

Credit for this annual report goes to the many scientists who performed the research and wrote the individual project reports, to the program managers who directed the research and coordinated the technical progress reports, to the editors who edited the individual project reports and assembled the four parts, and to Ray Baalman, editor in chief, who directed the total effort.

T. S. Tenforde
Health and Environmental Research Program

Previous reports in this series:

Annual Report for:

1951	HW-25021, HW-25709
1952	HW-27814, HW-28636
1953	HW-30437, HW-30464
1954	HW-30306, HW-33128, HW-35905, HW-35917
1955	HW-39558, HW-41315, HW-41500
1956	HW-47500
1957	HW-53500
1958	HW-59500
1959	HW-63824, HW-65500
1960	HW-69500, HW-70050
1961	HW-72500, HW-73337
1962	HW-76000, HW-77609
1963	HW-80500, HW-81746
1964	BNWL-122
1965	BNWL-280, BNWL 235, Vol. 1-4; BNWL-361
1966	BNWL-480, Vol. 1; BNWL-481, Vol. 2, Pt. 1-4
1967	BNWL-714, Vol. 1; BNWL-715, Vol. 2, Pt. 1-4
1968	BNWL-1050, Vol. 1;, Pt. 1-2; BNWL-1051, Vol. 2, Pt. 1-3
1969	BNWL-1306, Vol. 1;, Pt. 1-2; BNWL-1307, Vol. 2, Pt. 1-3
1970	BNWL-1550, Vol, 1;, Pt. 1-2; BNWL-1551, Vol. 2, Pt. 1-2
1971	BNWL-1650, Vol. 1;, Pt. 1-2; BNWL-1651, Vol. 2, Pt. 1-2
1972	BNWL-1750, Vol. 1;, Pt. 1-2; BNWL-1751, Vol. 2, Pt. 1-2
1973	BNWL-1850, Pt. 1-4
1974	BNWL-1950, Pt. 1-4
1975	BNWL-2000, Pt. 1-4
1976	BNWL-2100, Pt. 1-5
1977	PNL-2500, Pt. 1-5
1978	PNL-2850, Pt. 1-5
1979	PNL-3300, Pt. 1-5
1980	PNL-3700, Pt. 1-5
1981	PNL-4100, Pt. 1-5
1982	PNL-4600, Pt. 1-5
1983	PNL-5000, Pt. 1-5
1984	PNL-5500, Pt. 1-5
1985	PNL-5750, Pt. 1-5
1986	PNL-6100, Pt. 1-5
1987	PNL-6500, Pt. 1-5
1988	PNL-6800, Pt. 1-5
1989	PNL-7200, Pt. 1-5
1990	PNL-7600, Pt. 1-5

Foreword

Part 4 of the Pacific Northwest Laboratory Annual Report for 1991 to the DOE Office of Energy Research includes those programs funded under the title "Physical and Technological Research." The Field Task Program Studies reported in this document are grouped by budget category and each Field Task proposal/agreement is introduced by an abstract that describes the projects reported in that section. These reports only briefly indicate progress made during 1991. The reader should contact the principal investigators named or examine the publications cited for more details.

Contents

Dosimetry
Research

Chernobyl Database Management

The Chernobyl Database project is developing and maintaining an information system to provide researchers with data and resource materials relating to the Chernobyl nuclear accident of April, 1986. The system is the official United States repository for Chernobyl data. The system includes a collection of Chernobyl-related documents, a database of bibliographic references, and a collection of radiological measurements records. During FY 1991, end-user software products were prepared to make the resources more accessible and easy to use. These products include a personal-computer-based bibliographic search system (*ChernoLit*™[a]) and a personal-computer-based radiological measurements database system (*ChernoDat*).

Chernobyl Database

R. A. Kennedy, J. A. Mahaffey, F. Carr, Jr., and S. K. Smith

ChernoLit

In an effort to provide software tools to aid researchers studying the Chernobyl accident, the Chernobyl Bibliographic Search System (*ChernoLit*™) was developed, documented, and tested during FY 1991. *ChernoLit* provides bibliographic data and abstracts in a usable format for research studies relating to the Chernobyl accident. *ChernoLit* is an easy-to-use software package that includes search capabilities on bibliographic data. The user may specify names, words, and phrases of interest. These search criteria may be logically compounded. The user may also specify which database fields are to be searched. The user may interactively view the references, including the abstracts, or may generate a report. Reports may be directed to the screen, to the default printer, or accumulated in a folder that is written to a disk file.

ChernoLit will run on an IBM PS/2, AT,[b] or a fully-IBM-compatible computer configured with either a 5-1/4-inch or 3-1/2-inch high-density floppy disk drive and with 8 megabytes of free disk space. An operating system of DOS 3.3 or higher is required. For best performance, use of a mouse is recommended. If printed reports are desired, a printer must be available to the computer.

ChernoLit has been implemented as a FoxPro™[c] 2.0 run-time application consisting of pull-down menus, shortcut keys, text buttons, and dialog boxes as well as the bibliographic database. This stand-alone system is provided in compressed format on floppy disks. An automatic install procedure loads the application onto the user's computer. A version that executes on the Macintosh®[d] computer will be available in the future.

Over 4400 references concerning the accident, complete with abstracts, are included with *ChernoLit*. The data contained in the database was obtained from electronic literature searches and from requested donations from individuals and organizations. These literature searches interrogated the ENERGY SCIENCE AND TECHNOLOGY database (formerly DOE ENERGY) of the DIALOG®[e] Information Retrieval Service. ENERGY SCIENCE AND TECHNOLOGY, provided by the U.S. DOE, Washington, D.C., is a multidisciplinary database containing references to the world's scientific and technical literature on energy. All unclassified information processed at the Technical Information Center of the U.S. DOE is included in the database.

(a) ChernoLit is a trademark of Battelle Memorial Institute, Columbus, OH, USA.
(b) IBM, PS/2, and AT are trademarks of International Business Machines Corporation, Boca Raton, FL, USA.
(c) FoxPro is a trademark of Fox Software, Inc. Perrysburg, OH, USA.
(d) Macintosh is a registered trademark of Apple Computers, Inc., Cupertino, CA, USA.
(e) DIALOG is a registered trademark of Dialog Information Services, Inc., Palo Alto, CA, USA.

In addition, information on many documents has been manually added to *ChernoLit*. Most of this information was obtained in response to requests for data sent to people and/or organizations throughout the world.

A significant effort was undertaken to increase the readability of the bibliographic references contained in *ChernoLit* by: 1) capitalization of titles and acronyms, 2) standardization of radionuclide specification, and 3) standardization of superscripts, subscripts, and numeric references. Particular attention was paid to standardizing radionuclide specification because of the likelihood that searches would be conducted on this information.

ChernoLit underwent a beta test within PNL in late FY 1991. As a result of the beta test, several software modifications and documentation changes were made.

In cooperation with the technology transfer initiative within DOE, *ChernoLit* will be made available commercially by Battelle Memorial Institute.

ChernoDat

A companion software package to *ChernoLit* that allows the user to interactively browse the radiological measurements database is currently undergoing development and testing. The Chernobyl Radiological Measurements Information System (*ChernoDat*) is a software package that provides access to radiological measurements collected in response to PNL requests subsequent to the Chernobyl accident. Data in *ChernoDat* are organized into a central database that stores data in a standardized record format, with multiple satellite databases containing the data in their original record formats. *ChernoDat* allows the user to browse, query, and export the radiological data from both the central and satellite databases. The browsing feature allows the user to toggle between data in the original record and a standardized record. The query feature allows the user to obtain a data subset and then export the subset to an ASCII file for analysis.

ChernoDat will run on an IBM PS/2, AT, or a fully-IBM-compatible computer configured with a VGA monitor, 3-1/2-inch high-density floppy disk drive, and a hard drive with 7 megabytes of free disk space. An operating system of DOS 3.3 or higher is required. Performance will increase as the amount of available RAM is increased up to a limit of 16 megabytes.

ChernoDat is implemented as a Paradox®[(a)] Runtime 3.5 application consisting of pop-up menus, on-line help, and query-by-example filtering. The application requires Paradox Runtime files that are included with *ChernoDat* on the 3-1/2-inch high-density diskettes. An automatic installation program is used to install the compressed format files.

Currently, the central database consists of over 48,000 records that have been standardized from five satellite databases. The data records currently included in the satellite databases have been donated by the following agencies: State of Washington Department of Social and Health Services (Pickett 1986), Ministry of Agriculture, Fisheries and Food, Welsh Office (1988), Safety Analysis Unit, National Institute of Radiological Sciences, Japan (1988), Chernobyl Protective Measures Assessment Team, United States Nuclear Regulatory Commission (1986), and Stone & Webster Engineering Corporation (1986).

Interaction with Researchers

During FY 1991, letters were written to more than 100 researchers who provided us with either radiological measurements or bibliographic data. The letters acknowledged our appreciation of their assistance and noted we would provide them with *ChernoLit*, *ChernoDat*, and/or the printed bibliography.

Publication Preparation

A paper entitled "Chernobyl Database" was presented at a poster session of the Winter Technical Conference of the American Statistical Association.

(a) Paradox is a registered trademark of Borland International, Scotts Valley, CA, USA.

A report entitled *ChernoLit™ - Chernobyl Bibliographic Search System User's Guide* was published to document use of the *ChernoLit* software.

A printed bibliography of more than 4400 references included in *ChernoLit*, complete with author index, was published. Utility software was written that automated much of the work involved in generating this document.

An abstract has been accepted to present a poster on the Chernobyl Database at the IRPA 8 - International Radiation Protection Association meeting in Montreal, May 17-22, 1992. The paper entitled "U.S. Department of Energy Chernobyl Databases" will be published in the Conference Proceedings of IRPA8.

An abstract has been accepted for inclusion in the "New Horizons in Radiation Protection and Shielding" American Nuclear Society Topical Meeting to the held in Pasco, WA, April 26 - May 1, 1992. The paper entitled "*ChernoLit* - Chernobyl Bibliographic Search System" will be published in the proceedings.

Future Efforts

Completion and distribution of products developed during FY 1991 is scheduled for early FY 1992. In addition, a major task for FY 1992 will be to summarize data currently included in the information system and to analyze the information system in relation to the overall availability of information relating to the Chernobyl accident. If software is available, a Macintosh version of *ChernoLit* will be generated and released.

References

Chernobyl Protective Measures Assessment Team, U.S. Nuclear Regulatory Commission. 1986. *Preliminary Assessment of the Chernobyl Accident Radiological Data Provided to the NRC Through May 9, 1986.* NUREG-1219. Washington, D.C.

Ministry of Agriculture, Fisheries and Food, Welsh Office. 1988. *Radionuclide Levels in Food, Animals and Agricultural Products 1987, Post Chernobyl Monitoring in England and Wales.* ISBN 0 11 242828 2, HMS Stationery Office, London.

Pickett, B. 1986. *DSHS Activities Relating to the Chernobyl Nuclear Accident.* Office of Radiation Protection, Division of Health, Washington State Department of Social and Health Services, Olympia, Washington.

Safety Analysis Unit, National Institute of Radiological Sciences. 1988. *Environmental and Health Consequences in Japan due to the Accident at Chernobyl Nuclear Reactor Plant.* NIRS-M-69, Chiba, Japan.

Stone & Webster Engineering Corporation. 1986. *Compilation of Radiological Measurements from the Chernobyl Accident.* Prepared for Pacific Northwest Laboratory on behalf of the U.S. DOE, Boston.

Chernobyl Environmental Measurements

In 1990, the government of the USSR requested, through the auspices of the International Atomic Energy Agency (IAEA), the assistance of member countries in helping to assess the environmental, health, and safety aspects related to the Chernobyl accident in the inhabitated contaminated communities surrounding the Chernobyl area. As part of this assessment, a request was made to sample and analyze soils, sediments, selected biota, and water from these regions. The purposes of these measurements were to 1) verify the radiological environmental conditions established earlier by Soviet scientists, 2) determine the credibility of their results, conclusions, and recommendations, and 3) learn as much as possible about the environmental distribution and behavior of Chernobyl-origin radionuclides in the environs just outside of the 30-km "prohibited zone." Pacific Northwest Laboratory (PNL) participated in this measurement and assessment program. R. W. Perkins and D. E. Robertson served on several committees for planning and implementing the radiological measurements and assessments program, and PNL participated in analyses of selected environmental samples collected from the regions surrounding Chernobyl. This report summarizes the results of this participation.

Radiological Measurements

D. E. Robertson, R. W. Perkins, E. A. Lepel, C. W. Thomas, and R. A. Kiddy

Soil, sediment, vegetation, surface water, and air filter samples were collected from the communities surrounding the Chernobyl area by International Atomic Energy Agency (IAEA) sampling teams. A portion of these samples were sent to Pacific Northwest Labortory (PNL) for gamma spectrometric and radiochemical analyses. In general, the PNL measurements confirmed the earlier results of the Soviet scientists. Radionuclide concentrations and distributions in soils from this region were similar to the ranges reported by the Soviets.

Figure 1 illustrates the depth distribution of ^{137}Cs, the most abundant Chernobyl-origin radionuclide in the environs, in four soil cores collected from three communities surrounding the Chernobyl area. In the three undisturbed soil cores from Bragin and Polesskoye, the radiocesium had penetrated past a depth of 5 cm, although the concentrations at 5 cm were over two orders of magnitude lower than the surface values. The soil core from Gomel showed either a faster ^{137}Cs penetration with depth or some disturbance (physical mixing) of the upper layer of soil, or a combination of both processes.

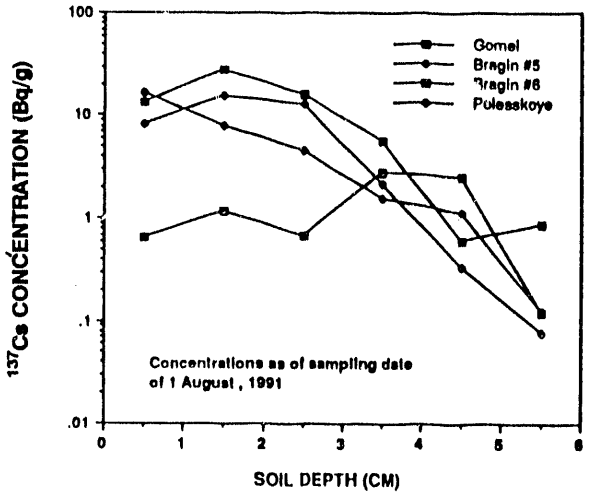

FIGURE 1. Depth Distribution of ^{137}Cs in Four Soil Cores Collected Near Chernobyl

Figure 2 shows the depth distribution of the detectible gamma emitting radionuclides in an undisturbed soil core from Bragin. The ^{137}Cs, ^{134}Cs, ^{106}Ru, and ^{144}Ce concentrations at a depth of 5 cm were only about 1% of the surface concentrations, whereas the ^{124}Sb and ^{154}Eu concentrations decreased only about 10% at a depth of 5 cm. This indicates that the radionuclides of cesium, ruthenium, and cerium were more tightly bound to the soil than those of antimony and europium. Radiochemical separations and measurements were also performed on samples of this core, and the results are shown in Figure 3. The ^{90}Sr, the transuranic radionuclides (TRUs), and the ^{129}I concentrations were

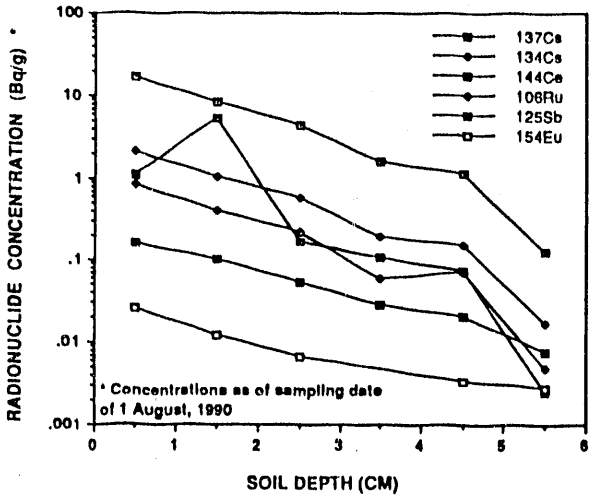

FIGURE 2. Gamma-Emitting Radionuclide Distributions in Soil Core #5 from Bragin Employing Long Counting Intervals

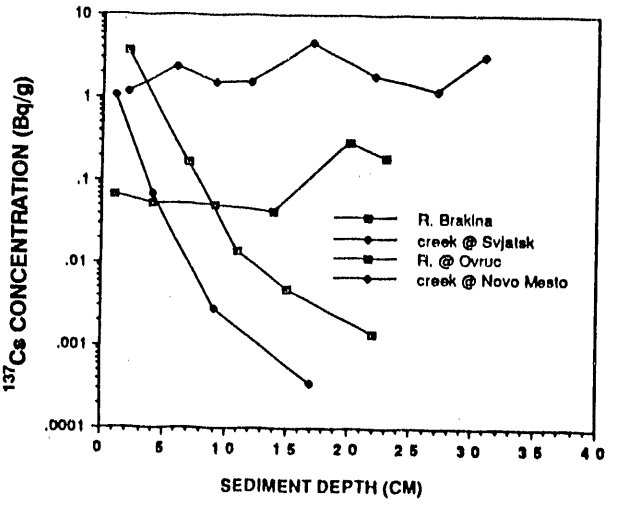

FIGURE 4. ^{137}Cs Distributions in Sediment Cores from Rivers and Streams Near the Chernobyl Region

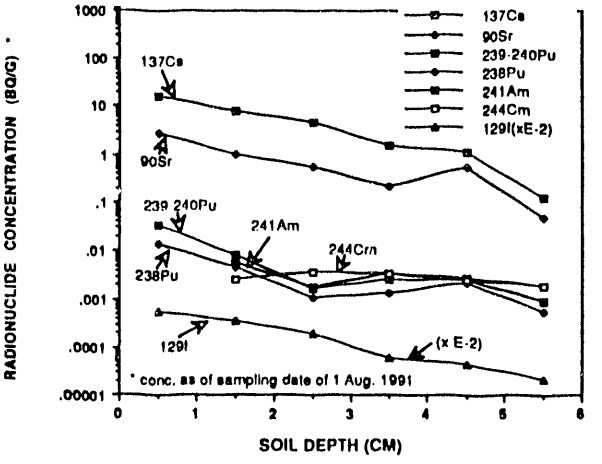

FIGURE 3. Radionuclide Concentrations in Soil Core #5 from Bragin

approximately 1, 3, and 6 orders of magnitude lower, respectively, than the ^{137}Cs. The ^{129}I measurements are the first known reported measurements of this radionuclide in the Chernobyl environs.

Gamma-emitting radionuclide concentrations were also measured in sediments from five rivers and streams near the Chernobyl region. Figure 4 shows the depth distributions of ^{137}Cs in four of the sediment cores having the highest concentrations. The sediment cores contained lower concentrations of ^{137}Cs compared with most of the soil cores sampled in this region. The cores from the River Braginka and a small creek near Novo Mesto showed rapid, nearly exponential decreases of about 4 orders of magnitude in ^{137}Cs concentrations over a sediment depths of 16 and 20 cm. The sedimentation rates for these bodies of water are obviously quite low, and the ^{137}Cs attached to the sediment particles does not migrate vertically very fast. In fact, the ^{137}Cs observed below a sediment depth of several cm is probably due to contamination of the deeper sediments during the sampling process. The sediment cores from the small creek/ponds near Svjatsk and the river on the boarder of Ovruc showed rather homogeneous mixing of the ^{137}Cs down to sediment depths of 20 and 32 cm. It is obvious that these two water bodies either have rapid sedimentation rates or the sediments have been turbulently mixed by physical processes.

Samples of grass and moss from the Bragin, Daleta, Polesskoye, and Soboli areas were measured for gamma-emitting radionuclides. The grass samples were limited in number, and since their exact sampling locations compared to the soil samples were not known precisely, it was not possible to determine accurate transfer coefficients for radiocesium from soil to grass.

The moss samples, because of their ability to efficiently collect and integrate atmospheric fallout deposition, were recounted for several

thousand minutes each to obtain more comprehensive analyses of gamma-emitting radionuclides. In addition to radiocesium, it was possible to measure ^{60}Co, ^{106}Ru, ^{110m}Ag, ^{125}Sb, ^{144}Ce, ^{154}Eu, and ^{155}Eu. The moss samples collected from house roofs in the Soboli area were particularly high in all gamma-emitting radionuclide concentrations. Effective decontamination of houses would certainly require removing as much of this material as possible from the rooftops. Moss samples A-4 and A-5 were selected for radiochemical analyses of Pu and ^{90}Sr. The $^{90}Sr/^{137}Cs$ and $^{239-240}Pu/^{137}Cs$ activity ratios for the moss were quite similar to those for surface (0-4 cm) soil cores collected in the same region, indicating no substantial biological fractionation of the Chernobyl fallout by the moss.

Eight air filter samples collected from six communities near Chernobyl were analyzed for gamma-emitting radionuclides. None of the air filter samples contained detectable concentrations of radiocesium. A few samples contained detectable ^{60}Co, but the counting uncertainties were so large that it could also be considered essentially non-detectable. The air sampling was conducted during a period following heavy rains, and resuspension of contaminated soil particles, which is the major source of airborne radionuclides, was at a minimum. Also, the air volumes sampled were not very large.

These measurements are being used, together with the results of other IAEA member participants, to assess the radiation dose received by the Soviet people in the regions surrounding Chernobyl.

DNA Adducts as Indicators of Health Risks

The objective of this program is to develop specific analytical methods for determining adducts formed in mammals by the reaction of carcinogenic compounds with cellular DNA. DNA adducts are closely associated with the formation of cancerous cells, and their concentrations are thought to be related to the amount of exposure to carcinogenic chemicals. This program is developing mass spectrometric methods to analyze adducts for studies of human exposure to carcinogens.

Analysis of DNA Adducts as the Nucleotide: Benzo[a]pyrene-Adducted Deoxyguanosine-5′-Monophosphate

S. D. Harvey, R. M. Bean, and H. R. Udseth

Metabolites of carcinogenic organic compounds have the ability to bond with deoxyribonucleic acids (DNA) to form DNA adducts. These species are retained for relatively long periods of time in the body and are thought to be associated with the formation of cancer. Analysis of DNA for adducts may, therefore, provide an estimate of individual exposure to carcinogens. The methods currently available lack sufficient sensitivity for environmental screening or qualitative specificity. The objective of this project is to develop methods for analyzing DNA adducts to identify and quantify adducted polycyclic aromatic hydrocarbon metabolites at environmental levels. This past year a major effort has focused on the application of powerful microcolumn liquid chromatography techniques for the specific analysis of adducted nucleotides.

Isolation and Characterization of Benzo[a]pyrene-Adducted Nucleotide

To prepare adducted nucleotide material for analytical studies, Benzo[a]pyrene diolepoxide was reacted with calf thymus DNA as previously described by Jannette et al. (1977) and then hydrolyzed to nucleotides by treatment with DNAase I and snake venom phosphodiesterase. The adducted nucleotide fraction was isolated from both non-adducted nucleotides and enzymes by LH-20 chromatography as described by Blobstein et al. (1975). The nucleotides were sorbed on a C-18 Sep-Pak and the buffer salts eluted with water. Subsequent washing with 75:25 methanol:water eluted the adducted nucleotide fraction. Direct infusion electrospray mass spectrometry of the B[a]P-adducted nucleotide fraction gave a full scan negative ion mass spectrum featuring the $(M - H)^{-1}$ ion at 648 amu. This ion indicated that our adducted fraction consisted primarily of B[a]P-adducted deoxyguanosine-5′-monophosphate (MW = 649). This experiment was conducted on approximately 3 ng of material and gave a 648-ion intensity of roughly 13 times the noise level. This gives an approximate detection limit of 460 pg. A projected detection limit of approximately 0.60 pg (1.2 femtomoles) could be achieved by selective ion monitoring.

Capillary Zone Electrophoresis of the Adducted Nucleotide

An objective of this research was to develop a separation technique that would be fully compatible with electrospray ionization mass spectrometric detection. Capillary zone electrophoresis (CZE) was chosen because of its very high separation efficiencies and the mass flow detection enhancement observed with it and other microcolumn separation techniques. A volatile ammonium carbonate buffer was chosen as the supporting electrolyte. Figure 1 illustrates the separation obtained at 30 kV with 30-mM-ammonium carbonate at pH of 8.8. The separation efficiency for the B[a]P-adducted deoxyguanosine peak was 258,000 theoretical plates. On-column fluorescence detection was utilized for this separation. An accurate detection limit was not determined; however, detectability was limited (approximately 1.0 - 0.1 ng) due to intramolecular quenching of the adducted nucleotide.

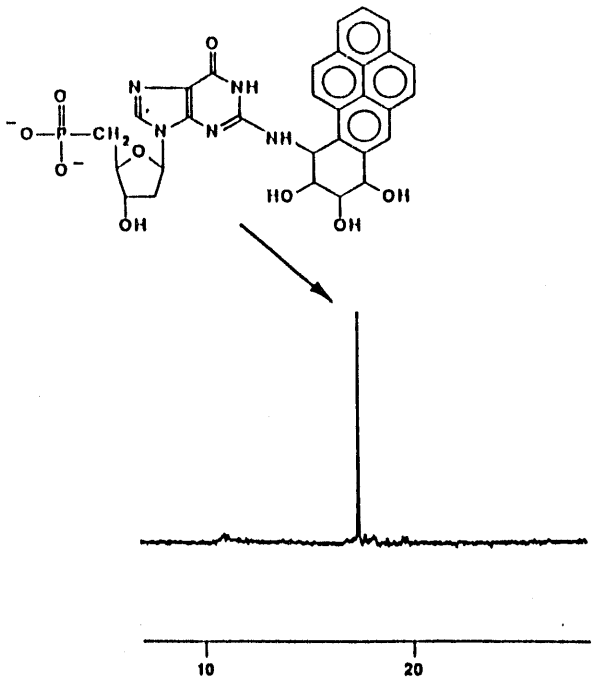

FIGURE 1. Capillary Zone Electrophoretic Separation of the B[a]P-adducted Nucleotide Fraction

Micellar Electrokinetic Capillary Chromatography of the Adducted Nucleotide

This separation strategy was pursued because it offers several advantages over the CZE approach. In comparison to CZE, micellar electrokinetic chromatography (MECC) offers the advantage of unique selectivity based on the partitioning process with the micellar phase. Additionally, an enhancement of fluorescence intensity is often observed for fluorescent analytes in the presence of micellar systems. This detection enhancement is due to both the inclusion of the analyte within the ordered micellar environment as well as protection of the sequestered analyte from molecular oxygen quenching (Love and Weinburger 1983; Liu et al. 1990). Unfortunately, inclusion of surfactants in the running buffer precludes use of mass spectrometric detection. The separation system chosen incorporated sodium dodecyl sulfate (SDS). The use of SDS surfactant has limited use for the analysis of negatively charged analytes because charge repulsion limits the interaction between micelle and analyte (Wallingford and Ewing 1989). However, for B[a]P-adducted deoxyguanosine-5′-monophosphate, the high affinity of the hydrophobic pyrene nucleus for the hydrophobic micellar environment would be expected to overcome charge repulsion and partition the adducted nucleotides into the micellar pseudostationary phase.

The separation of a concentrated adducted nucleotide preparation performed at 30 kV is presented in Figure 2. The running buffer chosen for this separation was 30-mM-ammonium bicarbonate at pH 7.9 containing 10 mM SDS. This electropherogram illustrates the unique selectivity of MECC. Although the principal peak is due to B[a]P-adducted deoxyguanosine-5′-monophosphate, the presence of several other fluorescent adducts are also evident. These additional peaks most likely result from B[a]P adducts of other DNA bases. Interestingly, the CZE electropherogram of the same fraction (Figure 1) does not resolve these additional fluorescent compounds. This difference in electrophoretic profiles is due to the unique selectivity of the micellar system. An injection of a more dilute sample of the adducted nucleotide fraction allowed calculation of the separation efficiency and detection limit for the B[a]P-adducted deoxyguanosine-5′-monophosphate. The separation efficiency was 239,000 theoretical plates. An injection of 20 femtomoles (13 pg) gave a signal equal to twice the baseline noise.

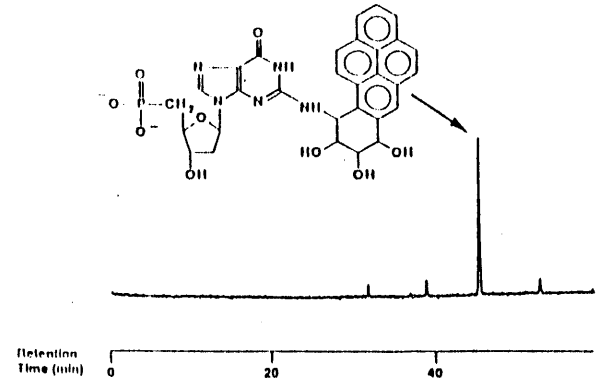

FIGURE 2. Micellar Electrokinetic Capillary Chromatographic Separation of the B[a]P-adducted Nucleotide Fraction

This detection limit is much lower than for the CZE separation of the same fraction. The lower detection limit obtained during MECC separation is due to the fluorescence enhancement discussed above.

It should be mentioned that the projected detection limit for combined CZE/electrospray ionization mass spectrometry compares favorably with on-column fluorescence detection. Because of the very selective nature of mass spectrometric detection, this strategy should be considered distinctly advantageous. The fluorescence detection limits reported here could be improved by approximately two orders of magnitude by use of laser-induced fluorescence detection. With this approach, detection limits considerably lower than those presently obtainable with mass spectrometry would be possible.

Capillary Zone Electrophoresis of B[a]P-tetrahydrotetrols

Another approach to analyzing DNA adducts is to treat the DNA with acid to liberate the B[a]P-tetrahydrotetrols. The structures of the B[a]P-tetrahydrotetrols are given in Figure 3. The advantage of this approach is that the B[a]P-tetrahydrotetrols are highly fluorescent and can be sensitively detected by fluorescence detection. The disadvantage of this approach is that information about the specific adducted DNA base is lost during the acid hydrolysis. As was the case for adducted nucleotides, microcolumn separation techniques were pursued due to the inherent high resolution and enhanced mass flow detection sensitivity. Analysis of B[a]P-tetrahydrotetrols can be readily accomplished by microcolumn HPLC as described previously (Bean et al. 1991). The detection limit for B[a]P-tetrahydrotetrols by microcolumn HPLC is approximately 1 pg (3 femtomoles). Capillary electrophoresis was evaluated as a complimentary technique for obtaining rapid separation and sensitive detection for the tetrahydrotetrols.

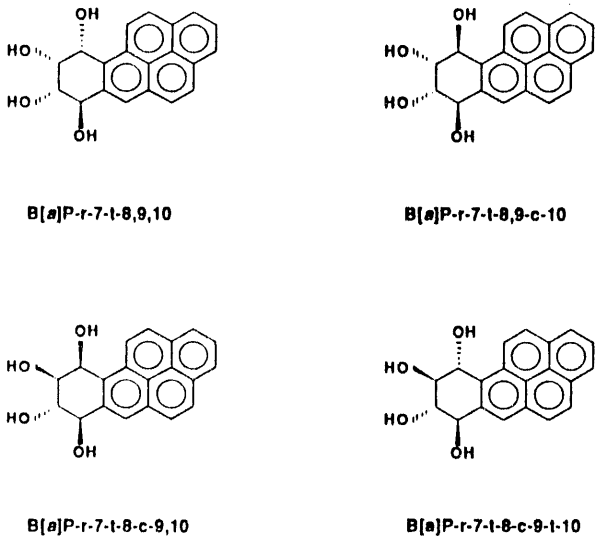

FIGURE 3. Structures of B[a]P-tetrahydrotetrols

Analysis of electrically neutral species can be facilitated by reaction of the analyte with a reagent that can impart a charge to the molecule. For B[a]P-tetrahydroptetrols, it should be possible to react the alcohol functionalities with borate to form the corresponding negatively charged borate complexes (Kuhn et al. 1991; Wallingford and Ewing 1988). The borate reaction is very specific for *cis* vicinal diol groups. As such, this separation strategy has been successfully applied to the CZE analysis of certain carbohydrates and catechols (Kuhn et al. 1991; Wallingford and Ewing 1988). By examining the structure of the B[a]P-tetrahydrotetrols shown in Figure 3, it is possible to predict the stability of the corresponding borate complexes. Borate can form two stable complexes with B[a]P-r-7-t-8,9,10-tetrahydrotetrol. Only one stable borate complex can form with either B[a]P-r-7-t-8,9-c-10-tetrahydrotetrol or B[a]P-r-7-t-8-c-9,10-tetrahydrotetrol. As based on the stearic interaction between the borate complex and the pyrene nucleus, the B[a]P-r-7-t-8,9-c-10-tetrahydrotetrol complex would be expected to be more stable than that formed with B[a]P-r-7-t-8-c-9,10-tetrahydrotetrol. Finally, due to the lack of a *cis* vicinal diol group, B[a]P-r-7-t-8-c-9-t-10-tetrahydrotetrol would not be expected to form a borate complex.

The reaction between borate and B[a]P-tetrahydrotetrol is an equilibrium influenced by both borate concentration and pH. These two variables can be manipulated to achieve the desired separation. Complexation is readily

accomplished by incorporating borate in the running buffer. An electropherogram illustrating the separation of B[a]P-tetrahydrotetrol standards is given in Figure 4. The separation was performed at 30 kV and utilized a running buffer containing 25 mM $NaHPO_4$ and 200-mM-borate at pH of 7.9. The tetraydrotetrols elute in ascending order of their borate complex stabilities. For example, B[a]P-r-7-t-8,9,10-tetrahydrotetrol is most likely to complex borate and spends a higher proportion of time as a negatively charged complex migrating countercurrent to the electroosmotic flow. B[a]P-r-7-t-8-c-9-t-10-tetrahydrotetrol, on the other hand, remains neutral throughout the electrophoretic separation and elutes coincident with the electroosmotic flow. The detection limit equal to twice the baseline noise was calculated to be 1 pg (3 femtomoles). The separation efficiency for the B[a]P-r-7-t-8,9,10-tetrahydrotetrol peak was determined to be 293,000 theoretical plates.

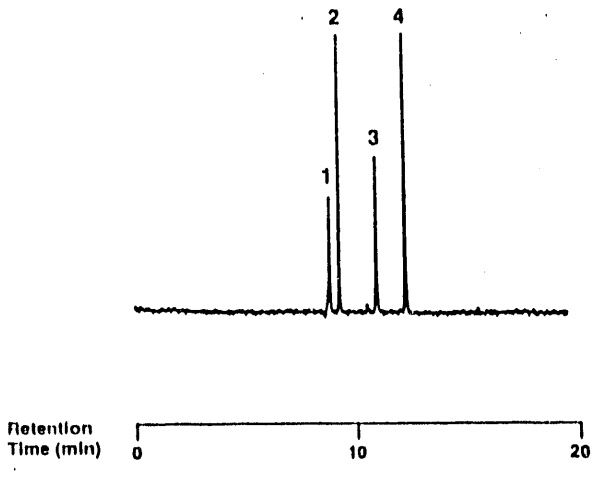

FIGURE 4. Electropherogram Illustrating the Separation of 1) [a]P-r-7-t-8-c-9-t-10-, 2) B[a]P-r-7-t-8-c-9,10-, 3) B[a]P-r-7-t-8,9-c-10-, and 4) B[a]P-r-7-t-8,9,10-tetrahydrotetrols as Their Negatively Charged Borate Complexes

References

Bean, R. M., S. D. Harvey, H. R. Udseth, and D. L. Springer. 1991. "DNA Adducts as Indicators of Health Risks." In *Pacific Northwest Laboratory Annual Report for 1990 to the DOE Office of Energy Research, Physical Sciences, Part 4.* PNL-7600. Pacific Northwest Laboratory, Richland, Washington.

Blobstein, S. H., I. B. Weinstein, D. Grunberger, J. Weisgras, and R. G. Harvey. 1975. "Products Obtained After In-Vitro Reaction of 7,12-Dimethylbenz[a]anthracene-5,6-Oxide with Nucleic Acids." *Biochemistry* 14:3451-3458.

Jannette, K. W., A. M. Jeffrey, S. H. Blobstein, F. A. Beland, R. G. Harvey, and I. B. Weinstein. 1977. "Nucleotide Adducts Form the In-Vivo Reaction of Benzo[a]pyrene-7,8-dihydro 9,10-Oxide or Benzo[a]pyrene 4,5-Oxide with Nucleic Acids." *Biochemistry* 16:932-938.

Kuhn, S. H., A. Paulus, E. Gassmann, and H. M. Widmer. 1991. "Influence of Borate Complexation on the Electrophoretic Behavior of Carbohydrates in Capillary Electrophoresis." *Anal. Chem.* 63:1541-1547.

Liu, J., K. A. Cobb, and M. Novotny. 1990. "Capillary Electrophoretic Separations of Peptides Using Micelle-Forming Compounds and Cyclodextrins as Additives." *J. Chromatogr.* 519:189-197.

Love, L. J. C., and R. Weinberger. 1983. "Recent Advances and Future Prospects in Fluorescence and Phosphorescence Spectrometry." *Spectrochimica Acta* 38B:1421-1433.

Wallingford, R. A., and A. G. Ewing. 1989. "Capillary Electrophoresis." In *Advances in Chromatography*, Vol. 29, eds. J. C. Giddings, E. Grushka, and P. R. Brown, pp.1-76. Marcel Dekker, Inc., New York.

Wallingford, R. A., and A. G. Ewing. 1988. "Retention of Ionic and Non-Ionic Catechols in Capillary Zone Electrophoresis with Micellar Solutions." *J. Chromatogr.* 411:299.

Biological Effectiveness of Radon Alpha Particles

Environmentally relevant exposures to alpha particles from radon decay products amount to only one or two particle tracks per cell. The consequences of these exposures, relative to the effects of the large numbers of electron tracks required to produce the same dose, are major concerns in establishing exposure limits for radon. Unfortunately, the number of particles from radioactive sources or from a charged-particle accelerator beam interacting with individual cells is a Poisson random variable. Since the desired mean is only one or two, the relative variance is so large that the results of such experiments do not adequately test theories about the consequences of exposure. A single-particle irradiation facility, which will provide the means to irradiate large numbers of cells with individually counted and controlled charged particles, is being tested. Techniques for aligning and collimating the beam and detecting the individual particles have been developed. The software necessary to position cells and control exposures has been written. Problems with beam shutter reliability and with illuminating the cells so they can be accurately positioned relative to the accelerator beam collimator are being resolved.

Single-Particle Irradiation System

L. A. Braby

A number of technical challenges must be met to control charged-particle irradiation so that specified numbers of particles interact with specific targets in each of the cells composing an experimental population. The principal problems arise in the areas of collimating the particle beam, detecting the individual particles, positioning the cells, stopping the irradiation, and controlling the system. Preliminary tests, conducted before the single-particle irradiation system was assembled, indicated that each of these areas was manageable. Now that the system has been assembled, the challenge is to ensure that the solutions to all of these problems are compatible.

The basic approach is illustrated in Figure 1. Beams of particles, protons or deuterons up to 4 MeV or ^{4}He or ^{3}He up to 6 MeV, from a tandem electrostatic accelerator are bent to a vertical upward path. The beam is collimated to a spot a few micrometers square using two sets of knife edges that can be positioned individually with 0.1-μm precision. A mechanical shutter stops the beam at the end of each irradiation. The beam exits the accelerator vacuum system through a thin plastic scintillator and passes directly into a cell growing on a thin mylar-bottomed petri dish. A photomultiplier detects the light flashes produced by each charged-particle interaction with the scintillator, and the control system activates the shutter when the desired number of particle interactions has been reached. A microscope with phase contrast epi illumination and an image intensifier video camera visualize the cells on the petri dish. A video processing system then determines the position of the cell relative to the beam through the collimator, and a motorized stage is used to position the cell so that the appropriate portion is irradiated.

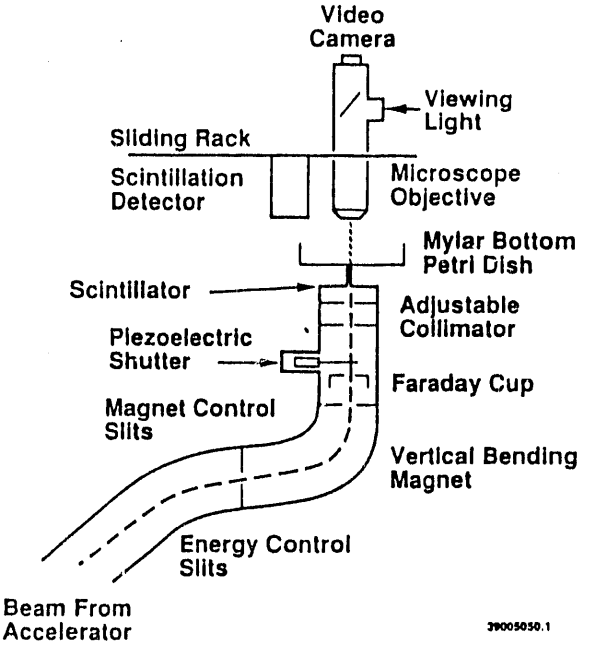

FIGURE 1. Schematic Drawing on the Single Particle Irradiation System

As discussed last year (Braby 1991), the combination of light losses in the microscope optics and the low light yield of the plastic scintillator necessitated using a photomultiplier directly over the plastic scintillator to collect the maximum number of photons from each charged-particle event. Figure 2 shows the pulse height distribution for 3 MeV protons passing through an 8-μm-thick plastic scintillator with the light collected by a 1 in. diameter photomultiplier 0.5 in. above the scintillator. This system works well, with only a very small probability of failing to detect a proton or mistaking noise for a particle event. The primary disadvantages are the added complexity and time required to move the lens and photomultiplier back and forth.

Aluminized mylar and other reflectors have been used to construct the vacuum window under the plastic scintillator. Also, the plastic scintillator itself has been aluminized to increase light-collecting efficiency and reduce the required scintillator thickness. However, these efforts have exacerbated a problem in locating cells to be irradiated. Initial tests of phase contrast imaging with epi illumination produced high resolution images with reasonable contrast. Several different backgrounds were employed to test the effect of reflections from below the cell being observed, but all of these backgrounds were fairly flat. Unfortunately, when used with the actual beam line, the vacuum caused the beam exit window to bow in, and the resulting curved surface reflected some of the light back into the objective. This reflected light reduced the contrast of the phase image, and where the reflecting surface was not uniform, produced a mottled background that prevented recognition of many of the cells. This problem appears to have been corrected by using an exit window slightly larger than the microscope field of view and covered with transparent plastic film. In this way, there is a small and relatively uniform fraction of the light reflected from all parts of the image area. The curved surface creates an image of the illumination phase ring, but it is completely defocused when the cells are in focus, so the image of the cells is relatively clear. The impact of this change on other aspects of system performance remains to be evaluated, but problems are not expected.

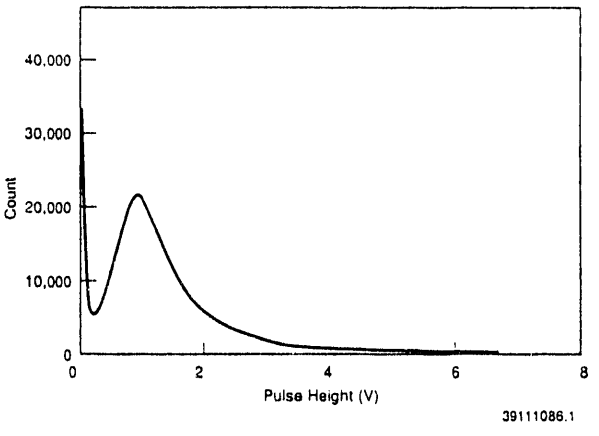

FIGURE 2. Pulse Height Spectrum of Scintillation Events Produced by 3-MeV Protons Through a 8-μm-Thick Scintillator Detected by a 2.54-cm photomultiplier 1.25 cm Away

Alignment of the beam collimator has become more of a problem than initially expected, in spite of the fact that each edge of each aperture is independently adjustable. Initially, the procedure by which the collimator was adjusted was based on using the light produced by the thin plastic scintillator to indicate the number of particles passing through the aperture. This assumption is valid when the beam is aligned, but if the beam is striking the edge of the exit window, then there can be more light produced than when the same number of particles passes through the center of the window. This leads to conflicting data on how to adjust the collimator and can cause mistakes in alignment that result in diffuse, scattered beams. Alignment procedures have been changed to rely on the image of the beam stopping in a thick plastic scintillator viewed by the image intensifier and charge-coupled device camera. The knife edges are then adjusted so that the beam is approximately centered in the exit window, avoiding the extra florescence produced by secondary particles when the beam hits the window edge. When the beam is aligned properly, spots as small as about 5 μm can be imaged directly with the video system, and the pixel address of the center of the beam can be determined directly. If a smaller beam is needed, the knife edges can be moved uniformly in from each side and the location of the center of the beam maintained.

The shutter that controls the beam must have a relatively rapid response time to allow it to close

in less than the average time between particles through the collimator. Both piezoelectric and electromechanical mechanisms have been tested and work satisfactorily. Each has advantages and disadvantages in areas of response time and reliability; therefore, research will continue on the design of the shutter mechanism.

The process of actually locating cells to be irradiated and carrying out the sequence of operations to perform the irradiation is complex. Individual computer subroutines for each of the operations were written and have been used to control the irradiation procedure, but the process proved exceptionally time consuming. Initial test experiments required several minutes to locate and irradiate each cell, far too long for practical experiments. To solve this problem, new menu-driven software was written to control the system. Figure 3 is an illustration of the control computer screen with the enlarged image of a cell in the upper left box. This enlarged image allows easy placement of the cross-hair over the portion of the cell to be irradiated. The center box indicates the areas within a given microscope field that have been shown as enlarged cell images at the left. If

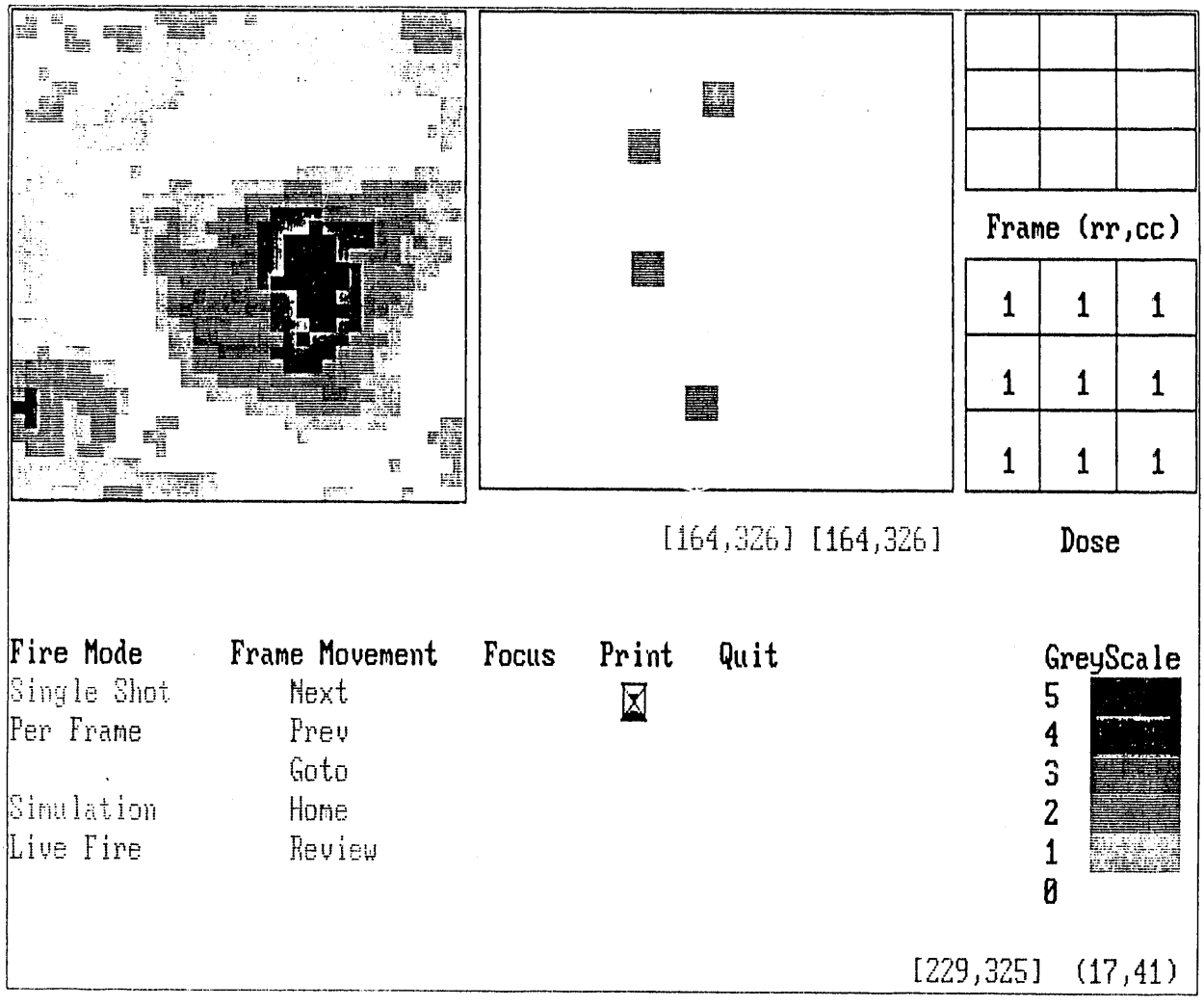

FIGURE 3. The Irradiation System Control Screen Showing the Enlarged Image of the Cell to be Irradiated and Its Position in the Current Microscope Field and in the Cell Culture Dish

there are two or more cells in a given field, each of them is marked for irradiation before the irradiations start. The dish is divided into nine areas (box, right, center), and each area can be dosed differently, helping to eliminate experimental variability due to different growth conditions on different dishes. The upper right panel shows the irradiated portion of the dish. This control screen, in combination with the video image of the microscope field, provides an efficient means to prepare and conduct experiments. The system currently uses a personal computer (PC) for irradiation control and the VAX 750 for image processing. Use of the VAX results in some delay when the magnified images are transferred to the PC, but this problem will be eliminated when a PC-based image processor replaces the current processor.

Preliminary irradiation experiments are being performed to isolate operational problems in the system, and initial cell survival experiments are being planned.

Reference

Braby, L.A. 1991. "Single-Particle Irradiation System." In *Physical Sciences, Part 4 of Pacific Northwest Laboratory Annual Report for 1990 to the DOE Office of Energy Research,* PNL-7600, pp. 15-17. Pacific Northwest Laboratory, Richland, Washington.

Measurement
Science

Capillary Electrophoresis-Mass Spectrometry

The analysis of environmental, hazardous mixed waste, or biological mixtures is best addressed by combined separation-mass spectrometry (MS) techniques. The development of these improved analytical methods rests upon the speed, selectivity, and efficiency of the separation combined with the sensitivity and flexibility of mass spectrometric analysis methods. This program is developing methods that are widely applicable to nonvolatile or highly polar compounds, intractable by more conventional methods such as gas chromatography-mass spectrometry. Currently, new methods based upon capillary electrophoresis-mass spectrometry (CE-MS) are being investigated. The goal of this research is to develop ultrasensitive CE-MS methods applicable at the attomole level for environmental and health-related problems.

Development of Capillary Electrophoresis-Mass Spectrometry

R. D. Smith, H. R. Udseth, C. J. Barinaga, B. E. Winger, C. G. Edmonds, and J. A. Loo

The history of analytical advances in mass spectrometry (MS) has highlighted the special importance of the combination of separation methods having high selectivity and resolving power in conjunction with the high sensitivity and specificity of mass spectrometric detection. "Real-world" samples are invariably mixtures and are often very complex. Any useful analytical method must accommodate contributions from the sample matrix, interfering substances, etc. The dynamic combination of capillary electrophoresis (CE), a separation method of high efficiency, speed, and flexibility, with electrospray ionization (ESI)-MS is thus particularly advantageous.

The on-line combination of capillary zone electrophoresis (CZE), one form of CE, with ESI-MS (Olivares et al. 1987; Smith et al. 1988b) was developed at PNL. Subsequently, a liquid sheath-electrode interface was developed from which the solvent composition and flow rate of the electrosprayed liquid could be controlled independently of the CZE buffer (which is desirable since high-percentage aqueous and high-ionic-strength buffers that are useful in CZE are not well tolerated by ESI) (Smith et al. 1988a). The interface provides greatly improved interface stability and performance and is adaptable to other forms of CE. Because CE relies on analyte charge in solution and the ESI process is nearly universal for charged species, the CE/ESI-MS combination is highly complementary. Thus, the CZE/MS approach offers previously unobtainable separation efficiencies (for the combination with MS) as well as detection limits that can greatly surpass existing methods (Edmonds et al. 1989; Loo et al. 1989a; Loo et al. 1989b; Smith et al. 1989b; Smith et al. 1990a; Smith et al. 1990d).

One reason for the current interest in CE-MS techniques is for identification and analysis of DNA adducts. This is an important but formidable analytical challenge due to the "difficult" nature of the compounds and their extremely low concentrations. Ideally, we desire the ability not only to detect "known" compounds, but also to determine the structure of unknown DNA adducts with sample sizes far too small to be addressed by other analytical methods. These desires lead to our interest in CE, ESI-MS, and ESI-MS/MS. In fact, it can be argued that the CE-MS/MS combination obtained using the ESI interface should provide a near-ideal analytical approach for DNA adducts. Potentially large segments of DNA can also be addressed because of the unique nature of the ESI method.

To realize the full potential of this new analytical marriage, several problems remain to be addressed:

- The utilization and transmission of ESI-produced ions must be improved. Currently, ESI losses in the interface and during transmission reduce potential sensitivity by 10^4 (Smith et al. 1990c).
- High-resolution separations utilizing an analyte enrichment scheme are required to both address the complexity of "real" samples and

obtain sufficient sensitivity with the small volumes utilized in CE.

- Improved MS and MS/MS sensitivity, resolution, and mass measurement accuracy are necessary to enhance detection and allow interpretation of mass spectra containing multiply-charged molecules.

We have recently shown that DNA and RNA segments having up to two million molecular weight can be electrosprayed and the highly charged (>1500 charges in some cases) molecular ions efficiently detected. Currently most of our efforts are focused on addressing the three problems outlined above.

Our efforts in development of more efficient ESI sources focus on the enhanced efficiency for transport of ions into the mass spectrometer from the atmospheric pressure source. A new approach based upon using magnetic fields in the moderate pressure interface region has the potential for a 10^2-10^3 gain in overall efficiency. A further gain based upon a "microspray" approach appears to offer another order-of-magnitude improvement in sensitivity. If these gains can, in fact, be realized, detection limits for ESI-MS could be reduced to under one zeptomole (i.e., 10^{-21} mole).

In the second area noted above, the multidimensional combination of capillary isotachophoresis (CITP) as a first stage and CZE as the second stage offers a significant advantage for ultra-trace level characterization (Smith et al. 1990a). The advantage of this combination is the ability to utilize large sample volumes, from which extremely low concentrations of targeted species can be identified.

The third area is being addressed by utilizing ion trapping mass spectrometers, both quadrupole (Paul) traps and ion cyclotron resonance (ICR) devices. Figure 1 shows a schematic illustration of a new 7-tesla ICR mass spectrometer which has been designed to obtain the ultrahigh vacuum conditions required for achieving high resolution for large molecular ions. Experimental

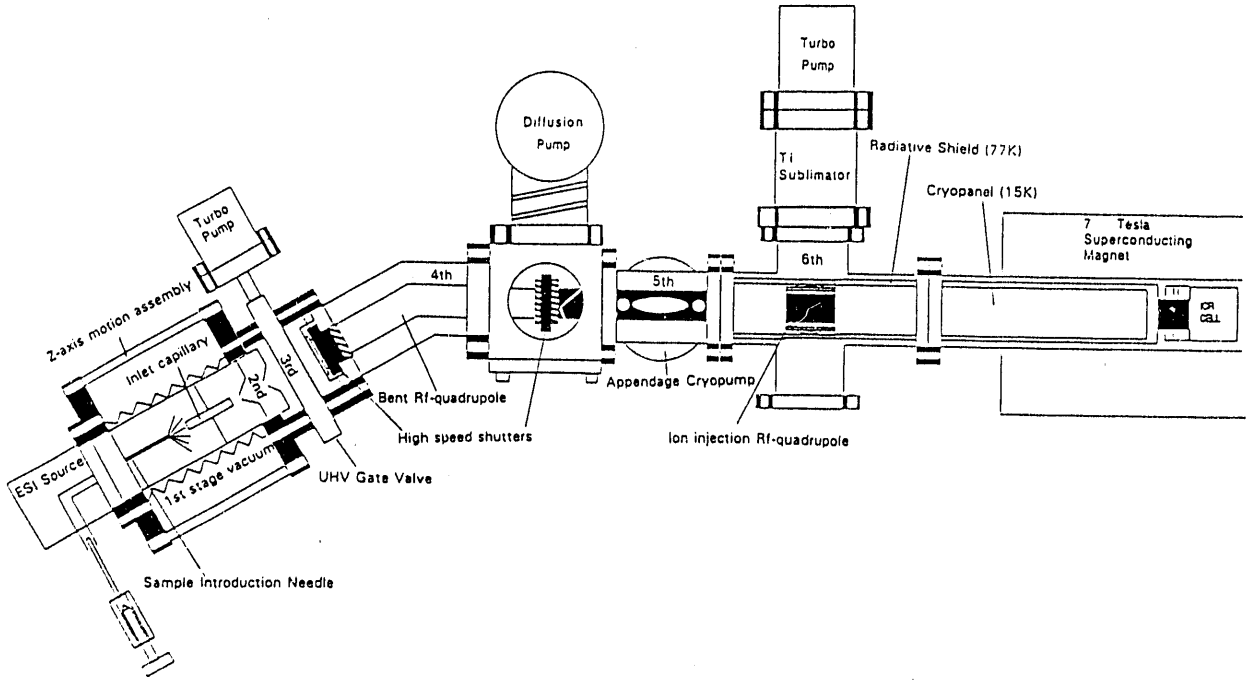

FIGURE 1. Schematic Illustration of a New 7-tesla ICR Mass Spectrometer Developed at PNL for the Characterization of Macromolecules

studies have been conducted during FY 1991 in conjunction with Professor F. W. McLafferty of Cornell University which have demonstrated the capability for achieving high resolution for large biomolecules. Figure 2 gives a high resolution spectrum for a small protein obtained using the Cornell 3-tesla ICR. A particular advantage of ICR is the capability for conducting high order multi-dimensional MS studies (i.e., MS^n), where detailed structural information is obtainable. This new approach would also offer the ability to examine long DNA segments to determine both the site and the identity of DNA adducts.

Related to this is our recent progress in obtaining both an experimental (Loo et al. 1990a; Loo et al. 1990b; Loo et al. 1991a; Loo et al. 1991b; Smith et al. 1989a; Smith et al. 1990b; Smith and Barinaga 1990) and theoretical (Rockwood et al. 1991) understanding of dissociation processes for large multiply charged biomolecules. This capability, if we succeed, would literally lead to a renaissance for analytical biochemical research.

High *m/z* resolution for *z* determination

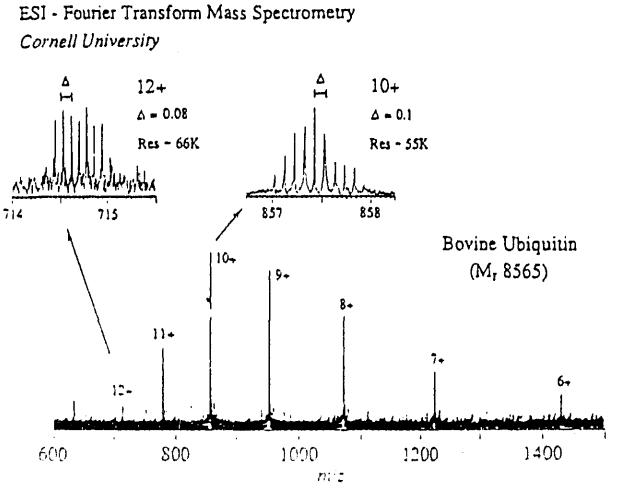

FIGURE 2. High Resolution ICR Mass Spectrum Obtained in Conjunction with F. W. McLafferty (Cornell University) Showing the Multiple Charge States Produced for Bovine Ubiquitin by Electrospray Ionization. Sufficient resolution (>60,000) is obtained to resolve the isotopic envelope and allow charge state determination.

References

Edmonds, C. G., J. A. Loo, C. J. Barinaga, H. R. Udseth, and R. D. Smith. 1989. "Capillary Electrophoresis-Electrospray Ionization-Mass Spectrometry." *J. Chromatogr.* 474:21-37.

Loo, J. A., C. G. Edmonds, H. R. Udseth, and R. D. Smith. 1990a. "Collisional Activation and Dissociation of Large Multiply Charged Proteins Produced by Electrospray Ionization." *Anal. Chim. Acta.* 241:167-173.

Loo, J. A., C. G. Edmonds, and R. D. Smith. 1990b. "Primary Sequence Information from Electrospray Ionization Tandem Mass Spectrometry of Intact Proteins." *Science* 248:201-204.

Loo, J. A., R. R. Ogorzalek-Loo, H. R. Udseth, C. G. Edmonds and R. D. Smith. 1991a. "Solvent-Induced Conformational Changes of Polypeptides Probed by Electrospray-Ionization Mass Spectrometry." Rapid Commun. Mass Spectrom. 5:101-105.

Loo, J. A., C. G. Edmonds, and R. D. Smith. 1991b. "Tandem Mass Spectrometry of Very Large Molecules: Serum Albumin Sequence Information from Multiply Charged Ions Formed by Electrospray Ionization." *Anal. Chem.* 63:2488-2499.

Loo, J. A., H. K. Jones, H. R. Udseth, and R. D. Smith. 1989a. "Capillary Zone Electrophoresis-Mass Spectrometry with Electrospray Ionization of Peptides and Proteins." *J. Microcolumn Sep.* 1:223-229.

Loo, J. A., H. R. Udseth, and R. D. Smith. 1989b. "Peptide and Protein Analysis by Electrospray Ionization Mass Spectrometry and Capillary Zone Electrophoresis-Mass Spectrometry." *Anal. Biochem.* 179:404-412.

Olivares, J. A., N. T. Nguyen, C. R. Yonker, and R. D. Smith. 1987. "On-Line Mass Spectrometric Detection for Capillary Zone Electrophoresis." *Anal. Chem.* 59:1230-1232.

Rockwood, A. L., M. Busman, and R. D. Smith. 1991. "Coulombic Effects in the Dissociation of Large Highly Charged Ions." *Int. J. Mass Spectrum. Ion Proc.* 111:103-130.

Smith, R. D., and C. J. Barinaga. 1990. "Internal Energy Effects in the Collision Induced Dissociation of Large Biopolymer Molecular Ions Produced by Electrospray Ionization: Tandem Mass Spectrometry of Cytochrome c." *Rapid Comm. Mass Spectrom.* 4:54-57.

Smith, R. D., C. J. Barinaga, and H. R. Udseth. 1988a. "Improved Electrospray Ionization Interface for Capillary Zone Electrophoresis-Mass Spectrometry." *Anal. Chem.* 60:1948-1952.

Smith, R. D., C. J. Barinaga, and H. R. Udseth. 1989a. "Tandem Mass Spectrometry of Highly Charged Cytochrome c Molecular Ions Produced by Electrospray Ionization." *J. Phys. Chem.* 93:5019-5022.

Smith, R. D., S. M. Fields, J. A. Loo, C. J. Barinaga, and H. R. Udseth. 1990a. "Capillary Isotachophoresis with UV and Tandem Mass Spectrometric Detection for Peptides and Proteins." *Electrophoresis* 11:709-717.

Smith, R. D., J. A. Loo, C. J. Barinaga, C. G. Edmonds, and H. R. Udseth. 1989b. "Capillary Zone Electrophoresis and Isotachophoresis-Mass Spectrometry of Polypeptides and Proteins Based Upon an Electrospray Ionization Interface." *J. Chromatogr.* 480:211-232.

Smith, R. D., J. A. Loo, C. J. Barinaga, C. G. Edmonds, and H. R. Udseth. 1990b. "Collisional Activation and Collision-Activated Dissociation of Large Multiply Charged Polypeptides and Proteins Produced by Electrospray Ionization." *J. Am. Soc. Mass Spectrom.* 1:53-65.

Smith, R. D., J. A. Loo, C. G. Edmonds, C. J. Barinaga, and H. R. Udseth. 1990c. "New Developments in Biochemical Mass Spectrometry: Electrospray Ionization." *Anal. Chem.* 62:882-899.

Smith, R. D., J. A. Loo, C. G. Edmonds, C. J. Barinaga, and H. R. Udseth. 1990d. "Sensitivity Considerations for Large Molecule Detection by Capillary Electrophoresis-Electrospray Ionization Mass Spectrometry." *J. Chromatogr.* 516:157-165.

Smith, R. D., J. A. Olivares, N. T. Nguyen, and H. R. Udseth. 1988b. "Capillary Zone Electrophoresis-Mass Spectrometry Using an Electrospray Ionization Interface." *Anal. Chem.* 60:436-441.

Laser Measurements of ^{210}Pb

The radioisotope ^{210}Pb is the first long-lived progeny in the decay of ^{222}Rn. It has, therefore, been suggested that the accumulation of ^{210}Pb in biological tissues and the environment can be used as a measure of long-term integrated radon exposure. The purpose of this project has been to develop an analytical methodology capable of measuring ^{210}Pb at the levels expected to be produced by radon exposure and to use this measurement capability to study the correlation between radon exposure and the levels of ^{210}Pb in human tissues and the environment. The measurement of ^{210}Pb at levels expected in small samples is generally beyond the capabilities of nuclear decay counting. Thus, methods using laser-induced ionization mass spectrometry have been developed to address these problems. In prior years this program has demonstrated that using high-resolution continuous wave lasers for these measurements permits the detection of ^{210}Pb at subfemtogram levels in the presence of a 10^{10} or greater excess of the stable naturally occurring Pb isotopes. In the past year, measurements have been performed on human tissue samples, including hair and brain sections.

Measurement of ^{210}Pb in Biological Samples

B. A. Bushaw and G. I. Lykken[a]

Laser-Induced Ionization

The capabilities of laser-induced ionization for measuring ^{210}Pb at subfemtogram levels have been described previously (Bushaw and Munley 1990, 1991), and the approach is only summarized here. Aqueous solutions containing the ^{210}Pb to be measured are evaporated in a graphite crucible, which is then placed within a vacuum system and heated electrothermally by passing a dc current through the graphite crucible material. As the temperature increases, the Pb salts in the sample are reduced to neutral metallic atoms on the graphite surface, which then vaporize and are ejected from the crucible. Just above the exit aperture of the crucible, the neutral metal atoms are subjected to three overlapped laser beams, which cause specific ionization of the isotope of interest via the double-resonance excitation:

$$6s^2\,{}^3P_0 \xrightarrow{\lambda_1} 6p7s\,{}^3P_1 \xrightarrow{\lambda_2} 6p16p(1/2,3/2),$$

$$J = 2 \xrightarrow{\lambda_3} Pb^+ + e^- \qquad (1)$$

where the resonance excitations (λ_1 = 283.3 nm and λ_2 = 420.9 nm) are accomplished with single-frequency continuous wave (CW) dye lasers, and the infrared photons for the ionization step (λ_3 = 10.6μm) are provided by a 10 watt CW CO_2 laser. The Pb^+ ions produced in this manner are then electrostatically extracted into a quadruple mass filter, which provides additional isotopic discrimination. We previously reported ^{210}Pb detection limits of 0.3 femtograms using this approach. Since then, our use of pyrolytic coatings on the graphite crucible and our increased experience have lowered these detection limits to 0.06 femtograms, as shown in Figure 1A.

Measurement of ^{210}Pb Content in Human Hair Samples

To test the capabilities of this analytical measurement technology for "real world" biological samples, hair samples were obtained from subjects with known bedroom radon levels, as determined by standard charcoal canister measurements. These samples were obtained by Dr. Glenn Lykken from persons in the Grand Forks, North Dakota, area where elevated radon levels in homes are known to occur. These samples can not be loaded directly into the graphite crucible, but must be subjected to chemical pretreatment before the analysis is performed. The procedure developed for these samples began with wet ashing of the samples (typically 0.3 to 0.5 grams of hair starting material)

(a) Dr. Lykken is a Professor of Physics at the University of North Dakota and has worked on this program through a NORCUS Summer Fellowship.

with nitric acid and hydrogen peroxide. The resulting Pb^{2+} ions in the resulting solution are converted to the $Pb(OH)_4^{2-}$ anion by treatment with concentrated ammonia solution. The Pb in this anionic form was then purified and concentrated by a two-step ion-exchange procedure using Dowex 1x4 anion-exchange resin, with the final elution evaporated to a volume suitable for loading into the graphite atomization crucible. The resulting temperature evolution curve, typical for these samples, is shown in Figure 1B. Compared to the reference standard solutions (Figure 1A), the evolution of the Pb atoms is spread out into several peaks. This is attributed to matrix effects caused by residual materials that are co-eluted from the ion exchange columns and delay the reduction of the Pb ions to the neutral atomic form. Standard addition techniques using samples spiked with the stable isotopes showed that ion exchange recoveries and/or lower atomization efficiency reduced overall measurement sensitivity by a factor of 2 to 3. However, the standard additions also served as an internal calibration, and it was still possible to obtain semiquantitative results by integration over the multiple evolution peaks. Table 1 tabulates the measured ^{210}Pb levels found in four different test hair samples and the corresponding measured bedroom radon levels.

Even with this rather limited data set, it is apparent that there is a strong correlation between the radon exposure levels and the ^{210}Pb concentrations. Continuing work in the area will focus on 1) improving the chemical procedures to reduce the matrix effects and 2) making measurements on a larger number of hair samples, particularly in the 0 to 20-pCi/L-expose range, to obtain a quantitative understanding of the correlation between radon exposure and ^{210}Pb levels in human hair.

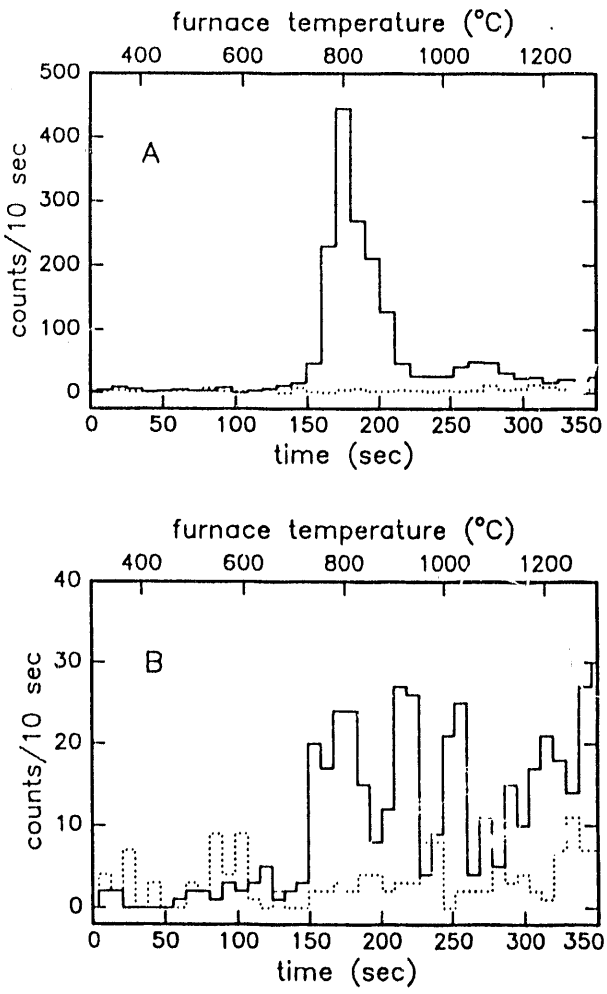

FIGURE 1. Laser-induced Ionization Measurements of ^{210}Pb. Ion counts are recorded while temperature of atomizing crucible is increased. A) Shows the result for a reference sample containing 4.4 femtograms ^{210}Pb (solid line), compared to a blank containing 2 micrograms of the stable isotopes (dotted line). Integration and comparison of the sample and blank signals yields 3σ detection limits of 0.06 femtograms. B) Shows the measurement on a chemically processed (see text) hair sample divided into two aliquots. The first aliquot (solid line), corresponding to 0.1 g hair measures the ^{210}Pb content. A background measurement (dotted line) is performed with the second aliquot by detuning the first excitation laser from the ^{210}Pb resonance.

Measurement of ^{210}Pb in Brain Sections of Alzheimer's Disease Victims

Although the predominant health risk associated with radon exposure has conventionally been thought to be an increased probability of lung cancer, it has been postulated recently that there may be additional risks (Henshaw et al. 1990). In particular, because of radon's high fat solubility, it has been suggested that elevated radon exposure may be a contributory factor in a number of fatty-tissue diseases, including brain tumors, Parkinson's disease, Alzheimer's disease, and certain types of bone marrow-related leukemias. We have begun testing these hypotheses by

TABLE 1. Measured ^{210}Pb Concentrations in the Hair of Persons with Known Bedroom Radon Levels

Bedroom Radon (pCi/L)	^{210}Pb in Hair (fg/g)[a]
0.3	1.2
10	5
65	22
80	18

(a) Semiquantitative measurement, estimated uncertainty is ± 30%.

performing ^{210}Pb determinations on brain sections from Alzheimer's disease victims and comparing them to age-matched control brain sections from unafflicted subjects. These samples were obtained by Dr. Lykken from the Ramsey Dementia Brain Bank in St. Paul, Minnesota. Initial chemical preparation involved microwave digestion with mineral acid (2 to 3 grams starting material) at the Human Nutrition Research Center at the University of North Dakota. The resulting solutions were transported to Pacific Northwest Laboratory, where they were freeze-dried to reduce the liquid volume, and then subjected to the same ion-exchange procedures described above for hair samples.

The results of the measurements or these samples are summarized in Table 2. In all cases the ^{210}Pb levels determined are extremely low, near the detection limits of the measurement system. Furthermore, there appears to be no significant difference between the Alzheimer's and control samples. Thus we conclude that we have no evidence to support the hypothesis that radon exposure is a contributory factor in the development of this disease. However, it should be realized that the limited number of samples and results very near the detection limits are not sufficient evidence to discount the hypothesis. Further efforts in this area will concentrate on improving the chemical procedures by using larger initial sample sizes and extending the measurements to bone marrow sections from leukemia victims.

TABLE 2. ^{210}Pb Concentrations Found in Brain Samples

Sample	Type[a]	fg ^{210}Pb/g tissue
BR-07	N	0.12 ± 0.04
BR-30	N	0.10 ± 0.07
BR-18	N	0.00 ± 0.02
BR-25	A	0.08 ± 0.04
BR-13	A	0.03 ± 0.03
BR-26	A	0.05 ± 0.04
BR-06	A	0.04 ± 0.04
BR-36	B	1.15 ± 0.10

(a) N: Normal brain, A: Alzheimer's disease victim, B: Bovine liver.

References

Bushaw, B. A., and J. T. Munley. 1991. "Isotopically Selective RIMS of Rare Radionuclides by Double-Resonance Excitation with Single-Frequency CW Lasers." *Inst. Phys. Conf. Ser.* 114:387.

Bushaw, B. A., and J. T. Munley. 1990. "Measurement of ^{210}Pb at the Subfemtogram Level with Relative Isotopic Concentrations of 10^{-10}." In *Physical Sciences, Part 4 of Pacific Northwest Laboratory Annual Report for 1989 to the DOE Office of Energy Research*, PNL-7600. Pacific Northwest Laboratory, Richland, Washington.

Henshaw, D. L., J. P. Eatough, and R. B. Richardson. 1990. "Radon: A Causative Factor in the Induction of Myeloid Leukaemia and Childhood Cancer." *Lancet* 23:1008.

Lasers in Environmental Research

This program has historically investigated the use of continuous wave (CW) lasers for atomic spectroscopy measurements of extremely rare isotopes. The extremely high resolution afforded by single-frequency dye lasers permits isotopic selectivity in the excitation of atoms. This selectivity can be combined with the selectivity of a mass spectrometer to unambiguously detect isotopes that occur at abundances of less than 10^{-10} with respect to other isotopes of the same element. Also, these CW lasers do not suffer the duty-cycle constraints that inherently limit the effectiveness of pulsed laser systems for ultratrace measurements. To overcome the ionization efficiency limits of low-power CW dye lasers, this program has developed the approach of using an auxiliary high-power infrared laser to efficiently ionize atoms that have been selectively prepared in high-lying Rydberg states by double-resonance dye laser excitation. Using this approach, detection limits in the subfemtogram range are now routinely achieved. During the last year, this methodology has been applied to detection of the radionuclide ^{90}Sr, which is a significant health risk and environmental contaminant generated by nuclear power and weapons cycles.

Detection of Strontium-90 at the Attogram Level

B. A. Bushaw

Methods for the rapid and accurate determination of low levels of the radioisotope ^{90}Sr are important for several reasons. The radioisotope is a high-yield fission product in nuclear reactors (and weapons), with approximately 1 1 kg produced for every gigawatt-year of reactor operation. It has a high potential for biological damage because it can chemically substitute for calcium in bone material and its radioactive half-life of 28.5 years is comparable to its retention time within the bone. However, the radioisotope is very difficult to measure by conventional radiochemical methods because its decay mode is pure β decay, without any associated gamma-ray emissions. Usual radiochemical methods involve a chemical separation of the strontium in a sample, followed by approximately one week for ingrowth and equilibration of the ^{90}Y progeny. Then, a gamma-ray spectroscopic determination of the ^{90}Y is performed. Even at moderately high ^{90}Sr levels, one to two weeks are required after the acquisition of a sample before analytical results can be delivered.

There are a number of applications, such as monitoring of site-remediation activities and personnel-exposure assessment, in which rapid analyses for ^{90}Sr would be most beneficial. Laser-based ionization techniques are not dependent on the intrinsic nuclear decay lifetimes, and it is possible to perform measurements in several minutes. Although some samples may require initial chemical preparations (e.g., a one-step ion-exchange purification and preconcentration), results may be obtained in less than one hour.

We previously performed initial spectroscopic measurements on the isotope shifts for ^{90}Sr in selected Rydberg states (Bushaw 1989). The shifts between ^{90}Sr and ^{88}Sr were found to be very small because of a serendipitous cancellation of normal mass shift and nuclear volume shift effects. The studies were curtailed at that time because optical isotopic selectivity of only ~100 could be achieved, and it appeared that there would not be enough overall selectivity, even with a mass spectrometer, to perform measurements at background ^{90}Sr abundances of $\sim 10^{-11}$ (residual from atmospheric weapons tests). In the interim, improvements in overall performance of the laser-induced ionization instrumentation and increased emphasis on site remediation, particularly the Hanford Site waste tanks, have caused us to resume these investigations.

The laser excitation scheme used in these measurements was

$$5s^2\,{}^1S_0 \xrightarrow{\lambda_1} 5s6p\,{}^1P_1 \xrightarrow{\lambda_2} 5s16d\,{}^1D_2 \xrightarrow{\lambda_3} Sr^+ + e^- \quad (1)$$

where the first two excitations are performed with single-frequency continuous wave CW dye lasers

operating at wavelengths of 460.86 and 428.94 nm, and a 10-watt CW CO_2 laser is used for the ionization step. The resulting ions were then analyzed with a quadruple mass spectrometer. Test sample solutions were prepared from a National Institute of Standards and Technology traceable radiochemical standard solution and diluted with solutions of the stable isotopes to produce the desired concentrations and relative isotopic abundances of ^{90}Sr. Figure 1 shows the measurement on a sample containing 2.7×10^{-17} grams of ^{90}Sr in the presence of a 1.8×10^{8} excess of the stable isotopes (solid line). This was compared to a blank without ^{90}Sr present, but with an equivalent amount of the stable isotope (dashed line). Integration of the signal for the two samples over the period of 200 to 600 seconds yields a 3σ detection limit of 2×10^{-18} grams, corresponding to 14,000 atoms or one radioactive decay every 20 hours. Further studies, with higher concentrations of the stable isotopes, determined that overall isotopic selectivity for ^{90}Sr against ^{88}Sr was 3×10^{9}. Of this, spectroscopic studies of the off-resonant ^{88}Sr line shape showed that optical selectivity was only ~75, and thus the remaining 4×10^{7} selectivity is provided by the mass spectrometer. While this selectivity is still not sufficient to address background-level measurements, it is adequate for many site-remediation needs. Also, the extreme sensitivity will allow microsampling techniques that can be used to minimize worker exposure to high-level radioactive wastes.

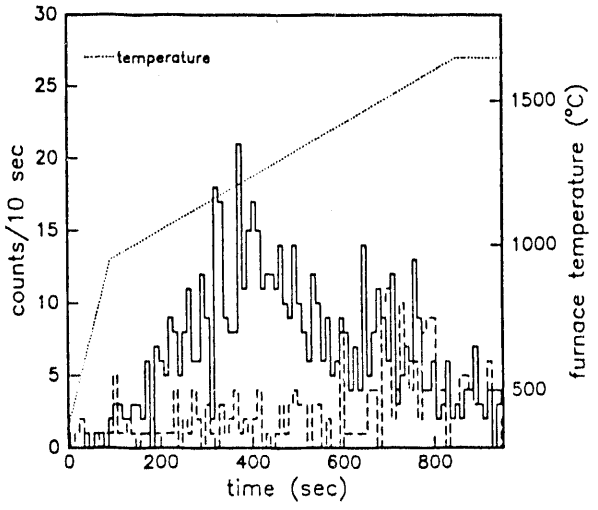

FIGURE 1. Double-Resonance Laser-Induced Ionization Measurement of ^{90}Sr at the Attogram Level. The solid line represents the measurement on a sample containing 2.7×10^{-17} g of ^{90}Sr in the presence of 5×10^{-9} g of the stable Sr isotopes, while the dashed line is for a sample containing only the 5×10^{-9} g of the stable isotopes.

The sensitivity that has been demonstrated in these measurements may also be sacrificed (to some extent) to improve selectivity to the level required for background environmental measurements. Currently, optical selectivity is limited by residual Doppler broadening resulting from close coupling of the graphite crucible atomization source to the ionization lasers. Increasing the source-ionization distance by a factor of 3 will cause a loss of an order of magnitude in sensitivity but will reduce Doppler broadening by a factor of 3. With the gaussian lineshape of Doppler broadening and the observed isotope shifts, this should improve the optical isotopic selectivity by a factor of ~200. These modifications are currently underway. Also, comprehensive, accurate measurements of isotope shifts and lineshapes are being performed to determine which Rydberg state will afford the maximum selectivity.

Reference

Bushaw, B. A., and G. K. Gerke. 1989. "Double Resonance Ionization Spectroscopy of ^{90}Sr." In *Physical Sciences, Part 4 of Pacific Northwest Laboratory Annual Report for 1988 to the DOE Office of Energy Research*, PNL-6800, p. 11. Pacific Northwest Laboratory, Richland, Washington.

Radiological and Chemical Physics

Radiation Physics

The spatial and temporal patterns of energy deposition by ionizing radiation play a dominant role in determining the subsequent chemical and biological processes leading to expression of radiation damage in biological systems. These patterns of energy deposition are established through the production and slowing down of secondary electrons that define the structure of charged particle tracks. Our studies focus on characterizing the absolute cross sections for interactions involving charged particles and electrons with atomic, molecular, and condensed phase targets that determine the structure of charged particle tracks in tissue-like material. Emphasis is on the study of differential ionization cross sections, charge-transfer processes, and on the fate of the target atom or molecule that has undergone an ionizing event. The information from these studies is then incorporated into Monte Carlo models developed to describe the charged particle track structure and the influence of that structure on subsequent chemical and biological processes.

The radiation physics studies continue to focus on understanding interactions of heavy charged particles with biologically relevant targets and implementing these data, along with more realistic target properties, into Monte Carlo simulations of energy deposition in tissue. Experimental studies have addressed the effects of both projectile and target structure on secondary electron production by high- and intermediate-velocity ions. Differential ionization cross sections were measured for a wide range of projectile charge states and preliminary data were collected for condensed phase targets. Collaborative measurements were also undertaken to determine charge transfer measurements of interest in radiation biology. Monte Carlo code developments include new models of the angular distribution of secondary electrons, and initial strides were made toward simulating electron emission from condensed phase targets. This latter development is intended to provide the framework for careful evaluation of condensed phase contributions to energy transport.

A Model of the DDCS for Ejection of δ-Rays by Fast Ions

W. E. Wilson

In ion-atom collisions, the angle at which the secondary electron is ejected relative to the ion direction is a very important quantity for determining the spatial extent of the ion track structure. For simulations, the angle of emission is obtained from the doubly differential cross sections (DDCS). The algorithm for the DDCS used in the MOCA series (Wilson et al. 1988) of positive ion track structure simulations is based on Bethe-Born theory (Inokuti 1971).

According to Bethe-Born theory, the doubly differential cross section for electron emission can be expressed as (Kim 1972),

$$\sigma(\theta,w) = \frac{4\pi a_0^2}{T/R}\left[A(\theta,w)\,\ln\left(\frac{T}{R}\right) + B(\theta,w) + 0(T^{-1})\right] \quad (1)$$

The first term in equation 1 describes the interactions involving small momentum transfers that arise from distant collisions and is often referred to as the "glancing collisions" term,

$$\sigma_{gc}(\theta,w) = \frac{4\pi a_0^2}{T/R}\,\ln\left(\frac{T}{R}\right) A(\theta,w) \quad (2)$$

The second term is the "hard collisions" term, which represents close collisions that often transfer significant momentum to the target particle,

$$\sigma_{hc}(\theta,w) = \frac{4\pi a_0^2}{T/R}\,B(\theta,w) \quad (3)$$

In the above equations, and throughout this discussion, the quantities a_0 and R have their usual meaning of Bohr radius and Rydberg energy, respectively. T is the kinetic energy of an electron having a velocity equal to that of the ion. In the present model, we ignore the higher-order terms O(1/T).

Glancing Collisions

In the optical approximation, the angular dependent part, A(θ,w), is given by (Kim 1972),

$$A(\theta,w) = \frac{1}{4\pi} \sum_j \left\{ \frac{R}{w + I_j} \cdot \frac{df_j}{dw} \left[1 + \frac{\beta_J}{2} P_2(\cos\theta) \right] \right\} \quad (4)$$

where

$$h_j(w) = \frac{R}{w + I_j} \frac{df_j}{dw} \quad (5)$$

is the dipole optical oscillator strength for shell j. In equation 4, β_j is the photoelectron asymetry parameter, P_2 is the Legendre polynomial of second order and I_j is the ionization threshold for shell j.

For the $h_j(w)$, we use a piece-wise polynomial representation of the Berkowitz tabulation of the total oscillator strength (Berkowitz 1979), and branching ratios of Tan et al. (1978), and of Blake and Carver (1967).

The asymmetry parameter, β_j, is theoretically equal to two for S states, (the $2a_1$ orbital of water); for other states, β_j is energy dependent (Kim 1972). We use a phenomenological fit to experimental DDCS data for water vapor (Toburen and Wilson 1977). Empirically, β_j is taken to be,

$$\beta_j = \max \begin{cases} 1 - \exp^{(0.168 - 0.024w)} \\ 0 \end{cases}, \quad j = 1,2,3,$$

$$\beta_4 = 2 \quad (6)$$

Finally,

$$P_2 = \frac{3}{2} \cos^2\theta - \frac{1}{2} \quad (7)$$

Hard Collisions

The hard collisions component of the experimental angular distributions (Toburen and Wilson 1977) are well represented by a (Gaussian) normal distribution (Wilson 1978). Therefore, we represent this term, equation 3, by a product of three functions,

$$\sigma_{hc} = g_w(\theta)\, S_{bea}(w)\, f_{bea}(w) \quad (8)$$

The angular dependence is described by a normalized Gaussian function $g_w(\theta)$,

$$g_w(\theta) = \frac{1}{\sqrt{2\pi}\Gamma} \exp\left[-\left(\frac{\cos\theta - \overline{\cos\theta}}{\Gamma} \right)^2 \right] \quad (9)$$

For unbound electrons, the centroid of the binary encounter peak is related to the energy transferred, E_R, by

$$\overline{\cos\theta} = \sqrt{E_R}$$

(See for example Evans 1955.) We find that better agreement is achieved with the experimental data for the bound electrons of water vapor if a small energy dependent correction term, δ, is added. Then

$$\overline{\cos\theta} = (1 + \delta) \sqrt{E_R} \quad (10)$$

where δ is given by the phenomenological power law relations,

$$\delta = \exp(\gamma)$$

$$\gamma = 2.303\ \alpha + \beta \log_{10}(E_R) \qquad (11)$$

$$\alpha = -2.5 + 2.27 \exp(-1.066\ E_{ion})$$

$$\beta = -1.25 + 0.635 \exp(-1.375\ E_{ion})$$

E_{ion} is the proton energy in MeV.

The Gaussian width parameter, Γ, is given by,

$$\Gamma = \frac{(E_2\ W)^{1/2}}{E_2 + W} \qquad (12)$$

with E_2 = 20 eV from least-squares fitting of the experimental data.

The amplitude of the hard collisions term is determined primarily by the second function, $S_{bea}(w)$, in equation 8. For it, we use a simple single differential binary-encounter treatment (Rudd and Macek 1972),

$$S_{bea}(W) = \frac{\sigma_0}{TE^3} \begin{cases} 0, & E < U \\ E + \frac{4}{3} E_k, & U \le E \le T_4 - \Delta T \\ \left(\frac{T_4}{E_k}\right)^{3/2} + \left(1 - \sqrt{E/E_k + 1}\right)^3, & T_4 - \Delta T < E \le T_4 + \Delta T \\ 0, & E > T_4 + \Delta T \end{cases} \qquad (13)$$

The terms in equation 13 are defined as follows:

- U = binding energy of shell electrons,
- E = w + U = total energy transferred to the electron,
- E_k = assumed kinetic energy of shell electrons,
- T = kinetic energy of an electron with velocity equal to that of the ion,
- T_4 = 4 T = classical maximum energy transfer by a proton to a free electron,
- $\Delta T = 4\sqrt{T\ E_k}$, and
- $\sigma_0 = 6.51 \times 10^{-14}$ cm^2/eV.

To achieve better agreement with experiment, the function f_b is introduced to force the hard collisions component, σ_{hc}, to tend to zero as w goes to zero,

$$f_{bea}(w) = \max \begin{cases} 1 - \exp\left(\frac{9 - w}{16.5}\right) \\ o \end{cases} \qquad (15)$$

Cross sections produced by this model are illustrated in Figure 1 for several energies of secondary electrons ejected by the positive ion.

For use in track structure simulations, the cross sections as probability density functions are integrated to give probability distributions and then inverted numerically to provide the cosine variate of the angle of emission.

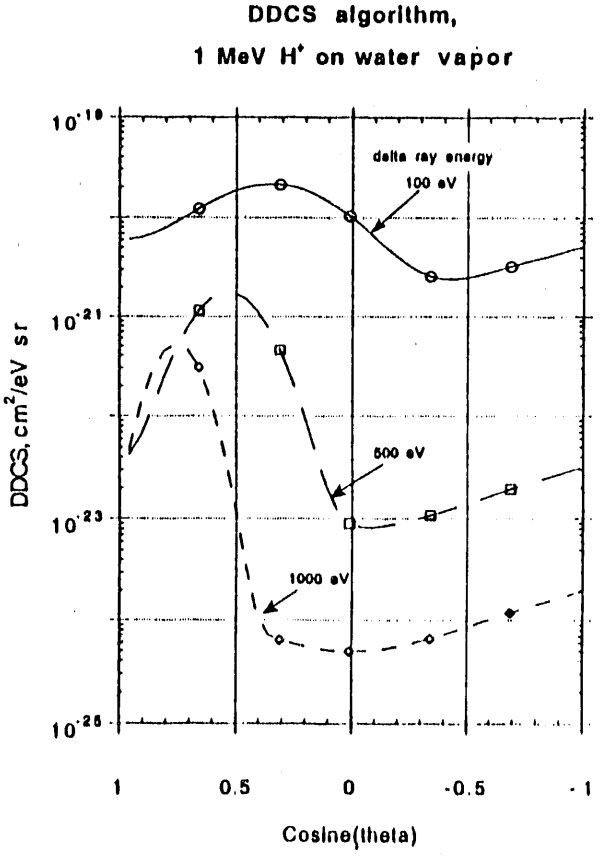

FIGURE 1. Doubly Differential Cross Section, DDCS, for Delta-Ray Emission as a Function of Cosine of Angle of Emission. Angular distributions for delta-rays of 100, 500, and 1000 eV energy are shown.

References

Berkowitz, J. 1979. *Photoabsorption, Photoionization, and Photoelectron Spectroscopy.* Academic Press, New York.

Blake, A. J., and J. H. Carver. 1967. "Determination of Partial Photoionization Cross Sections by Photoelectron Spectroscopy." *J. Chem. Phys.* 47:1038-1044.

Evans, R. D. 1955. *The Atomic Nucleus,* p. 835. McGraw-Hill.

Inokuti, M. 1971. "Inelastic Collisions of Fast Charged Particles with Atoms and Molecules-The Bethe Theory Revisited." *Rev. Mod. Phys.* 43:297-347.

Kim, Y. 1972. "Angular Distributions of Secondary Electrons in the Dipole Approximation." *Phys. Rev. A* 6:666-670.

Rudd, M. E., and J. H. Macek. 1972. "Mechanisms of Electron Production in Ion-Atom Collisions." *Case Studies in Atomic Physics* 3:47-136.

Tan, K. H., C. E. Brion, Ph. E. van der Leeuw, and M. J. van der Wiel. 1978. "Absolute Oscillator Strengths (10-60 eV) for the Photoabsorption, Photoionisation and Fragmentation of H_2O." *Chem. Phys.* 29:299-309.

Toburen, L. H., and W. E. Wilson. 1977. "Energy and Angular Distributions of Electrons Ejected from Water Vapor by 0.3-1.5 MeV Protons." *J. Chem. Phys.* 66:5202-5213.

Wilson, W. E. 1978. "Analytical Expression for Cross Section Data." In *Physical Sciences, Part 4 of Pacific Northwest Laboratory Annual Report for 1977 to the DOE Office of Energy Research,* PNL-2500, p. 2.7. Pacific Northwest Laboratory, Richland, Washington.

Wilson, W. E., N. F. Metting, and H. G. Paretzke. 1988. "Microdosimetric Aspects of 0.3- to 20-MeV Proton Tracks." *Radiat. Res.* 115:389-402.

Charge Transfer Cross Sections for Heavy Ion Impact

M. Rottmann,[a] L. H. Toburen, R. D. DuBois, R. Bruch,[a] and C. Drexler[b]

As energetic charged particles undergo energy-loss collisions and slow down, they capture and lose electrons in interactions with the atomic and molecular constituents of the medium. The number of bound electrons on a moving ion at any instant is a stochastic variable, and the mean charge state is a function of the ion velocity. The changes in charge state produced by electron capture and loss can have important consequences in radiological physics. In our studies of differential ionization cross sections (see other sections of this report) we found that bound projectile electrons have a dramatic effect on the energy distribution of electrons ejected in ionizing collisions. Electronic screening of the projectile charge by bound electrons thereby affects the mean energy lost in collisions with the absorbing medium and is reflected in the stopping power for the projectile. In addition, the processes of electron capture and loss contribute directly to the energy loss of charged particles.

From a more pragmatic point of view, the change in charge of the incident ion in collisions with target atoms or molecules can also influence the results of measurements intended to provide absolute interaction cross sections. This occurs because most experimenters use the transmitted ion beam current as a measure of the number of charged particles that pass through the target region. The correlation of measured ion current with number of particles through the interaction region is based on a presumed knowledge of the particle charge. Ion beam experiments generally rely on thin target conditions and expect

(a) University of Nevada, Reno, Nevada.

(b) Technical University, Munich, Germany.

negligible change in the incident charge when correlating charge with incident particle number. However, when considering heavy ions at low and intermediate energy, the charge transfer cross sections may be sufficiently large so that interactions with the target gas and with residual molecules in the accelerator beam lines may become significant. Unfortunately, there is little information in the literature concerning the charge transfer cross sections for low- and intermediate-energy ions of interest to radiobiology.

In order to provide additional data on charge transfer cross sections, we initiated a project in collaboration with Dr. Reinhard Bruch of the University of Nevada to experimentally determine cross sections of electron capture and loss relevant to radiological physics. A system for measuring charge transfer cross sections was initially set up at the Pacific Northwest Laboratory (PNL) Van de Graaff accelerator and later moved to the University of Nevada, where the measurements were conducted. The basic features of the system include a differentially pumped gas target cell and electrostatic deflection plates, which were used to analyze the final charge states of the transmitted beam. The charged and neutral beam components were detected by impinging them on metal surfaces and detecting the resulting secondary electrons with channel electron multipliers. Tests indicated that the detection system was 100% efficient for each of the beam components, C°, C^{1+}, and C^{2+}, for ion energies from 100 keV to 1500 keV. Measurements of the charge state fractions of the transmitted beam exiting the collision cell were made as a function of the target pressure. Cross sections for electron capture were determined from the linear increase in the neutral beam fractions with increasing target pressure.

Cross section measurements for a single electron capture have been completed for singly charged carbon ions with energies from 100 keV to 1525 keV passing through the gases H_2, He, Ne, Ar, N_2, O_2, CO, CH_4, NH_3, C_2H_6, and $(CH_3)_2NH$. In addition, cross sections were measured for H^+ collisions with H_2, He, N_2, and Ne for testing the reliability of the system against previously published cross sections. Within experimental uncertainties, the proton cross sections agreed with the recommended values given in the ORNL compilation (Barnett et al. 1990). Uncertainties in the present work are estimated at approximately 15% because of uncertainties in the detection efficiencies, pressure measurement, and statistical variations in determining the slope of the linear portion of the charge fraction versus pressure curves.

The only previously published data for singly charged carbon ions in the energy range from 100 keV to 1500 keV are for collisions with a molecular hydrogen target. Our results for electron capture in collisions of C^+ with H_2 are compared in Figure 1 to values recommended for this energy range in the compilation of Phaneuf et al. (1987). In general, the agreement is quite good; the data point at 300 keV from our measurement is somewhat lower than expected, but the other data are well within the uncertainties in the two sets of data. Cross sections for several of the molecules studied in this experiment are shown in Figure 2. Further analysis of these data is currently underway.

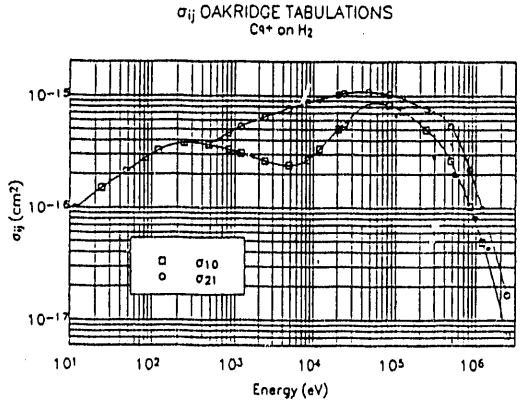

FIGURE 1. Comparison of Measured Cross Sections for Single Electron Capture (σ_{10}) by C^+ in Collision with H_2 (•) with Values Published by Phaneuf et al. (1987)

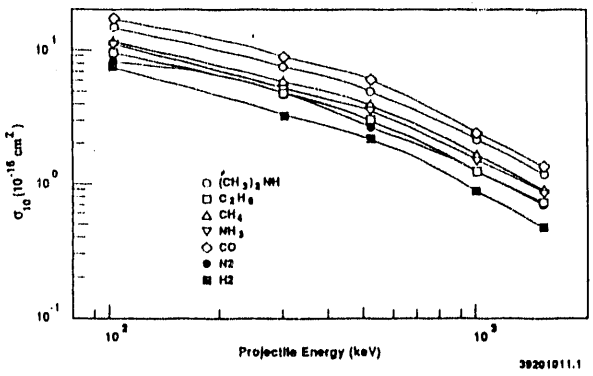

FIGURE 2. Measured Single Electron Capture Cross Sections (σ_{10}) for Interactions of C^+ with Several Molecular Targets

References

Barnett, C. F., H. T. Hunter, N. I. Kirkpatrick, I. Alvarez, C. Cisneros, and R. A. Phaneuf. 1990. *ORNL-6086 Vol. 1.* Oak Ridge National Laboratory, Oak Ridge, Tennessee.

Phaneuf, R. A., R. K. Janev, and M. S. Pindzola. 1987. *ORNL-6090 Vol. 5.* Oak Ridge National Laboratory, Oak Ridge, Tennesse.

Differential Cross Sections for Electron Emission in Carbon Ion-Helium Collisions

R. D. DuBois and R. Herrmann[a]

Fission neutrons interacting with biological tissue produce carbon, nitrogen, and oxygen recoil ions having energies from tens to hundreds of keV. Information about interactions involving these ions is important for microdosimetric descriptions of the energy deposition that results from neutron exposures. In contrast to interactions involving fast, fully stripped ion impact, ionization resulting from slower, partially stripped ions is poorly understood. This is because 1) the bound projectile electrons partially screen the incoming nuclear charge, 2) loosely bound projectile electrons can also be liberated during the collision, and 3) these recoil ions have lower velocities where electron capture processes can be important.

(a) Institute of Nuclear Physics, University of Frankfurt, Frankfurt, Germany.

To characterize collisions involving slow, partially stripped ion impact, we investigated electron emission produced in 100 and 150 keV/amu carbon projectile-helium target collisions. Helium was chosen as a target to emphasize projectile ionization effects and also because single electron removal dominates the target ionization spectra. The collision velocity was selected to provide data in an energy regime where the Born approximation can no longer be expected to provide reliable information. It is, however, in a region where the Classical Trajectory Monte Carlo (CTMC) technique has been used successfully (Reinhold et al. 1990).

Carbon projectile-helium target collisions were studied systematically as a function of the charge state of the incoming projectile. For the collision velocities studied thus far, a C^+ beam was passed through a gas stripper cell, and the transmitted beam components were electrostatically analyzed for charge state. This provided usable beams ranging from neutral carbon atoms to four-times-ionized ions. In the first stage of the experiment, absolute cross sections were measured for laboratory electron emission angles between 20° and 150° and for electron energies between 1 and 1500 eV.

Examples of the 100-keV/amu data for carbon atom and triply charged carbon are shown in Figures 1 and 2, respectively. The data demonstrate the strong forward peaking of the low energy electron emission that is indicative of these types of collisions. For neutral carbon impact, evidence of an "electron loss peak" centered at 55 eV is seen. This peak results from the ionization of loosely bound projectile electrons. Because the majority of the projectile electrons are emitted with little energy in the moving projectile frame, the peak is centered at the projectile velocity and is strongly forward-directed due to kinematic reasons. For C^{3+} impact no such peak is observed because the remaining projectile electrons are more tightly bound. It should be noted that the data for energies less than 10 eV are subject to larger experimental uncertainties due to background scattering, electron transmission and detection, etc. This is especially important in the backward direction since the signal rates are much smaller than in the forward direction. Thus, it is believed

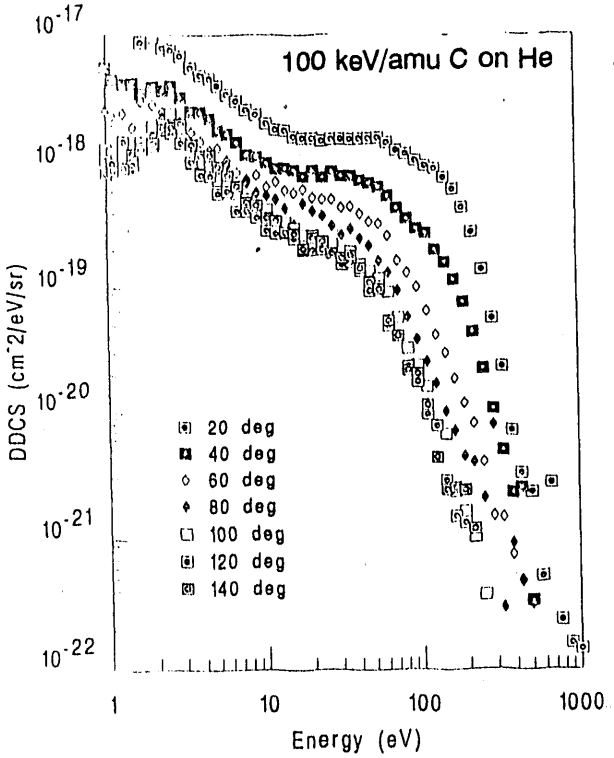

FIGURE 1. Doubly Differential Cross Sections for Electron Emission in 100 keV/amu Carbon Atom-Helium Collisions

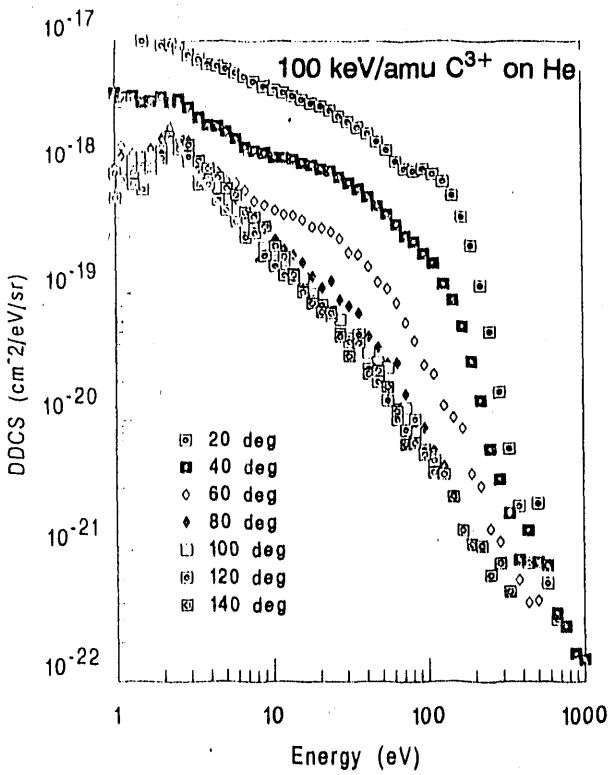

FIGURE 2. Doubly Differential Cross Sections for Electron Emission in 100 keV/amu C^{3+}-Helium Collisions

that the bump in the cross section observed near 2 eV for the larger angles of emission is an experimental anomaly.

One of the purposes of this experiment is to study how the bound projectile electrons screen the incoming nuclear charge and hence affect the target ionization spectra. In a simple picture, one expects that for very distant collisions that primarily result in low energy electron emission, the screening should be complete and the cross sections should scale according to the square of the net projectile charge. For very close collisions, the projectile-target separation can be smaller than the bound electron cloud, and the cross sections should scale according to the projectile nuclear charge, which for the present experiment is fixed. Thus, in the binary encounter region, the cross sections should be the same for all projectile charge states.

In Figure 3, 150-keV/amu 20° electron emission data are compared for different incoming charge states. Screening effects are clearly noticeable in the 10 to 100 eV region where the cross sections increase with incoming projectile charge. However, for electron energies less than 10 eV, the 0 to 3+ cross sections tend toward a common value at 1 eV. As discussed, data at these extremely low energies can be subject to larger *absolute* uncertainties. However, we are confident in the data shown because they were measured under identical conditions in a short time period. Thus, although the absolute magnitude of the cross sections may be subject to large uncertainties, the *relative* change in the cross section for various charge state projectiles is believed to be accurate within 20%. Note that charge states 0 to 3+ all tend toward a common value near 1 eV, whereas the C^{4+} data do not. This could be the result of long-lived metastable components of the +4 beam. Another possibility is that the +4 data might merge at a still lower electron energy. This behavior is not understood, nor is it predicted by any theoretical treatment and thus will require additional studies to verify these preliminary findings.

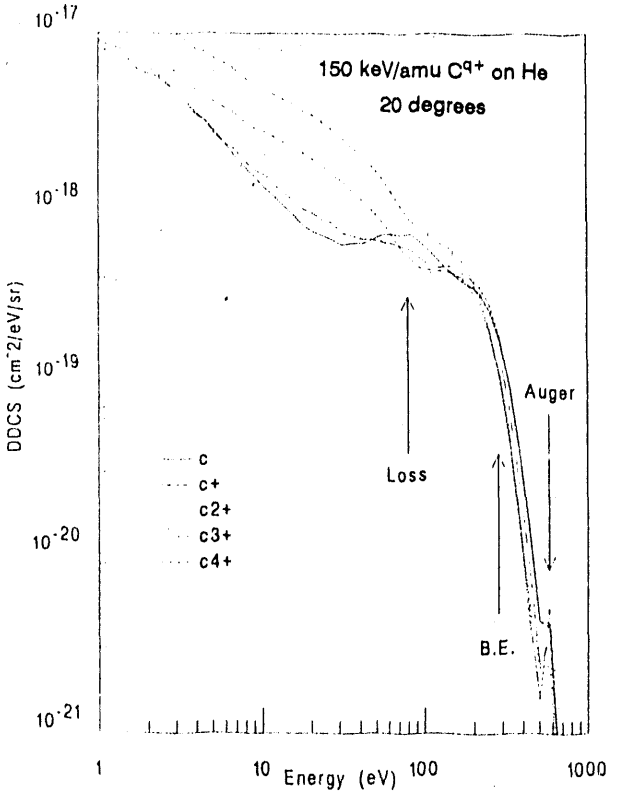

FIGURE 3. Differential Electron Emission for 150 eV/amu C^{q+}-He ($0 \le q \le 4$) Collisions. The laboratory emission angle was 20°. The arrows indicate features attributable to electron loss by the projectile, binary collisions between the projectile nucleus and the bound target electrons, and inner shell ionization of the projectile resulting in Auger relaxation.

In the binary encounter region, the simple picture discussed above predicts that all the cross sections should be the same. But the data exhibit an inverse q scaling effect that has been observed previously (Richard et al. 1990; Jagutzki et al. 1991). In a following section, this behavior will be discussed in more detail.

One last interesting feature of the data shown in Figure 3 is that ionization resulting from carbon-atom impact is quite similar to that produced by singly charged carbon-ion impact. This again demonstrates that a simple screening picture describing distant collisions is inappropriate because such a picture would predict a very small cross section for distant collisions between two atoms.

In a second stage of this experiment, coincidences between the various outgoing charge states of the projectile and the emitted electrons were measured. This was done to separate the electron emission resulting from direct target ionization from that resulting from electron-transferring (capture or loss) collisions. Figures 4 and 5 show typical results for carbon-atom and C^{3+} impact, respectively. For carbon-atom impact, emission resulting from single, double, and triple ionization of the projectile plus any target ionization is shown. For C^{3+} impact, only the single capture and loss channels were investigated. Studying other charge state projectiles at this collision energy showed that direct target ionization always dominates the total electron emission spectra. The importance of the capture channel was found to increase with increasing projectile charge state, whereas that of electron

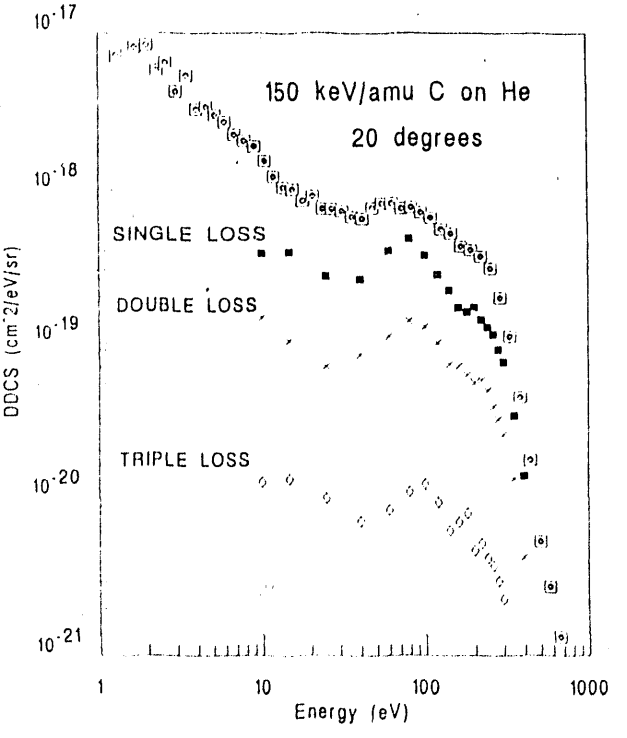

FIGURE 4. Differential Cross Sections for 20° Electron Emission in 150 keV/amu Carbon Atom-Helium Collisions. The upper curve is the electron emission from all processes, whereas the lower three curves are the contributions attributable to single, double, and triple ionization of the projectile *plus* any associated target ionization.

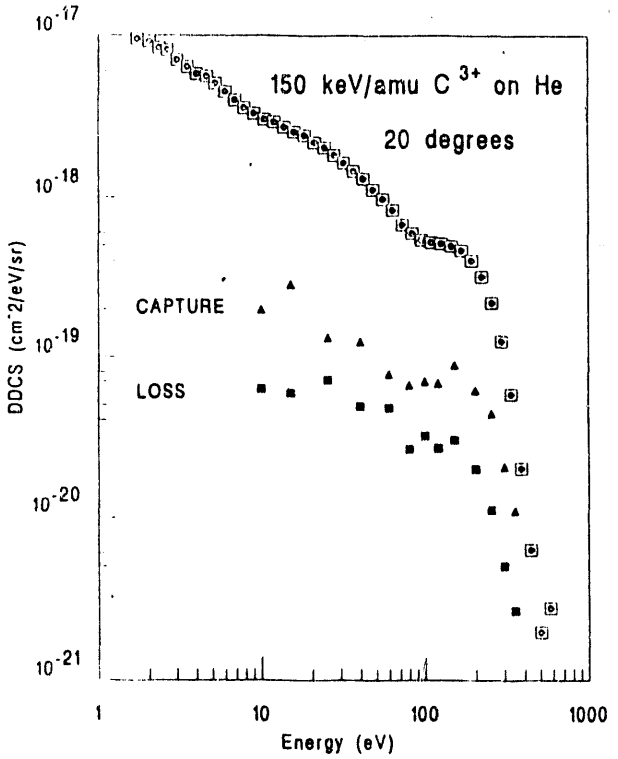

FIGURE 5. Differential Electron Emission for 150 eV/amu C^{q+}-He ($0 \le q \le 4$) Collisions. Same as for Figure 3, except the projectile is now C^{3+} and only the contributions associated with the projectile capturing or losing a single electron are shown.

loss decreased with increasing projectile charge state. Further research is planned to gather data on lower impact energies where electron capture processes become increasingly more important.

References

Jagutzki, O., S. Hagmann, H. Schmidt-Böcking, R. E. Olson, D. R. Schultz, R. Dörner, R. Koch, A. Skutlartz, A. Gonzalez, T. B. Quinteros, C. Kelbch, and P. Richard. 1991. "Abnormal Behavior of Zero Degree δ-electron Emission on the Projectile Ionic Charge." *J. Phys. B.* 24:2579.

Reinhold, C. O., D. R. Schultz, R. E. Olson, L. H. Toburen, and R. D. DuBois. 1990. "Electron Emission from Target and Projective in C^+ + He Collisions." *J. Phys. B* .23:L297-302.

Richard, P., D. H. Lee, T.J.M. Zouros, J. M. Sanders, and J. L. Shinpaugh. 1990. "Anomalous *q* Dependence of 0° Binary Encounter Electron Production in Energetic Collisions of F^q (q=3-9) with He and H_2 Targets." *J. Phys. B.* 23:L213.

Differential Electron Emission for 0.5 MeV/amu Boron, Carbon, Oxygen, and Fluorine Ions on Helium

R. D. DuBois, O. Jagutzki,[a] and L. H. Toburen

Understanding how bound electrons influence the ionization process is important in modeling the energy deposition as heavy ions slow down in various media. For fast, fully stripped ion impact it is well established that the differential cross sections will scale according to z^2, where z is the projectile nuclear charge. This scaling will hold unless z becomes so large that additional effects become important (Schneider et al. 1989; Stolterfoht et al. 1987).

The situation is more complicated for projectiles bringing bound electrons of their own into the collision. These electrons can partially screen the nuclear charge or, if they are loosely bound, can be ionized during the collision. To date, an accurate theoretical treatment of ionization resulting from heavy, partially stripped ion impact does not exist. One of the essential features of such a theory is knowing how the bound electrons screen the projectile nucleus.

In order to provide additional insight into partially stripped ion-atom collisions, we measured the differential electron emission resulting from 0.5 MeV/amu boron, carbon, oxygen, and fluorine impact on a helium target. Neon and argon targets were also studied but only for carbon-ion impact. The incoming charge states studied ranged from 2+ to 5+ for boron and carbon ions and from 3+ to 6+ for oxygen and fluorine ions. The electron emission was measured for 10°, 15°, 30°, 45°, and 60° since our primary interest was to investigate the inverse q scaling that has previously been observed in the binary encounter region (Jagutzki et al. 1991; Richard et al. 1990).

Of interest in this study was the determination of how the differential cross sections scale for

(a) Institute of Nuclear Physics, University of Frankfurt, Frankfurt, Germany.

fixed q (the incoming charge state) when z is varied, how they scale for fixed z when q is varied, and what is the effective projectile charge during the ionization process. For the first case, fixed q, absolute cross sections are required. Therefore data were also accumulated for proton impact under the same experimental conditions as for the heavy ion data. By normalizing the proton data to known cross sections (Rudd et al. 1976), absolute cross sections can then be determined for the heavy ion impact data.

For the second case, fixed z, and for determining the effective projectile charge, only relative cross sections are required. We have determined the effective projectile charge as a function of electron emission angle and energy by comparing the partially stripped projectile data with that measured for fully stripped boron, e.g., $z_{eff} = 5[DDCS_{Pq+}/DDCS_{B5+}]$. Results for q = 3 are shown in Figure 1 for an emission angle of 45°. z_{eff} is shown versus the electron emission velocity that is given in units of the projectile velocity divided by cos(45°). Thus v = 1.4 corresponds to the projectile velocity and is where the projectile ionization contribution is maximum. This angle of emission was chosen in order to minimize any projectile ionization contributions. The binary encounter peak is at v/cos(45°) = 2.

The data demonstrate that the effective projectile charge is slightly smaller than the net ionic charge, q, for electrons emitted with velocities less than the projectile velocity. For harder collisions, the screening of the projectile nuclear charge is less effective and z_{eff} increases. z_{eff} continues to increase and eventually becomes larger than z. Figure 2 shows similar results for q = 5 ions. It also demonstrates that in the binary encounter region z_{eff} is larger for lower charge state ions. This is the inverse q scaling effect alluded to earlier.

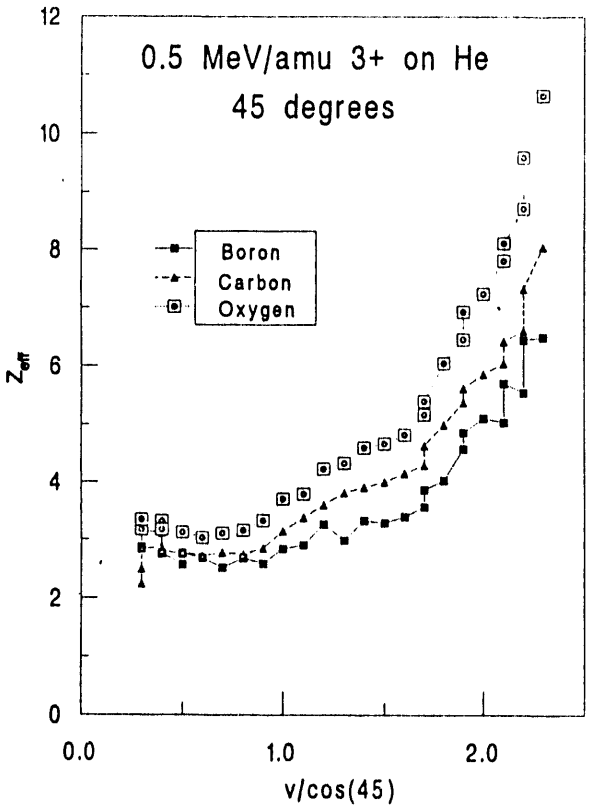

FIGURE 1. Effective Charges are Shown for Triply Ionized Boron, Carbon, and Oxygen Ions Interacting with Helium. The effective charges are shown as a function of the emitted electron velocity given in units of the projectile velocity.

References

Jagutzki, O., S. Hagmann, H. Schmidt-Böcking, R. E. Olson, D. R. Schultz, R. Dörner, R. Koch, A. Skutlartz, A. Gonzalez, T. B. Quinteros, C. Kelbch, and P. Richard. 1991. *J. Phys. B.* (in press).

Richard, P., D. H. Lee, T.J.M. Zouros, J. M. Sanders, and J. L. Shinpaugh. 1990. "Anomalous *q* Dependence of 0° Binary Encounter Electron Production in Energetic Collisions of F^{q+} + (*q*=3-9) with He and H_2 Targets." *J. Phys. B.* 23:L213.

Rudd, M. E., L. H. Toburen, and N. Stolterfoht. 1976. "Differential Cross Sections for Ejection of Electrons from Helium by Protons." *At. Data Nucl. Data Tables* 18:413.

Schneider, D., D. DeWitt, A. S. Schlachter, R. E. Olson, W. G. Graham, J. R. Mowat, R. D. DuBois, D. H. Loyd, V. Montemayor, and G. Schiwietz. 1989. "Strong Continuum-Continuum Couplings in the Direct Ionization of Ar and He Atoms by 6-MeV/uU^{38+} and Th^{38+} Projectiles." *Phys. Rev. A.* 40:2971.

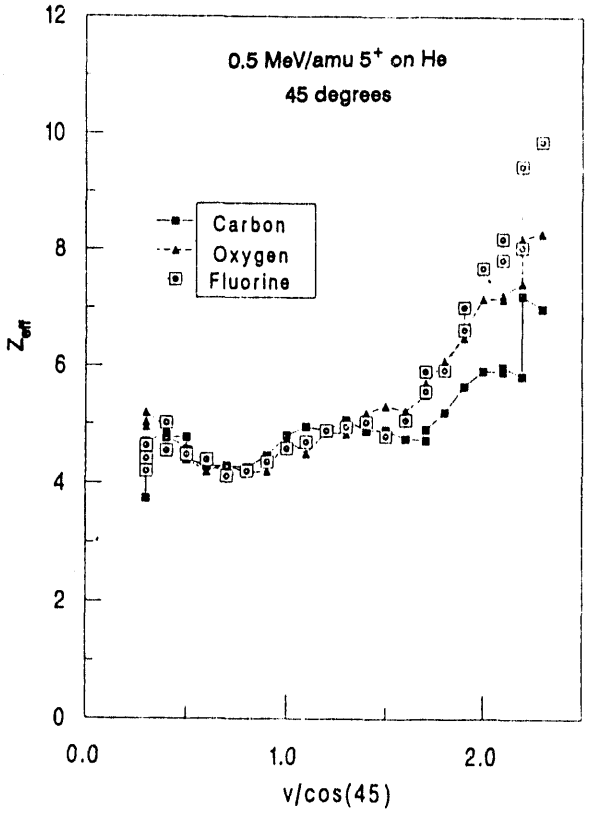

FIGURE 2. Effective Charges are Shown for Five-Times-Ionized Carbon, Oxygen, and Fluorine Ions Interacting with HeliumL The effective charges are shown as a function of the emitted electron velocity given in units of the projectile velocity.

Stolterfoht, N., D. Schneider, J. Tanis, H. Altevogt, A. Salin, P. D. Fainstein, R. Rivarola, J. P. Grandin, J. N. Scheurer, S. Andriamonje, D. Bertault, and J. F. Chemin. 1987. "Evidence for Two-Centre Effects in the Electron Emission from 25-MeV/uMo^{40+} + He Collisions: Theory and Experiment." *Euro. Phys. Lett.* 4:899.

Ionization in Fast Atom-Atom Collisions

R. D. DuBois

Doubly differential cross sections for electron emission occurring for 0.5-MeV/amu hydrogen and helium atom impact were measured in collaboration with Dr. O. Heil from the Institute for Nuclear Physics, University of Frankfurt, Germany. In addition, ionized projectile ion-emitted electron coincidences were measured to separate projectile ionization, target ionization, and simultaneous projectile-target ionization events. These measurements were discussed in detail in last year's annual report. During the past year, some of these data were reported in *Nuclear Physics and Methods* (1990) and a paper has been submitted for publication in *Physical Review A* (1991).

References

Heil, O., R. D. DuBois, R. Maier, M. Kuzel, and K. O. Groeneveld. 1990. "Electron Emission in H^0 Atom Collision: A Coincident Study of Angular Dependence." *Nucl. Inst. and Meth.* B56/7:282-84.

Heil, O., R. D. DuBois, R. Maier, M. Kuzel, and K. O. Groeneveld. 1991. "Ionization in Fast Neutral Particle Atom Collisions: H and He Atom Impacting on He." Submitted to *Phys. Rev. A.*

Measurement of Secondary Electron Spectra from Gases and Thin Foils

C. Drexler,[a] R. D. DuBois, and L. H. Toburen

Very fast computers, using parallel processing, make it possible to conduct detailed model calculations of energy transport in complex heterogeneous target materials. When studying radiation-induced genetic damage, the target of interest is DNA in a cellular environment. Several different Monte Carlo models have been developed to study energy transport. These models are based on either gas phase interaction cross sections or on largely untested theoretical models of condensed phase interactions. The main goal of this project is to obtain experimental secondary electron emission and transport data for interactions of protons with DNA and other condensed phase materials. Such data can stringently test the validity of existing models of electron transport.

During the past year, an ultrahigh vacuum system was instrumented to measure the spectra of electrons emitted from foil targets traversed by fast protons. The spectra were recorded using the Time-of-Flight (TOF) electron energy analysis

(a) Technical University, Munich, Germany.

technique. We chose TOF analysis for these studies because differences in secondary electron production cross sections between gas phase targets and condensed phase targets are expected to be most important in the ejected electron energy range below 100 eV, where TOF techniques are most efficient. Special care was taken to avoid any influence of the low energy electrons by residual magnetic and electric fields. All high voltage and signal cables were electrically shielded from the interaction region; contact potentials were minimized by applying a carbon coating to exposed surfaces; and local magnetic fields were reduced by using nonmagnetic materials. The residual magnetic field was reduced to less than 0.2 mG in the interaction region by use of magnetic shielding and a field-compensating current coil.

A pulsed proton beam was obtained from our 2-MV Van de Graaff accelerator by using a 2-MHz oscillator that supplied a high voltage to vertical and horizontal (90°-phase-shifted) electrostatic beam deflection plates. This electrostatic beam "chopper" created one proton pulse every 500 ns. Geometric considerations and beam current factors indicated that the proton pulse width was less than 0.5 ns. Electrons ejected from the foil by the pulse of protons traversed a flight path of approximately 8.9 cm and were detected by microchannel plates (MCP). With this system, ejected electron spectra can be measured reliably for electron energies from approximately 0.1 eV to 200 eV in an angular range of 15° to 165°.

Initial measurements of the spectra of ejected electrons were conducted using gas targets to test the performance of the system by comparing results to the extensive literature of gas phase cross sections. Preliminary results for ionization of xenon by 1-MeV protons are shown in Figure 1. This TOF spectra, plotted against the logarithm of the ejected electron energy, clearly shows the NOO-Auger electron spectra resulting from de-excitation of inner shell vacancies produced in proton-xenon collisions. The observed energies of these lines are in excellent agreement with published values. In addition, there is structure in the spectrum in the 0.5 to 1 eV region resulting

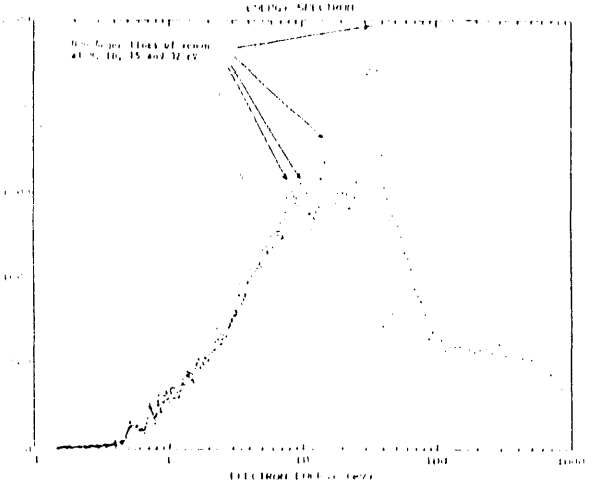

FIGURE 1. Energy Spectra for 1-MeV Protons on Xenon Measured for Electron Ejection at 150°. Auger electron energies from K. Siegbahn (p. 163 1969).

from decay of autoionizing states of xenon. These autoionization lines agree well with the published transition energies verifying the accuracy of our energy analysis to electron energies as low as 0.5 eV. This TOF spectrum is converted to an energy spectrum and replotted in Figure 2. After conversion to the energy spectra, the Auger transitions are much less dramatic and we see the more commonly recognized spatial

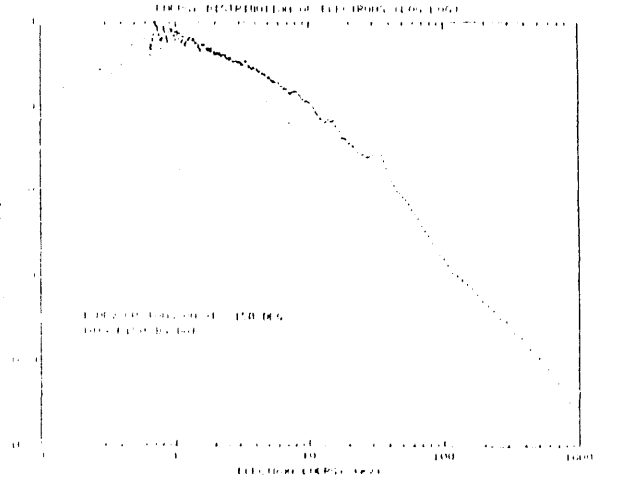

FIGURE 2. Energy Distribution for 1-MeV Protons on Xenon Derived from the Energy Spectrum Shown in Figure 1

shape representing electrons ejected from atomic targets by charged particle impact. Preliminary data for electrons emitted from a foil target are shown in Figure 3. The primary difference in the foil spectrum relative to the gas spectrum is the rapid decrease in the yield of low energy electrons as the ejected electron energy decreases below about 1.5 eV. Studies are underway to explore differences in the spectra for gases and foils as a function of electron energy and emission angle, target thickness, and target composition.

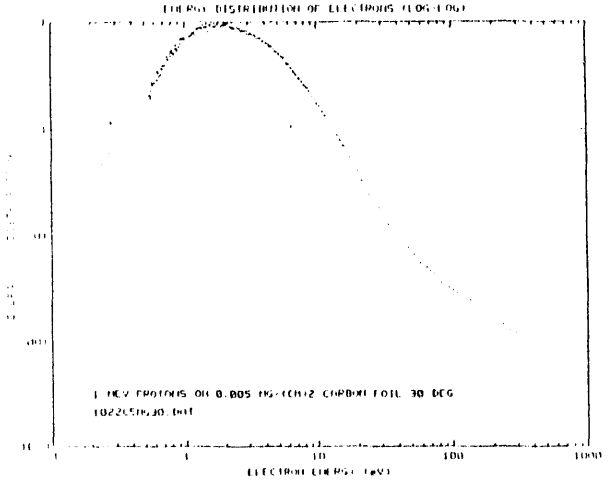

FIGURE 3. Energy Distribution for 1-MeV Protons on 5 $\mu g/cm^2$-Carbon Foil for Secondary Electrons Emitted at 30°

Reference

Siegbahn, K. 1969. ESCA Applied to Free Energy Molecules. North-Holland Publishing Company-Amsterdam.

Radiation Dosimetry

The primary goal of the Radiation Dosimetry program is to understand the connections between the physical events produced by the interaction of ionizing radiation with matter and the biological consequences of those events. These consequences result from complex sequences of events involving a variety of initial radiochemical products as well as the products of later chemical reactions and biological responses. However, differences in responses occur when only the type of charged particle that deposits the energy is changed. This indicates that the spatial and temporal relationships of those initial products profoundly influence the subsequent processes.

Dosimetry research attempts to provide realistic models of the physical processes and to combine them with information on likely chemical and biological processes to produce models for response at the cellular level. The models are designed to be testable by experiment at each level of the system. Models of energy deposition along individual charged particle tracks have been used to calculate energy deposition in small volumes. Volumes a few nanometers in diameter, as well as those a few micrometers in diameter, appear to be directly relevant to the biological damage, while energy deposition in the larger volumes can be measured experimentally and used to test the validity of the calculations. The impact of the difference in energy deposition patterns in solids as compared to vapors is being investigated by calculating the spectrum of electrons ejected by collisions of ions with thin foils, a configuration which can also be measured experimentally.

In order to determine characteristics of the energy deposition patterns of different radiations that are relevant to the biological response, it is necessary to develop and test representative models that depend on those characteristics. Both phenomenological and mechanistic models can be used to discriminate between types of mechanisms and different dependences on initial damage patterns. As models are developed, data from the literature or from specific experiments conducted in the Radiation Biophysics program are used to determine if the model is applicable to a specific biological system. As inappropriate models are rejected, those that remain converge to form an acceptable description of the relevant damage and biological processes.

Modeling Cell Lethality and Mutation as Consequences of the Same Type of Damage

L. A. Braby and T. L. Morgan[a]

Last year we began the process of exploring models of cell response which assume that reproductive death, mutation, and transformation are different manifestations of the same type of biochemical damage (Braby 1991). Because mutation obviously involves DNA damage, and because there is a great deal of evidence suggesting that lethality also results from DNA damage, the simplest model would assume that both endpoints come from the same type of damage. This assumption has not generally been used in modeling because the relative biological effectiveness for a specific radiation is higher for cell mutation than it is for cell survival. This has led people to consider models that assume that different types of DNA damage are responsible for mutation and for lethality. However, most radiation-induced mutations involve deleting a significant segment of DNA. If too large a segment is deleted, the mutation will not be detectable because the deletion will be lethal. These observations show that a single type of damage, DNA deletion, can be responsible for both mutation and lethality. Because DNA deletion will have to be included as a mechanism for both mutation and lethality in any complete model of cellular effects, it is important to explore the possibility that this type of damage is the dominant source (possibly even the only source) of these effects.

(a) Present address, Department of Radiation Oncology, Kaiser Permanente Regional Medical Center, 4950 Sunset Boulevard, Los Angeles, CA 90027.

The presence of well-defined split-dose repair and delayed-plating repair for cell survival following low-linear-energy transfer (LET) exposure, and the absence of these effects for high-LET exposures, initially led people to believe that the damage produced by high-LET irradiation was not repairable. However, measurements (Ngo et al. 1981) of the interaction of damage produced by high- and low-LET radiations show that the damage produced by high-LET exposures is repairable. As a result, a concept of variable damage severity is being developed. In general terms, it is assumed that the more energy deposited in a limited volume, the more chemical alterations will occur, and the less likely that a repair system will be able to eliminate the damage.

We have concentrated on developing a comprehensive understanding of the response of Chinese hamster ovary (CHO) cells, to radiation as a function of as many different exposure characteristics as possible. Our studies have shown that 1) two repair processes with different repair rates are active in CHO cells, 2) the radiation damage is potentially lethal, and 3) the LPL model (Curtis 1986) describes the response of each type of damage as a function of dose and dose rate. Our studies of DNA deletion lengths in HPRT mutant lines of CHO cells (Morgan et al. 1991) have shown that there is very little, if any, difference in deletion lengths for high- and low-LET-induced mutations or for mutations produced by low-LET with or without extensive opportunity for repair. This suggests that the initial type of damage or its severity does not determine the length of the deletion. However, it may be the length of the deletion that determines whether it will be detected as a mutation.

One possible model for the production of lethal and mutagenic damage from the same initial damage begins with the production of very large deletions by unrepaired, or misrepaired, potentially lethal damage. Repair of this damage would reduce the size of the deletion and possibly eliminate it. But repair would sometimes result in a deletion of the length that is characteristic of observed mutations; that is, repair may occur with poor fidelity. In this model, as in other applications of the LPL model, it is assumed that the cells have some opportunity to repair damage even when they are actively growing and the dose is delivered at a high rate. As a result, much of the initial damage is repaired and most mutations are the result of repair with poor fidelity.

In the plateau-phase CHO cells, we observed two repair rates that seem to be related to different types of initial damage, and that may relate to the two types of damage, of different severity, that Goodhead (1987) has suggested as the origin of the increase in Relative Biological Effectiveness (RBE) with LET. His data for the frequency of energy-deposition events greater than 100 eV in a 2-nm-diameter cylinder 2-nm long, and for events greater than 350 eV in a 10-nm-diameter cylinder 5-nm long (Figure 1) show that the larger events in the larger site increase more rapidly with LET than do the smaller events. If both types of damage are repaired, but damage produced predominantly by high-LET radiation is more likely to be repaired with poor fidelity, then the RBE for mutation will be higher than the RBE for lethality. This model requires that the majority of the damage produced by high-LET radiation be repaired; it also requires that the amount repaired not depend on dose rate or delayed plating. This would be the case if the time for damage to be fixed is long as compared to the repair time for this type of damage, and if the probability of binary misrepair is small.

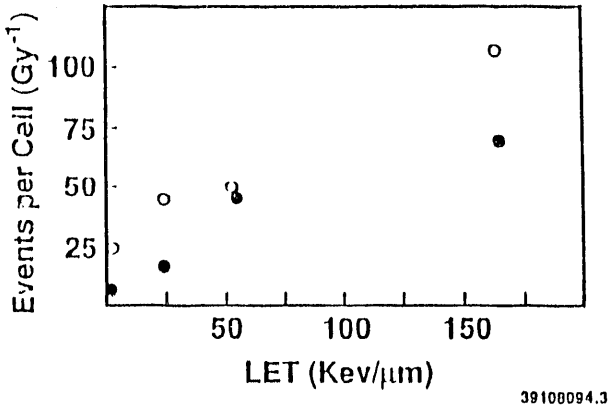

FIGURE 1. The Number of Events ○ Greater Than 100 eV in a 2-nm-Diameter Cylinder 2-nm Long and • Greater Than 350 eV in a 10-nm-Diameter Cylinder 5-nm Long per Cell per Gray as a Function of LET

This model seems to be consistent with the major features of the response of CHO cells, but many details remain to be explored. One of the major unknowns concerns the distribution of energy deposition within those events that are characteristic of high-LET radiation. These events may each contain one of the 100 eV in 2 x 2-nm events that are also produced by low-LET radiations. This possibility, which will be investigated by Monte Carlo calculations, may change the interpretation of the two types of damage.

References

Braby, L. A. 1991. "Modeling Survival and Mutation." In *Physical Sciences, Part 4 of Pacific Northwest Laboratory Annual Report for 1990 to the DOE Office of Energy Research*, PNL-7600, pp. 43-46. Pacific Northwest Laboratory, Richland, Washington.

Ngo, F.Q.H., E. A. Blakely, and C. A. Tobias. 1981. "Sequential Exposures of Mammalian Cells to Low- and High-LET Radiations 1. Lethal Effects Following X-ray and Neon-Ion Irradiation." *Radiation Research*, 87:59-78.

Goodhead, D. T. 1987. "Relationship of Microdosimetric Techniques to Applications in Biological Systems," in *The Dosimetry of Ionizing Radiation Vol II*. ed. by K. R. Kase, B. E. Bjarngard, and F. H. Attix, Academic Press

Morgan, T. L., E. W. Fleck, J. Thacker, and J. H. Miller. 1991. "Genetic Consequences of Radiation Damage to Mammalian Cells." In *Physical Sciences, Part 4 of Pacific Northwest Laboratory Annual Report for 1990 to the DOE Office of Energy Research*. PNL-7600, pp. 53-55. Pacific Northwest Laboratory, Richland, Washington.

Optimum Inactivation Dose and Indices of Radiation Response Based on the Linear-Quadratic Survival Equation

B. S. Jacobson[(a)]

The rationale for hyperfractionation and traditional dose fractionation in radiotherapy is either based on the hypothesis of different growth and repair kinetics between normal and tumor cells or based on the hypothesis of different survival curve shapes.

Following a single irradiation, the ratio between the fraction of cells killed to the radiation dose administered is a continuously decreasing function of dose unless the survival curve is sufficiently shouldered, in which case it has a maximum value at a finite dose. When choosing a radiation-dose fractionation regime, it would seem desirable to maximize that ratio for the target cells while maintaining a low corresponding ratio for adjacent cells. This is possible if the shapes of the dose-survival curves of the two populations are different.

Insofar as it fits the experimental data, the linear-quadratic survival equation, $S = \exp(-\alpha D - \beta D^2)$ has consequences that are independent of the interpretation of α and β. The degree of "shoulderedness" is frequently measured by the ratio β/α or α/β (for example, Thames 1985; Deschavanne and Malaise 1989; Barendsen 1990). The values of these ratios depend on the units chosen to measure dose. Curves with the same shape, but showing different radiosensitivity will yield different values of α/β. However, the ratios $\alpha/\sqrt{\beta}$ (Bettega et al. 1991) or $\sqrt{\beta}/(\alpha + \sqrt{\beta})$ used here will not change under these conditions; they are also independent of the choice of units and correlate with an overall radiosensitivity index, $\alpha + \sqrt{\beta}$, which has dimensions of $(\text{dose})^{-1}$. It will be shown that the reciprocal of this parameter is approximately equal to the dose needed to reduce the surviving fraction to 1/e and conversely that survival after receiving a dose of $1/(\alpha + \sqrt{\beta})$ lies between exp(-1) and exp(-3/4). The quantity, $1/(\alpha + \sqrt{\beta})$, is also approximately equal to the mean inactivation dose.

The linear-quadratic equation for survival can be written in the form

$$(1) \qquad -\ln S = L = (1-r)Ds + r^2D^2s^2$$

where $s = \alpha + \sqrt{\beta}$ (the sensitivity index) and $r = \sqrt{\beta}/(\alpha + \sqrt{\beta}) = \sqrt{\beta}/s$ (the shape index). For simplicity, let us choose a unit of dose so that $s = \alpha + \sqrt{\beta} = 1$. Then, $L = 1$ for $D = 1$ if r is at either of its limits, 0 or 1. Thus, survival is equal to 1/e, or 0.368 after receiving a dose $D = 1/s$ if

(a) Visiting professor, Central Michigan University, Mt. Pleasant, Michigan.

either $\alpha = 0$ or $\beta = 0$. Otherwise, survival is somewhat greater. At this dose, equation (1) reduces to

$$L = 1 - r + r^2 \quad (2)$$

which has a minimum (i. e., survival has a maximum) at $r = 1/2$, where $L = 3/4$, $S = 0.472$, and $\alpha = \sqrt{\beta}$. Using this dose unit, the mean inactivation dose varies between 0.88 and 1.14.

If, on the other hand, survival is held constant at 1/e or $L = 1$, then, for $s = 1$, equation (1) reduces to

$$r^2 D_{37}^2 + (1-r)D_{37} = 1 \quad (3)$$

which defines D_{37} as a function of r. Setting $dD_{37}/dr = 0$, D_{37} is found to have a maximum of 5/4 (in units of s) occurring when $r = 2/5$. The minimum value of $D_{37} = 1$ occurs at $r = 0$ and $r = 1$. In other words, the dose needed to reduce the surviving fraction to 1/e lies between 1/s and 1.25/s.

In Figure 1, a family of dose-survival curves is plotted as a function of dose in units of s, which cross the $S = 1/e$ line between $D = 1$ and $D = 1.25$. As can been seen here, 1/e survival changes little throughout the normal range of shape index, r.

In Figure 2, the ratio of fraction killed to normalized dose, i.e., (1-S)/Ds, is plotted. For a shape index, $r = \sqrt{\beta}/(\alpha+\sqrt{\beta})$, greater than 0.4, this ratio, which is tabulated in Table 1, has a maximum or optimum value. The maximum or optimum shown in Figure 2 is also plotted in Figure 3 and tabulated in Table 2.

Implications for Therapeutic Dose Fractionation

Figure 3 compares the mean inactivation dose and the 37-percent survival dose, in units of s; it also shows the optimum or maximum value of the ratio of fraction-inactivated to normalized dose. If $r > 0.5$, in the case of various malignant and non-malignant cells, the optimum dose approximates the traditional radiotherapeutic fraction of 2 Gy. For smaller values of r, the inactivation-dose ratio is greatest for doses approaching zero. For cells with this characteristic, very small fractions might be more efficient. Table 2 shows optimum doses,

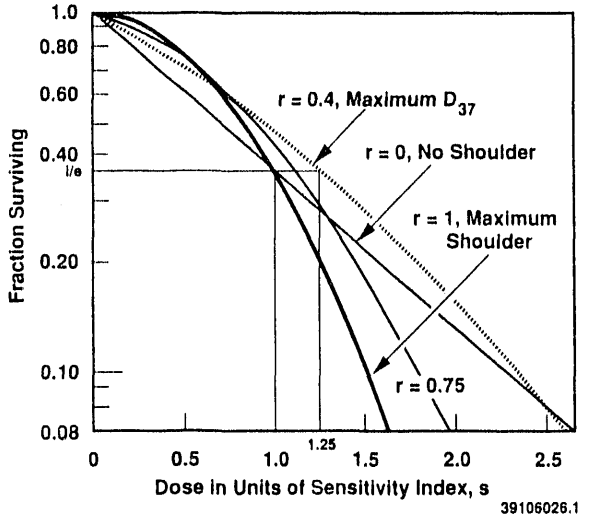

FIGURE 1. Linear-Quadratic Dose-Survival Cureves Having Different Shape Indices, Plotted Against Dose in Units of Sensitivity Index, s. When dose is expressed in these units, the dose for 1/e survival falls between 1.0 and 1.25 sensitivity-index units.

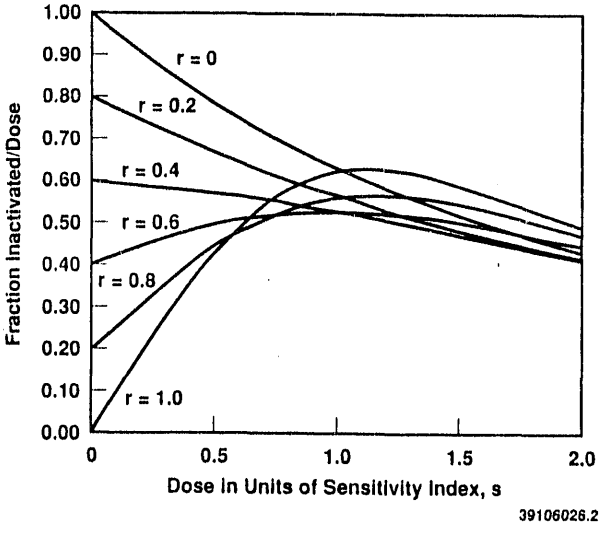

FIGURE 2. Ratio of the Fraction Killed to the Relative Dose for Several Values of Shape Index, r, Plotted Against Dose in Units of Sensitivity Index, s

TABLE 1. Optimum Values for Shape Index, r

Shape Index, r	Optimum dose in "s" Units
0.41	0.000
0.415	0.008
0.42	0.060
0.43	0.160
0.44	0.243
0.45	0.323
0.46	0.396
0.47	0.463
0.48	0.524
0.49	0.581
0.50	0.632
0.525	0.744
0.55	0.833
0.575	0.906
0.60	0.964
0.625	1.010
0.65	1.048
0.675	1.077
0.70	1.099
0.75	1.129
0.80	1.144
0.85	1.147
0.90	1.143
0.95	1.133
1.00	1.121

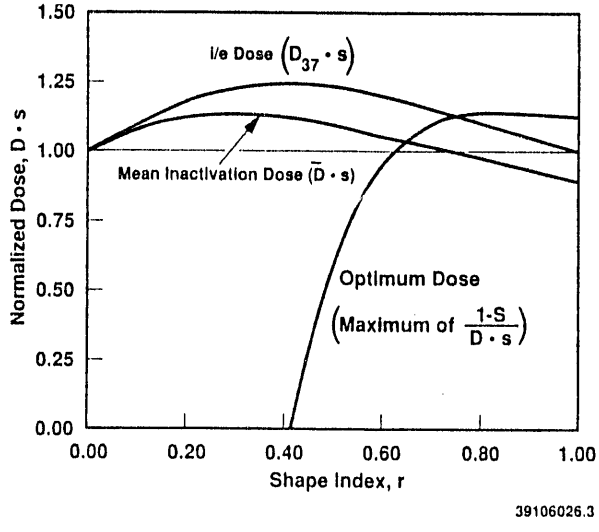

FIGURE 3. Normalized Optimum Dose, Mean Inactivation Dose, and 1/e Dose, Plotted as a Function of Shape Index, r

with respect to that ratio, based on various published values of α and β. Most of these cell lines fall in the second category.

Summary

For any linear-quadratic dose-survival curve, the fraction surviving a dose of $1/(\alpha + \sqrt{\beta})$ falls between exp(-1) and exp(-3/4). That dose is approximately equal to the mean inactivation dose. The dose corresponding to a surviving fraction equal to 1/e falls between $1/(\alpha + \sqrt{\beta})$ and $5/4(\alpha + \sqrt{\beta})$ for all non-negative values of α and β. The sum, $\alpha + \sqrt{\beta}$, easily obtainable from a least squares fit of the data, is proposed as a radiosensitivity index and its reciprocal as a convenient alternative to mean inactivation dose. The dimensionless ratio $\sqrt{\beta}/(\alpha + \sqrt{\beta})$ is proposed as a simple index of the shape of the survival curve. Any linear quadratic dose-survival curve of the form $S = \exp(-\alpha D + \beta D^2)$ can be completely described by these two parameters.

Using these parameters, the ratio of the fraction of cells inactivated to the dose can be determined as a unit-independent quantity. For values of $\sqrt{\beta}/(\alpha+\sqrt{\beta})$ greater than 0.55, this ratio has a maximum when the dose is approximately 1/s. However, for values of $\sqrt{\beta}/(\alpha+\sqrt{\beta})$ less than 0.4, this ratio is greatest when the dose is zero.

References

Barendsen, G. W. 1990. "Mechanisms of Cell Reproductive Death and Shapes of Radiation Dose-Survival Curves of Mammalian Cells." *Int. J. Radiat. Biol.* 57:885-896.

Bettega, D., P. Calzolari, A. Ottolenghi, and L. T. Lombardi. 1991. "Criteria and Techniques for Analyzing Cell Survival Data." *Radiat. Environ. Biophys.* 30:53-70.

Deacon, J., M. J. Peckham, and G. G. Steel. 1984. "The Responsiveness of Human Tumours and the Initial Slope of the Cell Survival Curve." *Radiotherapy and Oncol.* 2:317-323.

Deschavanne, P. J., and E. P. Malaise. 1989. "The Relevance of Alpha/Beta Ratios Determined in Vitro for Human Cell Lines to the Understanding of In Vivo Values." *Int. J. Radiat. Biol.* 53:539-542.

TABLE 2. Optimum Doses Calculated From Published Data for Various Cell Lines

Cell Type	Alpha	Beta	Shape(r) Index	Unit Dose(Gy)	Optimum Dose(Gy)
Grp. A (Deacon, 6 cell lines)	0.779	0.0129	0.127	1.12	0.0
SW403 (Leith)	0.347	0.0100	0.224	2.24	0.0
SW48 (Leith)	0.658	0.0531	0.259	1.13	0.0
Head & neck mean[b]	0.372	0.0250	0.298	1.89	0.0
SW1116 (Leith)	0.337	0.0261	0.324	2.01	0.0
Ovarian ca mean[b]	0.352	0.0300	0.330	1.90	0.0
Sarcoma mean[b]	0.438	0.0660	0.370	1.44	0.0
HT-29 (Leith)	0.246	0.0291	0.409	2.40	0.0
Grp. E (Deacon,25 cell lines)	0.250	0.0433	0.454	2.18	0.77
SW948 (Leith)	0.261	0.0502	0.462	2.06	0.84
LS174T (Leith)	0.277	0.0568	0.462	1.94	0.79
Mouse lung (Travis)[a]	0.310	0.0720	0.464	1.73	0.73
HCT-8 (Leith)	0.289	0.0726	0.482	1.79	0.90
HCT-15 (Leith)	0.266	0.0820	0.518	1.81	1.29
WIDR (Leith)	0.176	0.0421	0.538	2.62	2.07
STSAR-21[c]	0.259	0.0990	0.548	1.74	1.44
SW480 (Leith)	0.185	0.0644	0.578	2.28	2.08
D (Leith)	0.206	0.0810	0.580	2.04	1.87
CaCO-2 (Leith)	0.140	0.0381	0.582	2.98	2.75
COLO320HSR (Leith)	0.227	0.1220	0.606	1.74	1.70
Skin(AT) (Turesson)[a]	0.100	0.0240	0.608	3.92	3.84
HN-SCC-68[c]	0.117	0.0410	0.634	3.13	3.20
SW620 (Leith)	0.172	0.0927	0.639	2.10	2.17
Rat spinal cord (Ang)[a]	0.066	0.0190	0.676	4.91	5.29
STSAR-35[c]	0.141	0.1210	0.712	2.05	2.27
HN-SCC-29[c]	0.068	0.0340	0.731	3.96	4.43
LoVo (Leith)	0.106	0.0844	0.733	2.52	2.82
A (Leith)	0.053	0.0961	0.854	2.76	3.17

(a) Cited in Hall (1991)
(b) Welchselbaum et al. (1989), 14 to 24 cell lines per group.
(c) Welchselbaum et al. (1989), individual cell lines.

Hall, E. J. 1991. "The Dose Rate Factor in Radiation Biology." (Weiss Lecture)., *Int. J. Radiat.* 59:595-610.

Leith, J. T., L. A. Faulkner, G. Papa, P. Quinn, and S. Michelson. "In Vitro Radiation Survival Parameters of Human Colon Tumor Cells." *Int. J. Radiat. Oncol. Biol. Phys.* 20:203-206.

Thames, H. D. 1985. "An 'Incomplete-Repair' Model for Survival After Fractionated and Continuous Irradiations." *Int. J. Radiat. Biol.* 47:319-339.

Welchselbaum, R., J. Rotmensch, S. Ahmed-Swan, and M. A. Beckett. 1989. "Radiobiological Characterization of 53 Human Tumor Cell Lines." *Int. J. Radiat. Biol.* 56:553-560.

Secondary Electron Emission from Foils

W. E. Wilson and J. Song[a]

We have adapted MOCA14 to compute the spectra of low-energy electrons emitted from a thin (simulated water) foil for fast penetrating ions. The intent is to compare the predictions of simulations based on vapor-phase cross sections with experimental measurements of emission from solid foils (Drexler et al. in this report).

A schematic diagram defining the quantities scored is shown in Figure 1. The track structure of fast positive ions is computed for ion paths

(a) Visiting scientist, from The Institute of Biophysics, The Chinese Academy of Sciences, Beijing, China.

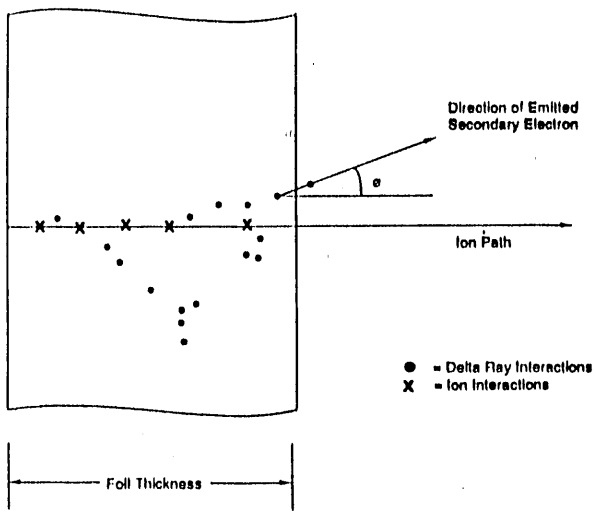

FIGURE 1. Schematic Diagram of the Solid Foil and the Ion-Path Orientation. The number of secondary electrons emitted as a function of their energy and their direction cosine relative to the ion path was scored.

perpendicular to and penetrating through a semi-infinite absorber. The track structure data are then scanned for secondary electrons (delta-rays) that exit the foil, and their energy and Z - direction cosine are scored; the path of the ion defines the Z axis.

Algorithms were developed to score the two quantities in correlation; that is, the computed yield of secondary electrons is doubly differential in solid angle and in energy. Because of the wide dynamic range of the possible electron energies and the very low production of primary high-energy electrons by the positive ions, scoring bins are defined on a piecewise-linear logarithmic (base 2) scale. Each factor of two of the log-arithmic scale is subdivided into four bins of equal width. This manner of defining a scoring template or scale is natural in numerical computations for any variate in the form of a real number in binary representation; the method is also easily imple-mented in most high-level computer languages frequently used in scientific computation. Equal-width bins are used to score the Z - direction cosine; preliminary results were obtained with eleven bins covering 0 to 1 in cosine (90 to 0 degrees).

The last collision experienced by the electron before exiting the foil determines the pertinent direction cosine and may be elastic or inelastic. This feature of the problem means that individual computer runs require more memory and time than most previous track-structure calculations because the elastic collisions must be stored for scoring. Generally, the actual loci of the elastic collisions are unimportant to the microscopic distributions of ionization and energy deposition, provided elastic scattering is included in the simulation to produce realistic (diffusion-like) transport of the secondary electrons. Elastic scattering does contribute to the ultimate spatial distribution of the energy and ionization deposi-tion, but otherwise is not involved in the dosimetry.

The results of a preliminary computation are shown in Figures 2 through 4. This example is for 1-MeV protons passing through a 20-nm-thick semi-infinite slab of simulated water (vapor). The

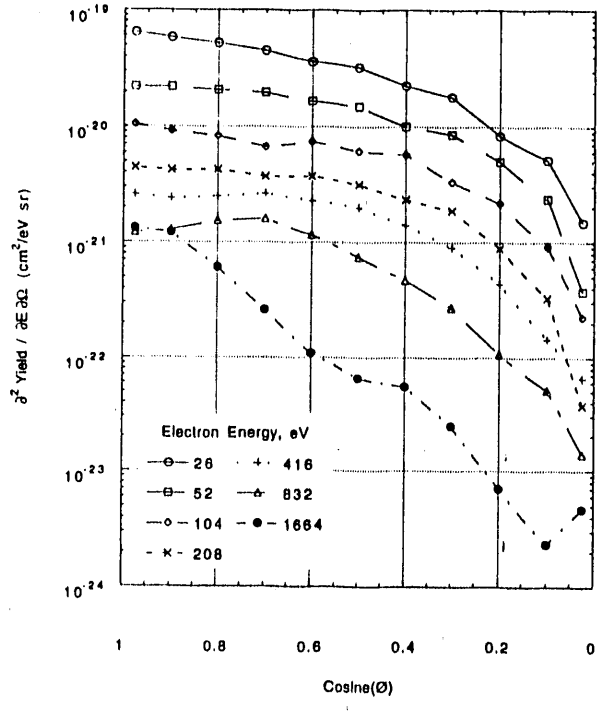

FIGURE 2. Computed Angular Distributions of the Doubly-Differential Yield of Secondary Electrons for Electron Energies of 26 to 1664 eV. The electrons are ejected by a 1-MeV proton passing through a simulated 20-nm-water (vapor) foil.

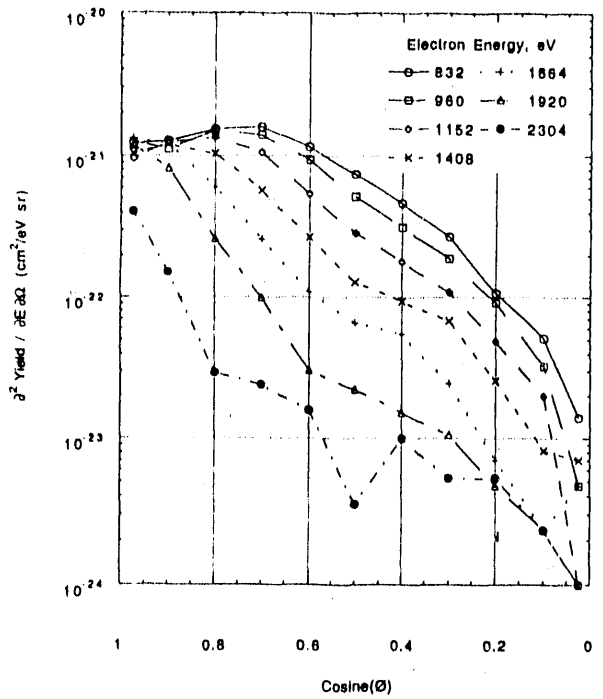

FIGURE 3. Computed Angular Distributions of the Doubly-Differential Yield of Secondary Electrons for Electron Energies of 832 to 2304 eV. The electrons are ejected by a 1-MeV proton passing through a simulated 20-nm-water (vapor) foil.

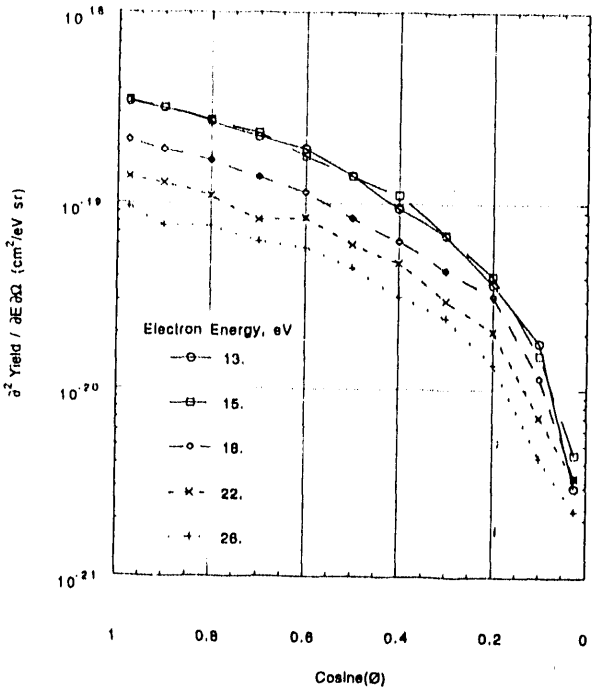

FIGURE 4. Computed Angular Distributions of the Doubly-Differential Yield of Secondary Electrons for Electron Energies of 13 to 26 eV. The electrons are ejected by a 1-MeV proton passing through a simulated 20-nm-water (vapor) foil.

Figures show the angular distribution of the doubly differential yield of secondary electrons for various secondary electron energies. For low-energy secondaries (Figure 2), the angular distributions exhibit no real structure and simply monotonically decrease from zero degrees toward ninety degrees, and likewise decrease monotonically with energy to beyond 416 eV. This behavior is consistent with what one would expect for multiply scattered low-energy electrons. At 832 eV and above (Figures 2 and 3), the peak yield occurs at angles greater than zero degrees, but the peak angle shifts toward zero with increasing energy. This dependence is a reflection of the binary-encounter peak or Bethe-ridge in the doubly-differential cross sections for the production of the primary delta rays. The secondary structure that occurs roughly between a cosine of 0.0 and a cosine of 0.5 (Figure 3) probably arises from once-scattered primary electrons.

For Figures 2 and 3, the sample size was 5×10^5 proton tracks, and the electron cut-off energy, below which secondaries are not followed, was 25 eV. In order to see electron emission down to sub-ionization energy, we reduced the cut-off energy to 12.6 eV (Figure 4). We reduced the corresponding sample size to 2×10^5 because the elastic scattering of the very low-energy electrons increases the computation time by more than a factor of two.

Radiation Biophysics

The Radiation Biophysics project conducts radiobiological studies to test specific aspects of the mathematical models developed in the Radiation Dosimetry and Modeling Cellular Effects programs. These studies, at the cellular, subcellular, and molecular levels, are designed to determine whether specific mathematical expressions, intended to characterize the expected effects of biochemical mechanisms on cellular response, are consistent with the behavior of selected biological systems. Mammalian cells, cultured by special techniques and grown under conditions that minimize biological variability during dose protraction and long-interval split-dose or dose-rate studies, are used to meet the stringent requirements placed on the cellular system by many of these experiments. Carefully characterized cell populations that have ceased progression through the cell cycle provide data on the extent of repair following low doses of radiation and on the changes in the types of damage that can be repaired as the cells reenter the growth cycle and progress toward mitosis.

Other experiments attempt to identify the mechanisms of physical and chemical damage to DNA and to determine the spatial distribution of DNA single-strand breaks. Particular attention is given to investigating the influence of higher-order structure, such as supercoiling of plasmid DNA and scaffold attachment, on the probability of strand scission. It appears that these structures and the resulting molecular strain lead to local sequence-dependent areas of increased susceptibility to chemical and physical attack.

Another significant consequence of radiation damage is mutation and transformation of mammalian cells. Though it is well established that most radiation-induced mutations result from the deletion of a portion of the genome, there are not enough data to characterize the processes leading from the initial DNA damage to the subsequent deletions. Initial damage probably involves only a few base pairs at most, but this rather innocuous lesion leads to deletions of a few hundreds or even thousands of base pairs. Experiments to explore the characteristics of deleted regions are providing information to help evaluate the role of higher-order chromatin structure and the repair of base damage in the production of large deletions. These studies will help to identify physical and biochemical mechanisms responsible for the observed changes and facilitate extrapolation of biological effects from the high doses and dose rates typical in the laboratory to very low environmental levels.

Relationship Between Mutation Type and Growth Rates of CHO Cells Containing X-Ray-Induced *HPRT* Mutations

B. S. Jacobson[a] and T. L. Morgan[b]

The hypoxanthine-guanine phosphoribosyl transferase (HPRT) gene is commonly employed in the study of radiation-induced mutagenesis in various mammalian cell lines (Chu et al. 1969; Cox and Masson 1978). When induced by ionizing radiation, a majority of these mutations are accompanied by detectable DNA deletions or rearrangements at or near the HPRT locus (Thaker 1986; Morgan et al. 1990). This study was designed to test the hypothesis that large deletion-type lesions frequently involve neighboring genes whose loss causes a reduction in growth rate and consequent underrecovery of potential mutant clones when extended expression times are used. This hypothesis implies a broad range of growth rates among our population of mutant clones (Morgan et al. 1990), in which the slowest growing strains are those that have large (i.e., full) deletions.

At the TK (thymidine kinase) locus in murine L5178Y cells, large chromosomal changes are associated with small colony size, i.e., slow

(a) Visiting professor, Central Michigan University, Mt. Pleasant, Michigan.
(b) Present address, Department of Radiation Oncology, Kaiser Permanente Regional Medical Center, 4950 Sunset Boulevard, Los Angeles, CA 90027.

growth, and vice versa (Moore et al. 1987). We have searched for a similar effect at the HPRT locus in CHO cells. The HPRT enzyme system is not required for growth on standard tissue culture media; however, the possible significance of loci closely linked to this one is unknown. We have attempted to correlate the growth rate or generation time with the type and probable size of the induced mutation, as determined by Southern blot analysis of DNA from mutant cell strains.

The cells used in this study were derived from 31 mutant clones isolated previously (Morgan et al. 1990), following x-irradiation, and an unirradiated control clone. They had been classified by Southern blot analysis according to mutation type. Each mutant was classified as *full deletion* if no HPRT coding sequences were detected, *alteration* if only a portion of the gene remained or if band patterns were rearranged, or *no change* if no change in HPRT coding sequences was visible. Seven of the clones had been classified *no change*, 13 *alteration*, and 11 *full deletion*. Two controls, derived from the unirradiated parent cells, were run. Each clone was grown to confluence, then diluted into a uniform set of 60-mm diameter Petri plates, and grown for 7 to 10 days. Two plates were counted daily at 1, 2, 3, and 4 days after plating, and again at 5 to 10 days. Growth was nearly always exponential between days 1 and 4. Growth rates were determined by unweighted least squares log-linear regression using data from 1 to 4 days after plating.

Mean generation times for each class of mutant are shown in Table 1. None of the differences between means of mutant classes is statistically significant by the criterion of Student's *T* test. Mean doubling times for the *no change* mutants and the *full deletion* mutants were essentially identical. The mean for *alteration* mutants was about 7 percent longer, while that for the controls was about 4 percent shorter. Eight of the mutant clones produced generation times slightly, but not significantly, shorter than the non-mutant controls.

There was no evidence of any relationship between deletion type and growth rate. Evidently, the maximum size of an observable DNA deletion is limited by the presence of outlying genes that are indispensable. Within this window of viability, detection of nonlethal mutations depends on the presence of one or more functional but nonessential genes. The information lost in HPRT-containing deletions in this system has a negligible effect on growth under the conditions of this experiment.

References

Chu E. H. Y., P. Brimer, K. B. Jacobson, and E. V. Merriam. 1969. "Mammalian Cell genetics I. Selection and Characterization of Mutations Auxotrophic for L-Glutamine or Resistant to 8-Azaguanine in Chinese Hamster Cells <In Vitro>." *Genetics* 62: 359-377.

Cox R., and W. K. Masson. 1978. "Do Radiation-Induced Thioguanine-Resistant Mutants of Cultured Mammalian Cells Arise by HGPRT Gene Mutation or X-Chromosome Rearrangement?" *Nature* 276: 629-630.

Moore M. M., K. H. Brock, D. M. Demarini, and C. L. Doerr. 1987. "Differential Recovery of Induced Mutants at the *TK* and *HPRT* Loci in Mammalian Cells." In *Banbury Rept. 28: Mammalian Cell Mutagenesis* M. M. Moore, D. M. Demarini, F. J. DeSerres and K. R. Tindall, eds., pp. 93-108. Cold Spring Harbor Laboratory, Cold Spring Harbor.

TABLE 1. Generation Times

Class	Number	Mean doubling time/hrs	Standard Deviation	Range/hrs
No change	7	13.1	0.96	11.9 - 14.2
Alteration	13	14.1	1.6	11.8 - 16.9
Full deletion	11	13.2	1.5	11.6 - 16.7
All mutants	31	13.4	1.4	11.6 - 16.7
Control	2	12.7	---	12.6 - 12.7

Morgan T. L., E. W. Fleck, K. A. Poston, B. A. Denovan, C. N. Newman, B. J. F. Rossiter, and J. H. Miller. 1990 "Molecular Characterization of X-Ray-Induced Mutations at the HPRT Locus in Plateau-Phase Chinese Hamster Ovary Cells." *Mutat. Res.* 232: 171-182.

Thacker J.. 1986. "The Nature of Mutants Induced by Ionizing Radiation in Cultured Hamster Cells. III. Molecular Characterization of HPRT-Deficient Mutants Induced By ∫-rays or `-particles Showing that the Majority have Deletions of All or Part of the *HPRT* Gene. *Mutat. Res.* 160: 267-275.

Implications of Repair Observed at Low Doses

L. A. Braby and J. M. Nelson

At the Workshop on Biophysical Modeling of Radiation Effects, an invited paper based on conclusions drawn from our measurements of repair at low doses was presented as a part of the concluding session. The abstract of this paper, which will be published by Adam Hilger, summarizes the conclusions we have reached from several years' work.

Models for the response of cells exposed to low-LET radiation can be grouped into three general types on the basis of assumptions about the nature of the interaction that is produced in the shoulder of the survival curve. The three forms of interaction are 1) sublethal damage becoming lethal, 2) potentially lethal damage becoming irreparable, and 3) potentially lethal damage saturating a repair system. The effects that these three forms of interaction would have on the results of specific types of experiments are investigated. Comparisons with experimental results indicate that only the second type is significant in determining the response of typical cultured mammalian cells.

Excess Iron and Cellular Radiation Sensitivity

J. M. Nelson and R. G. Stevens

Indirect radiation effects, instigated by radical formation in and around the target DNA, dominate the lethal and mutagenic actions of ionizing radiation in cells. Oxygen and hydroxyl radicals are probably the most abundant and reactive species associated with this effect. Their formation and moderation is affected by the ionic composition of the milieu adjacent to the genome. Transition metals are often associated with this process, and iron and copper are no exception because both catalyze radical formation of these most active forms.

Iron is the most abundant transition metal in mammals, and it plays a central role in metabolism. The deleterious consequences of iron deficiency are well documented. However, the potential risks associated with excess iron have been largely ignored; these risks are considered only when severe iron overload occurs. Iron is readily available, particularly in the Western diet, and there is growing skepticism of the conventional wisdom concerning the importance of iron maintenance. This suggests that the biological consequences of only moderately elevated cellular iron deserve serious attention.

Increased stores of available body iron may increase the risk of radiation-induced cancer by either or both of two possible mechanisms reviewed by Stevens and Kalkwarf (1990). Iron can catalyze the production of oxygen radicals that may deplete available reducing equivalents. This would render the cell more susceptible to the variety of radicals produced by ionizing radiations. Iron bound to DNA may also be particularly effective in increasing the ability of radiation to damage DNA at that particular site. Further, iron may interfere with normal cellular repair processes or even be a limiting nutrient required for the growth and replication of transformed cells. Exposure to ionizing radiation, whether occupationally or from environmental sources, underscores the need to identify tissue characteristics that might influence an individual's risk of radiation injury. Tissue iron level may be one such characteristic.

Iron concentrations vary substantially, both day-to-day for the same individual and between one individual and the next. The iron content in adult human blood is around 420-560 μg/ml; most of this is associated with the heme and is contained in erythrocytes. Serum levels in normal healthy adults contain 0.75-1.75 μg/ml of iron, almost completely found in the ferric form in

transferrin. Tissue iron content shows extreme variations, considerably greater than those found in serum. Normal liver tissue contains 28 to 162 μg/g; kidney, 3.3 to 10.1 μg/g; and spleen, 85 to 169 μg/g. The highest levels are found in lung and brain, where iron concentrations are found to be around 200 μg/g and 222 to 510 μg/g, respectively.

We have cultured stationary-phase Chinese hamster ovary (CHO) cells in a medium containing ferritin (~19% iron by weight) added in concentrations ranging from 0 to 128 μg/ml. One set of cultures was unirradiated, while another set was exposed to 4 Gy of x-rays. Clonogenic cell survival was assessed for each set of cultures. Preliminary experiments have shown that ferritin (~19% iron by weight) is toxic at concentrations above 100 μg/ml, while apoferritin (the iron-free protein) showed no toxicity at concentrations up to and including 1000 μg/ml, indicating that the protein itself does not play a significant role in this toxicity.

Results of the initial experiment are shown in Table 1. In this experiment, ferritin doses ranging from 0 μg/ml (control) to 32 μg/ml were used. The adjusted survival for cells in irradiated (ferritin) control plates (assay plates prepared from ferritin-free cultures) was 51% when normalized to 100% for cells in unirradiated control plates. This indicates that 4 Gy, in the absence of ferritin, killed ~49% of the population (column 2). Assuming that ferritin killing is independent of x-ray killing, the ratio of each set of irradiated plates at a given ferritin concentration to their respective unirradiated plates should then be 0.51; this ratio is given in column 3, and is shown normalized to 1.00 in column 4. Ratios greater than 0.51 would therefore indicate radioprotection, whereas those lower would indicate radiosensitization. At concentrations of 0.5, 2, and 8 μg/ml, these ratios were 0.45, 0.48, and 0.44, respectively, showing virtually no interaction between ferritin and x-rays ($p > 0.05$). However, at 32 μg/ml ferritin, this ratio fell to 0.14 ($p < 0.001$) and the adjusted ratio (column 4) fell to 0.27. This indicates a significant killing enhancement not caused by the chemical toxicity of ferritin, because the relative survival of unirradiated ferritin plates was effectively the same as unirradiated ferritin-free controls (relative survival = 0.95; column 1). Taken together, these results indicate that 32 μg/ml ferritin effectively sensitizes these cells to x-rays; yet by itself, this dose of ferritin is not toxic.

Results of this initial experiment were supported by the results of four additional experiments, all of which are shown in Figure 1. These subsequent experiments confirmed the earlier findings detailed above. In all of these experiments, 32 μg/ml of added ferritin was not toxic (relative survivals of 0.95, 1.16, 0.82, 1.04, and 1.47), whereas it augmented radiation killing (loss of reproductive integrity) so that survival after 4 Gy x-rays was only 27%, 42%, 14%, 25%, and 20% (mean = 25.6%; $p < 0.001$ for each ratio) of that expected if ferritin had no effect. No killing was observed in unirradiated plates at ferritin

TABLE 1. Effect of Ferritin on X-Ray Sensitivity of Stationary-Phase CHO Cells. The column labeled "ferritin" shows the survival of cells exposed to ferritin adjusted to the cloning efficiency of ferritin-free plates; "ferritin + x-ray" shows the adjusted survival of cells exposed to both ferritin and x-rays; "ratio" is the ratio of column 2 to column 1; and "adjusted ratio" is the ratio shown in column 3 normalized to give a 0 μg/ml ratio of 1.00.

	Adjusted Survival			
	Ferritin	Ferritin + x ray	Ratio	Adjusted Ratio
0 μg/ml	1.00	0.51	0.51	1.00
0.5 μg/ml	0.98	0.44	0.45	0.88
2 μg/ml	1.05	0.50	0.48	0.94
8 μg/ml	1.13	0.50	0.44	0.86
32 μg/ml	0.95	0.13	0.14[a]	0.27

(a) Significantly lower than the ratio at 0 μg/ml ($p < 0.001$).

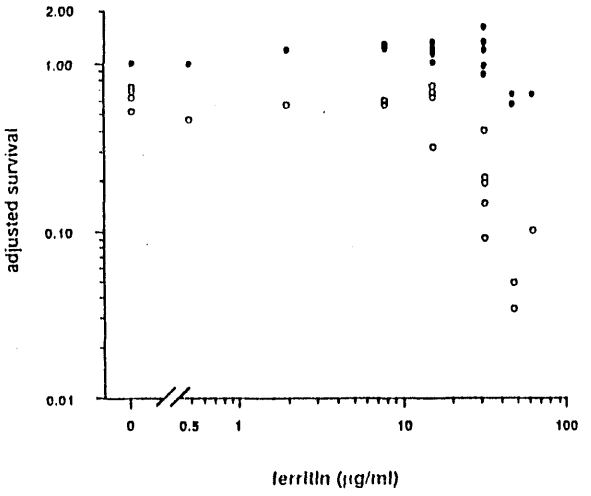

FIGURE 1. Effect of Added Ferritin on Reproductive Survival of Chinese Hamster Ovary Cells. Relative survival, adjusted to that of controls, is shown at several added ferritin concentrations with 4 Gy of x-rays (open circles) and without x-rays (solid circles). Results of five replicate experiments; each data point represents ~36 assay plates.

concentrations up to 32 μg/ml. However, at 64 μg/ml ferritin, survival of unirradiated plates falls to about 60%, and at 128 μg/ml, to about 1.0% of the control value. Although toxic at 64 and 128 μg/ml, ferritin still enhanced radiation cell killing. In addition to being nontoxic, apoferritin had no effect on radiation sensitivity (data not shown).

As shown in Figure 1, relative survival at each ferritin concentration, with and without x-irradiation, appears approximately parallel up to 16 μg/ml. At higher concentrations, x-ray killing is significantly enhanced, indicating radiosensitization by ferritin.

Ferritin is the normal tissue iron storage protein, although it is also present in serum at low concentrations ranging from 15 to 300 μg/ml. Normal serum contains 1 to 2-μg/ml iron, primarily bound to transferrin. The growth medium in which these cells are maintained contains ~10% fetal calf serum, or ~0.1 to 0.2-μg/ml iron. Since the ferritin used in these experiments contained ~19% iron by weight, 32-μg/ml-ferritin represents only ~6-μg/ml iron. Therefore, even though ferritin added at 32 μg/ml increased the iron content of our medium 30 to 60 fold, this represents only 3 to 6 times the normal iron concentration of the milieu surrounding cells in serum and tissue. Yet, this modest elevation in iron added as ferritin was a potent radiosensitizer to our stationary CHO cells.

Reference

Stevens, R. G. and D. Kalkwarf. 1990. "Iron Radiation and Cancer." *Environ. Health Perspec.* 87:291-300.

Base Composition and the Probability of Radiation Strand Scission

J. M. Nelson, J. H. Miller, M. Ye,[a] and E. W. Fleck[b]

Double-strand breakage of the DNA molecule, with the concurrent rearrangement, substitution, or deletion of information, appears to be the principal and most significant radiation-induced lesion associated with cellular radiation effects. Although the initial physical interactions and depositions of energy are entirely random, the subsequent distribution of biologically important lesions, such as strand breaks, appears not to be random. Plasmids are naked circular DNA molecules with defined primary and higher-order structures. Plasmids are particularly useful for studies, such as the investigation of such non-random phenomena, because they are not associated with stabilizing proteins, as is genomic DNA, and the structure and its alteration can be relatively easily identified.

We demonstrated a correlation between negative linking differences and susceptibility of pristine supercoiled plasmid DNA to induction of the first single-strand break by ionizing radiation (Miller et al. 1991). We then sought to determine if this breakage was non-random and most prevalent in the AT-rich regions of the molecule where transient strand separation is most probable.

Theoretical considerations suggest that spontaneous strand separation in duplex DNA will most likely occur within the AT-rich regions of

(a) Present address, Montech Environmental Technology, Inc., P.O. Box 1198, Kerr Laboratory Road, Ada, OK 74820.
(b) Visiting professor, Whitman College, Walla Walla, Washington.

highly stressed molecules. Because transient disruptions of base pairing in plasmid DNA would be associated with the torsional stress of negative supercoiling, we expect that this would increase the probability of their occurrence within the AT-rich sequences. Hence, if open states are involved in the increased sensitivity to radiation-induced strand scission observed in underwound plasmids, then at least part of this increase should be caused by non-random breakage at the AT-rich regions.

Theory also predicts that the probability of denaturation will increase with temperature and decrease with the ionic strength of the buffer in which the molecules are irradiated. We have investigated this hypothesis by assessing non-random break induction in the plBI-30 plasmid. Our findings indicate that preferential breakage does occur at the most probable site, as suggested.

Replicate samples of the plBI-30 plasmid were irradiated with x rays sufficient to produce about one break per molecule. Following irradiation, circular DNA was made linear by cutting it at its unique Pst-I restriction site. The duplex molecule was then denatured, i.e., separated into single strands, by treatment with glyoxal. The single-strand fragments produced by this procedure were then separated electrophoretically using a denaturing gel to prevent their spontaneous recombination into the double-strand form.

If strand scission is non-random and associated with momentary strand separation, then single-strand breaks (SSBs) should occur within one or the other of two AT-rich regions with considerably greater frequency than at other sites throughout the molecule. Methods developed by Benham (1990) have been used to calculate the probability of helix-to-random-coil transitions as a function of sequence location in plBI 30. These calculations, although based on a somewhat higher negative linking difference, predict that melting of the double helix should be most probable near base sequence 2000. Single-strand breaks at these predicted locations should increase the yield of 18K and 12K base fragments.

These fragment lengths were identified in plasmids irradiated within a specific temperature range, in phosphate buffer having very low ionic strength, and at a sufficiently low radiation dose. The low radiation dose was required to avoid the complication of supplemental breaks that could mask the appearance of fragments produced by only the preferentially located breaks.

The optimum dose of x-rays was chosen to produce approximately one SSB in each supercoiled molecule. This dose was determined by observing the change in structure with increasing dose. Negative supercoiling is an element of tertiary structure common in plasmids and to most double-stranded DNA. It is found in both the prokaryotic and eukaryotic genomes. The excess free energy associated with this structural feature is related to gene stability and is believed to influence several biological functions of DNA, including both DNA replication and transcription.

Plasmids can exist in three different forms. The covalently closed circular supercoiled plasmid (Form I) is small, compact, and migrates quickly in an electric field. If a single phosphodiester bond has been broken, the relaxed circular plasmid (Form II) is no longer supercoiled and migrates much more slowly in an electric field. The linear form (Form III) is produced when two closely located phosphodiester bonds are broken; it migrates between the other two forms. Because Form II results from the first separation of *any* single phosphodiester bond, conversion from Form I to Form II can be used to determine the sensitivity of supercoiled DNA to SSB induction. Figure 1 illustrates this progressive conversion from Form I to Form II, and subsequent conversion of Form II to Form III, with increasing doses of low ionizing radiation. From these data we find that nearly all molecules of plBI 30 have acquired at least one SSB after only 10 Gy of x rays.

Several 5 to 10-μl samples of plasmid were irradiated simultaneously in micro-pipette tips at 46°C to 54°C. In each case, the temperature during exposure was held to within 0.1°C. Following exposure, the plasmid was cut at the Pst-I restriction site, denatured with glyoxal, and separated by gel electrophoresis in a 1.0% agarose gel prepared and run in 10 mM (pH 7.2) phosphate buffer.

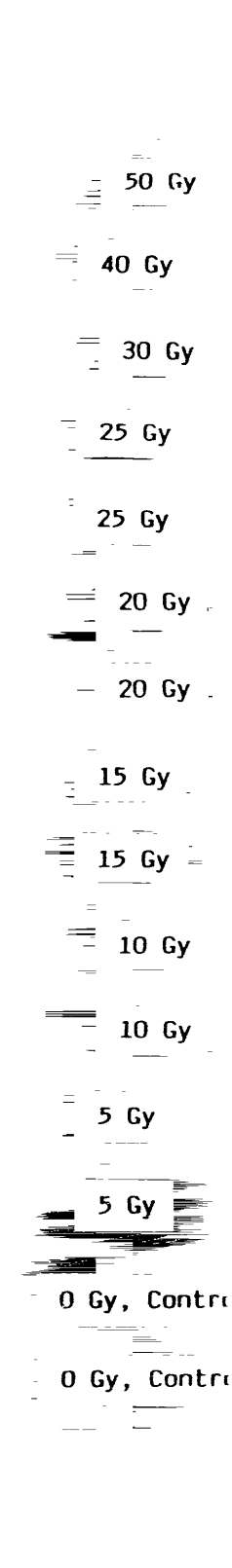
50 Gy
40 Gy
30 Gy
25 Gy
25 Gy
20 Gy
20 Gy
15 Gy
15 Gy
10 Gy
10 Gy
5 Gy
5 Gy
0 Gy, Contr
0 Gy, Contr

Figure 2 is an example of such a gel showing fragments of DNA irradiated with 5 Gy of x rays. Most of the DNA remains as intact single-strand molecules of about 3000 bases (bright bands), but ahead of these brighter spots (slightly below each) is a distinct band of lighter weight material. This band is seen in each lane (at each temperature). Two nearby bands of denatured Hind-III digest of lambda DNA (outer lanes) are 2322 bases (upper) and 2028 bases (lower). This indicates that the band of lighter weight material excised from the irradiated plBI 30 plasmid contains about 1700-1900 bases. In addition, a smear representing variable size fragments of single-strand DNA leads the bright band and surrounds this lighter one, indicating random nicking of the duplex DNA.

Ethidium-bromide fluorescence is very weak in Figure 2 because RNA and single-strand DNA stain only very weakly relative to duplex molecules, and this DNA has been denatured. When intercolated into the DNA helix, ethidium-bromide fluorescence is enhanced many fold.

References

Benham, C. J. 1990. "Theoretical Analysis of Heteropolymeric Transitions in Superhelical DNA Molecules of Specified Sequence." *J. Chem. Physics* 92(10):6294-6305.

Miller, J. H., J. M. Nelson, M. Ye, C. E. Swenberg, J. M. Speicher, and C. J. Benham. 1991. "Negative Supercoiling Increases the Sensitivity of Plasmid DNA to Single-Strand Break Induction by X Rays." *Int. J. Radiat. Biol.* 59(4):941-949.

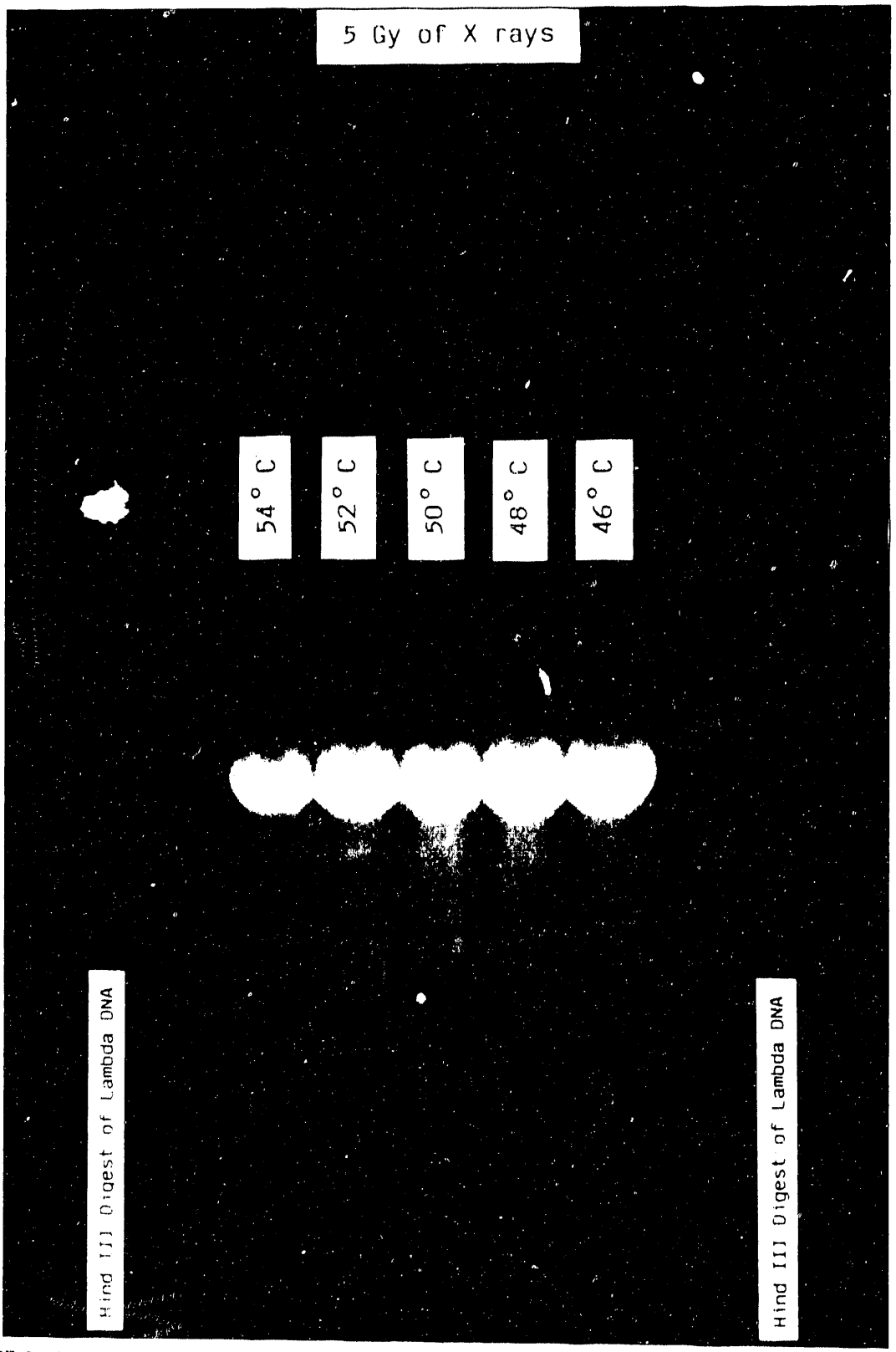

FIGURE 2. Agarose-Gel Electrophoresis of Denatured pIBI 30 Plasmid DNA. Most of the DNA is found as intact single-strand molecules of about 3000 bases (bright bands). A large fragment is found as a light band of lighter-weight material slighly below the bright band. The location of this lighter band, just ahead of the two marker fragments (2322 and 2028 bases) of denatured Hind-III digest of lambda DNA (outer lanes), confirms that this single-strand molecule contains about 1800 bases. The smear representing variable-size fragments leading the bright band, and surrounding the lighter one, indicates that random nicking of the duplex DNA also occurs.

Modeling Cellular Response to Genetic Damage

This project investigates mechanisms of damage to the genetic material of mammalian cells by exposure to energy-related environmental pollutants. Currently, the work is focused on the role of damage to deoxyribonucleic acids (DNA) in cell killing and mutation induction by ionizing radiation. The conformation and chemical environment of DNA in cells is carefully controlled to ensure proper expression of genetic information. These regulatory mechanisms also influence the interaction of DNA sequences with radiation and chemicals. Hence, studies of DNA damage as a basis for understanding cellular response to carcinogenic agents must allow for the wide variety of secondary structures, proteins, and smaller molecules that are associated with DNA in cells. Negative supercoiling is a property of active genes that simulates the strand separation needed for transcription. Results obtained with a plasmid DNA system suggest that negative supercoiling increases the sensitivity of DNA to strand scission by x-rays. We are currently investigating the mechanism for this effect. Results obtained at other laboratories indicated that base stacking and water of hydration facilitate long-range energy and charge migration on DNA chains. We have used proton-beam irradiation of oriented DNA fibers to look for effects of energy or charge migration on the yield of radiation-induced free radicals.

Mechanisms for Enhancing Radiation-Induced Strand Scission by Negative Supercoiling of DNA

J. H. Miller

We have observed that the torsional stress developed in the DNA double helix by negative supercoiling increases the sensitivity of the molecule to induction of strand breaks by ionizing radiation (Miller et al. 1991). Under our irradiation conditions, direct ionization of a supercoiled plasmid is much less likely than attack by OH radicals, which are produced by energy absorbed in the aqueous environment of the molecule. The primary modes of OH-radical attack on DNA are abstraction of hydrogen from the sugar-phosphate backbone and addition to the double bonds in bases moieties. In relaxed DNA sequences, about 20% of the OH radicals attacking a double-stranded molecule abstract hydrogen from sugar and result in strand scission. The remaining 80%, which form a wide variety of addition products with base moieties, are usually not considered to contribute to strand-break induction.

The easiest way to interpret our observations within the existing theory of the indirect mode of DNA damage by ionizing radiation is to assume that the probability of interaction between OH radicals and sugar moieties is increased by negative supercoiling. If this is true, the increase is unlikely to be caused by increased accessibility of sugar moieties to solvent. As part of the backbone, ribose is usually considered to be maximally exposed unless folding of the DNA chain hinders access to solvent. Based on solvent accessibility, the compactness of supercoiled DNA, which is usually given as the explanation of its higher electrophoretic mobility, should decrease OH-radical attack on sugar moieties and consequently reduce the yield of DNA strand breaks.

Ward has shown that in the normal B conformation, the accessible area of OH-reactive sites on sugar moieties is about 10 times greater than it is on the bases (1985). Moreover, 80% of the OH radicals scavenged by DNA add to the double bonds of base moieties. Hence these factors indicate that OH abstraction of hydrogen from sugar is not diffusion controlled. Hence, a decrease in the energy barrier to OH abstraction of hydrogen from sugar (primarily the C4′ position) by negative supercoiling would explain its effect on strand scission. This effect fits the currently accepted framework of oxidative damage to DNA in dilute aqueous solutions by sparsely ionizing radiation.

The following observations suggests that an effect of negative supercoiling on OH-reactivity with sugar moieties is probably not the correct explanation for our data on x-ray induced strand breaks in supercoiled plasmid DNA (Miller et al.

1991). In single crystals of oligonucleotides, Fratini et al. (1982) found that sugar pucker was correlated with helical winding so that C3′-endo is more likely to be found in underwound DNA, and C2′-endo is more likely to be found in overwound DNA. Önal et al. (1988) observed that the efficiency of strand scission by OH radicals was much less in poly(A) than in poly(dA) and attributed this difference to the fact that the most probable sugar puckers in poly(A) and poly(dA) are C3′-endo and C2′-endo, respectively. The torsional stress of negative supercoiling tends to produce underwound DNA (i.e., more base pairs per helical turn than in the relaxed B conformation); thus these observations suggest that the effect of negative supercoiling on sugar pucker should reduce the sensitivity of DNA to strand breaks by OH-radical attack on sugar moieties.

The arguments given above encouraged us to look at secondary radical processes for ways that negative supercoiling could enhance strand scission. In the presence of oxygen, peroxyl base radicals are the most probable result of interaction between OH and DNA bases. Because 80% of the OH radicals scavenged by DNA interact with base moieties, we can expect a high yield of peroxyl base radicals under our irradiation conditions. The lifetime of these base radicals is on the order of seconds, and the kinetics of their decay in polyuridylic acid (poly[U]) parallels the induction of strand breaks in this single-stranded homopolymer (Schulte-Frohlinde et al. 1986). Hence, a possible explanation for our experimental findings is that negative supercoiling increases the decay of peroxyl base radicals to strand breaks.

The lifetime of peroxyl base radicals in poly(U) is three orders of magnitude longer than the lifetime of the peroxyl radical of uracil. Since peroxyl radicals in poly(U) are probably chemically identical to their monomeric form, the long lifetime in the polynucleotide is attributed to limited access to potentially reactive species. The observation that addition of salts decreases the lifetime of peroxyl base radicals in poly(U) suggests that folding of the homopolymer is a rate-limiting step. Folding is required to bring the base-centered radical close enough to a sugar moiety on the chain to allow abstraction of hydrogen from the C4′ position, which leads to strand scission just as is the case with direct OH-radical attack at this position (von Sonntag 1984).

The salt dependence of the decay of peroxyl base radicals in poly(U) is only one of several observations that point to a relationship between DNA flexibility and the induction of strand breaks by ionizing radiation. This is the most likely mechanism for the greater yield of strand breaks in poly(dA) relative to poly(A), since the differences in sugar pucker and base stacking make the former more flexible (Evans and Sarma 1976). The observation that OH-radical mediated strand scission is reduced in double-stranded DNA at runs of three or more adenines (Burkhoff and Tullius 1987) may be due to a rigidity of these sequences that is similar to that found in poly(dA•dT). Figure 1 compares electron micrographs of relaxed and supercoiled plasmids (Stryer 1981). The branched interwound secondary structure of the supercoiled plasmid brings together nucleotides that are distant from each other in the primary sequence. We speculate that this type of secondary structure is more favorable for the decay of peroxyl base radicals to strand breaks than is the unfolded conformation of relaxed closed-circular DNA.

References

Burkhoff, A. M., and T. D. Tullius. 1987. "The Unusual Conformation Adopted by Adenine Tracts in Kintoplast DNA." *Cell* 48:935-943.

Evans, F. E., and R. H. Sarma. 1976. "Nucleotide Rigidity." *Nature* 263:567-572.

Fratini, A. V., M. L. Kopka, H. R. Drew, and R. E. Dickerson. 1982. "Reversible Bending and Helix Geometry in a B-DNA Dodecamer: CGCGAATT^{Br}CGCG." *J. Biol. Chem.* 257:14686-14707.

Miller, J. H., J. M. Nelson, M. Ye, C. E. Swenberg, J. M. Speicher, and C. J. Benham. 1991. "Negative Supercoiling Increases the Sensitivity of Plasmid DNA to Single-Strand Break Induction by X-rays." *Int. J. Radiat. Biol.* 59:941-949.

Önal, A. M., D. G. E. Lemaire, E. Bothe, and D. Schute-Frohlinde. 1988. "Gamma-Radiolysis of poly(A) in Aqueous Solution: Efficiency of Strand Break Formation by Primary Water Radicals." *Int. J. Radiat. Biol.* 53:787-796.

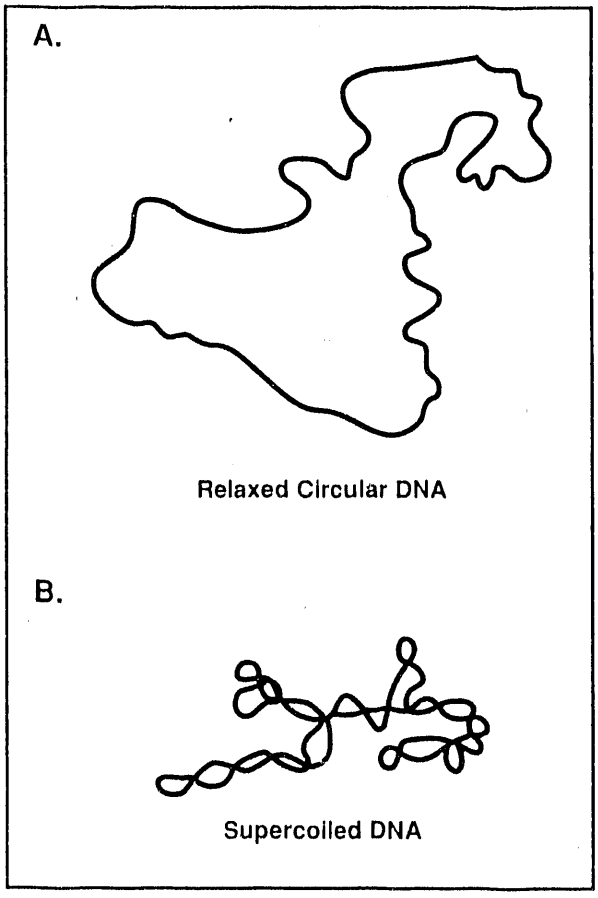

FIGURE 1. Electron Micrographs of Mitochondria Plasmid DNA in Relaxed (A) and Supercoiled (B) States

Schulte-Frohlinde, D., G. Behrens, and A. Önal. 1986. "Lifetime of Peroxyl Radicals of Poly(U), Poly(A), and Single- and Double-Stranded DNA and Their Reaction with Thiols." *Int. J. Radiat. Biol.* 50:103-110.

Stryer, L. 1981. *Biochemistry*, 2nd ed. (W.H. Freeman, San Francisco), p. 574.

Von Sonntag, C. 1984. "Carbohydrate Radicals: from Ethlene Glycol to DNA Strand Breakage." *Int. J. Radiat. Biol.* 46:507-519.

Ward, J. F. 1985. "Biochemistry of DNA Lesions." *Radiat. Res.* 104:S103-S111.

Proton Irradiation of Solid-Oriented DNA Samples at Low Temperature

J. H. Miller and D. L. Frasco[a]

Critical lesions in radiation biology result from clustering of ionizations on a nanometer scale. This assumption is supported by analysis of cell killing by radiations with different linear-energy-transfer (LET) based on computer simulations of track structure in water (Goodhead 1989). Although these biophysical models ignore the complexity of the cellular medium and the macromolecular structures that regulate its function, their basic conclusion can be rationalized by the high scavenging capacity of the chemical environment of DNA and the efficiency of enzymatic repair of minor perturbations of DNA structure.

If the most common precursor of cytotoxic and mutagenic effects from radiation exposure is a cluster of ionization in or, at least, very near to the DNA molecule. Then, involvement of macromolecules in the early stages of lesion production opens the possibility of intramolecular energy and charge transfer following excitation or ionization by the radiation field. These processes acting in the presence of traps for energy and charge provide a mechanism for concentrating energy deposited in macromolecular systems, a mechanism that is independent of stochastic processes in the slowing down of charged particles. Conversely, energy and charge transfer along DNA chains may dissipate clusters of excitation and ionization before biologically significant lesions are formed. In general, the existence of energy and charge migration in macromolecules tends to decouple lesion production from the stochasitics of energy deposition just as ordinary diffusion tends to decouple radiation chemistry on a long-time scale from track effects in the radiolysis of homogeneous solutions of small molecules.

Recent findings at several laboratories have raised questions about the assumption that radiation-induced DNA damage remains localized on the nanometer scale during lesion formation. Arroyo et al. (1986) observed that the yield of

(a) Department of Chemistry, Whitman College, Walla Walla, Washington.

neutron-induced free radicals in oriented DNA fibers depended on the orientation of the sample relative to the neutron flux. These observations were attributed to energy transfer between stacked DNA bases. Al-Kazwini et al. (1990) presented evidence that electrons can move along DNA chains for distances up to about 100 base pairs. Data obtained by van Lith et al. (1986) on microwave conductivity in pulsed radiolysis indicated that electrons can migrate for distances on the order of 100 nm in the structured-water layers around macromolecular chains.

We used direct proton-beam irradiation of oriented DNA samples to look for effects like those reported by Arroyo et al. (1986) for neutrons. Samples were prepared by Professor Allan Rupprecht at the University of Stockholm. For proton irradiation, they were placed on a copper block in contact with a reservoir of liquid nitrogen and held in place by a thin polyester film. After cooling to 77K, the sample was placed in a vacuum chamber attached to the beam line of the accelerator. Samples were exposed to graded doses of 4-MeV protons in the range of 20 to 60 kGy at a dose rate of about 2.5 kGy/min. After irradiation, the samples were placed in a precooled quartz tupe for transfer to an Electron Paramagnetic Resonance (EPR) Spectrometer. Samples exposed to gamma-rays for comparison with published data (Gräslund et al. 1971) and the results of proton irradiation could be sealed into an EPR tube before irradiation because of the penetrating power of the radiation.

Figure 1 compares EPR spectra of free radicals produced by gamma-rays and protons. The proton flux was incident on the sample either parallel or perpendicular to the orientation of DNA chains. All three spectra contain a central line that is associated with anions and cations of DNA bases (Gräslund et al. 1971). For the proton irradiated samples, we see clear evidence of another radical species which is the protonated form of the thymine radical anion (TH•). The samples were kept in contact with liquid nitrogen cooled surfaces, and the magnitude of the central line relative to the structure in the wings did not change as a function of proton dose. Thus the presence of TH• in proton-irradiated samples is

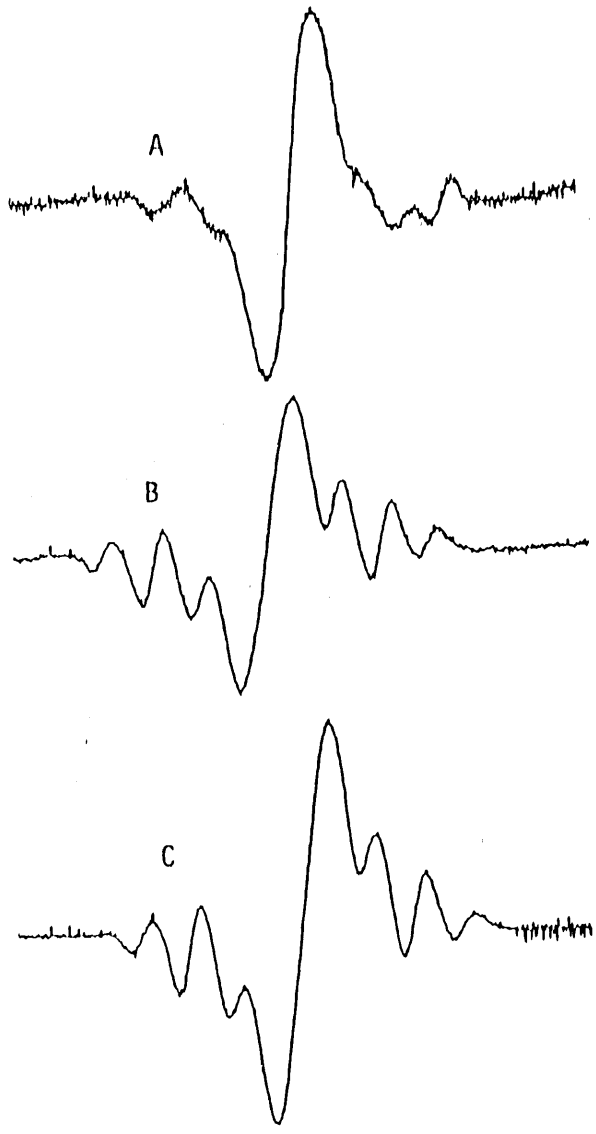

FIGURE 1. EPR Spectra of Oriented DNA Exposed to 4 kGy of Gamma-Rays (A), 56 kGy of Protons Incident Perpendicular the Fiber Orientation (B), and 48 kGY of Protons Incident Parallel to the Fibers Orientation (C)

not likely to be caused by sample warming during the transfer from the proton beam line to the EPR spectrometer. TH• radicals may have been produced by warming of the samples during irradiation because of the high dose rate. Our dose rate was less than the 10 kGy/min recommended by Henriksen and Smith (1970); however, this recommendation is based on their experience with 6.5-MeV electron irradiation, where

conversion of energy deposition into heat is probably less than with protons that stop in the sample.

Unlike the results reported for neutrons (Arroyo et al. 1986), EPR spectra of radicals produced by direct proton irradiation of oriented DNA in parallel and perpendicular geometries were not significantly different. Figure 2 shows that, within experimental error, total radical yields were also independent of the orientation of DNA fibers relative to the proton flux. To obtain these results, differential EPR spectra were recorded digitally and double integrated to give the area under the absorption lines. This area was converted to number of spins by comparison with a standard sample of 2,2 diphenyl-1-picrylhydrazyl (DPPH) dissolved in paraffin. Hence, we did not find any evidence for long-range energy or charge transfer in DNA from experiments in which oriented DNA was exposed to direct proton-beam irradiation. This may be due to the high doses and dose rates in the proton exposures. Experiments with larger samples, higher proton energies for greater penetration, and improved EPR detection sensitivity might reveal orientation effects that are not present in our data due to sample heating or processes that destroy free radicals at high exposure levels (Bernhard 1981).

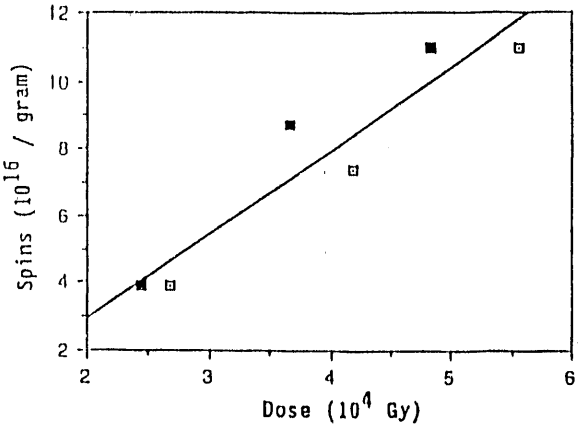

FIGURE 2. Total Radical yields in parallel (■) and Perpendicular (□) Proton Irradiation of Oriented DNA at 77° K

References

Al-Kazwini, A. T., P. O'Neill, G. E. Adams, and E. M. Fielden. 1990. "Radiation-Induced Energy Migration within Solid DNA: The Role of Misonidazole as an Electron Trap." *Radiat. Res.* 121:149-153.

Arroyo, C. M., A. J. Carmichael, C. E. Swenberg, and L. S. Myers, Jr. 1986. "Neutron-Induced Free Radicals in Oriented DNA." *Int. J. Radiat. Biol.* 50:789-793.

Bernhard, W. A. 1981. "Solid-State Radiation Chemistry of DNA: The Bases." *Adv. Radiat. Biol.* 9:199-280.

Goodhead, D. T. 1989. "The Initial Physical Damage Produced by Ionizing Radiation." *Int. J. Radiat. Biol.* 56:623-634.

Gräslund, A., A. Ehrenberg, A. Rupprecht, and G. Ström. 1971. "Ionic Base Radicals in Gamma-Irradiatied DNA." *Biochim. Biophys. Acta* 254:172-186.

Henriksen, T., and W. Snipes. 1970. "Radiation-Induced Radicals in Thymine: ESR Studies of Single Crystals." *Radiat. Res.* 42:255-269.

van Lith, D., J. M. Warman, M. P. de Haas, and A. Hummel. 1986. "Electron Migration in Hydrated DNA and Collagen at Low Temperature. Part I. Effects of Water Concentration." *J. Chem. Soc., Faraday Trans.* 1 82:2933-2943.

Publications and Presentations

Publications

Badhwar, G. D., A. Konradi, A. Hardy, L. A. Braby. 1991. "Active Dosimetric Measurements on Shuttle Flights." *Nucl. Tracks Radiat. Meas.*, Pergamon Press, Great Britain (in press).

Bean, R. M., B. L. Thomas, E. K. Chess, J. G. Pavlovich, and D. L. Springer. 1991. "Quantitative Determination of Polycyclic Aromatic Hydrocarbon Adducts to Deoxyribonucleic Acid Using GC/MS Techniques." In *Polynuclear Aromatic Hydrocarbons: Measurement, Means, and Metabolism*, pp. 121-130. 11th International Symposium, Battelle Press, Columbus, Ohio.

Braby, L. A. 1991. "Microbeam Studies of the Sensitivity of Structures Within Living Cells." *International Journal Scanning Microscopy.* 6 167-175 (1992).

Braby, L. A. 1991. "Phenomenological Models." In *Proceedings of the Physical and Chemical Mechanisms in Molecular Radiation Biology 1990*, Woods Hole, Massachusetts (in press).

Braby, L. A., and T. L. Morgan. 1991. "Role of DNA Deletion Length in Mutation and Cell Survival." In *Biophysical Modeling of Radiation Effects*. Institute of Physics, Padua, Italy (in press).

Braby, L. A., and J. M. Nelson. 1991. "Linear-Quadratic Dose Kinetics or Dose-Dependent Repair/Misrepair." In *Biophysical Modeling of Radiation Effects*. Institute of Physics, Padua, Italy (in press).

Braby, L. A., L. H. Toburen, W. E. Wilson, and N. F. Metting. 1991. "Microdosimetric Measurements of Heavy Ion Tracks." *Advances in Space Research* (in press).

Busman, M., A. L. Rockwood, and R. D. Smith. 1991. "Activation Energies for Gas Phase Dissociations of Multiply Charged Ions from Electrospray Ionization Mass Spectrometry." *Journal of Physical Chemistry* (in press).

Clark, M. W., J. A. Tanis, E. M. Bernstein, N. R. Badnell, R. D. DuBois, W. G. Graham, T. J. Morgan, V. L. Plano, A. S. Schlachter, and M. P. Stockli. 1991. "Cross Sections for Resonant Transfer and Excitation in Fe^{Q+} + He Collisions." *Physical Review A* (in press).

DuBois, R. D. 1991. "Coincidence Measurements of Electron Capture and Loss in Ion-Atom Collisions." *Lecture Notes in Physics, High-Energy Ion-Atom Collisions*, eds., D. Berenyi and G. Hock, pp. 33-45. Springer Verlag, Berlin, Germany.

DuBois, R. D. 1991. "Ionization in Few Electron Atom-Atom Collisions." In *Proceedings of Third U.S.-Mexico Cooperative Joint Symposium on Atomic and Molecular Physics*. Cuernavaca, Mexico (in press).

DuBois, R. D., H. Berg, O. Jagutzki, R. Dorner, J. A. Tanis, C. Kelbch, H. Schmidt-Bocking, J. Ullrich, A. S. Schlachter, R. Prior, L. Blumenfeld, B. d'Etat, S. Hagmann, A. Gonzales, et al. 1991. "Double Ionization of Helium by High-Velocity U^{90+} Ions." Submitted to *Physical Review A* (in press).

DuBois, R. D., O. Heil, R. Maier, M. Kuzel, K.-O. Groeneveld. 1991. "A Systematic Investigation of Ionization Occurring in Few Electron Collision systems: H^0, He^0, Impact on He." *Zeitschrift für Physik D.*

DuBois, R. D., O. Heil, R. Maier, M. Kuzel, K.-O. Groeneveld. 1991. "Ionization in Fast Neutral Particle-Atom Collisions: H and He Atoms Impacting on He." *Physical Review A.* 45 2850-8 (1992).

DuBois, R. D., R. Herrman, J. Feng, R. Dörner, J. Euler, and K. Ullman. 1991. "Correlations Between Charged Particles Emitted in Ion-Molecule Collisions." *Atomic Physics of Highly Charged Ions*, eds., E. Salzborn, P. H. Mokler, A. Müller, p. 259. Springer-Verlag, Berlin, Germany.

DuBois, R. D., J. A. Tanis, A. S. Schlachter. 1991. "Comment on 'Double and Single Ionization of Helium by High-Velocity N^{7+} Ions'." Submitted to *Physical Review Letters*. 68 897 Published (1992).

Edmonds, C. G., J. A. Loo, R. R. Ogorzalek-Loo, and R. D. Smith. 1991. "Electrospray Ionization Mass Spectrometry and Tandem Mass Spectrometry for the Characterization of Proteins and Proteolytic Digests." Chapter 47 in *Techniques in Protein Chemistry II*, pp. 487-495. Academic Press, Inc.

Harvey, S. D., R. M. Bean, and H. R. Udseth. 1991. "High-Resolution Separation and Detection of DNA Adducts of Benzo[a]pyrene." *J. Microcolumn Separations* (in press).

Heil, O., R. D. DuBois, R. Maier, M. Kuzel, and K. O. Groeneveld. 1991. "Electron Emission in H°-Atom Collisions: A Coincidence Study of the Angular Dependence." *Application of Accelerators in Research and Industry*, eds., J. L. Duggan and I. L. Morgan, pp. 282-84. North Holland, Amsterdam, Netherlands.

Heil, O., R. Maier, R. D. DuBois, M. Kuzel, K. O. Groeneveld. 1991. "Doubly Differential Electron Emission Cross Sections for He° (0.5 MeV/amu) → He Collisions." *Atomic Physics of Highly Charged Ions*, eds., E. Salzborn, P. H. Mokler, A. Müller, p. 333. Springer-Verlag, Berlin, Germany.

Loo, J. A., R. R. Ogorzalek-Loo, K. J. Light-Wahl, C. G. Edmonds, and R. D. Smith. 1991. "Multiply Charged Negative Ions by Electrospray Ionization from Polypeptides and Proteins." *Anal. Chem.* (in press).

Loo, J. A., R. R. Ogorzalek-Loo, H. R. Udseth, C. G. Edmonds, and R. D. Smith. 1991. "Solvent-Induced Conformational Changes of Polypeptides Probed by Electrospray Ionization-Mass Spectrometry." *Rapid Commun. Mass Spectrom.* 5(3):101-105.

Loo, J. A., C. G. Edmonds, and R. D. Smith. 1991. "Tandem Mass Spectrometry of Very Large Molecules: Serum Albumin Sequence Information from Multiply Charged Ions formed by Electrospray Ionization." *Anal. Chem.* 63:2488-2499.

Maier, R., O. Heil, R. D. DuBois, M. Kuzel, and K.-O. Groeneveld. 1991. "New Aspects of Simultaneous Projectile and Target Ionization in H° (0.5 MeV/1.0 MeV) → He Collisions." *Lecture Notes in Physics, High-Energy Ion-Atom Collisions*, eds., D. Berenyi and G. Hock. pp. 88-96. Springer-Verlag, Berlin, Germany.

Miller, J. H. 1991. "Role of Energy and Charge Transfer in DNA Damage by Densely Ionizing Radiation." *The Early Effects of Radiation on DNA*, NATO ASI Series, Vol. H54, eds. E. M. Fielden and P. O'Neil. pp. 157-158. Springer-Verlag, Berlin, Germany.

Miller, J. H., and S. T. Manson. 1991. "Relativistic Model of Secondary-Electron Energy Spectra in Electron-Impact Ionization." *Phys. Rev.* 44:4321-4327.

Miller, J. H., M. Ye, J. M. Nelson, C. E. Swenberg, J. M. Speicher, and C. J. Benham. 1991. "Negative Supercoiling Increases the Sensitivity of Plasmid DNA to Single-Strand-Break Induction by X Rays." *International J. of Radiation Biology.* 59:941-949.

Miller, J. H., D. L. Frasco, M. Ye, C. E. Swenberg, L. S. Myers, Jr., and A Rupprecht. 1991. "Free-Radical Yields in Proton Irradiation of Oriented DNA: Relationship to Energy Transfer Along DNA Chains." *Biological Effects and Physics of Solar and Galactic Cosmic Radiation, NATO ASI Series*, eds., C. E. Swenberg, C. Hornect, and E. G. Stassinopoulas (in press).

Miller, J. H., D. L. Frasco, C. E. Swenberg, and A. Rupprecht. 1991. "Energy Transfer Mechanisms in DNA: Relationship to Energy Deposition in Sub-microscopic Volumes." In *Proceedings of the 9th International Congress of Radiation Research*, 1991, Toronto, Ontario, Canada (in press).

Miller, J. H., J. M. Nelson, E. W. Fleck, C. J. Benham. 1991. "Effects of Torsional Stress

on the Interaction of DNA with Radiation and Chemicals." *Applied Occupational and Environmental Hygiene* (in press).

Nelson, J. M. and R. G. Stevens. 1991. "Ferritin-Iron Increases Killing of Chinese Hamster Ovary Cells by X-Irradiation." *Radiation Research*. Cell Proliferation (in press).

Nelson, J. M. and R. G. Stevens. 1991. "Body Iron Stores May Modify Sensitivity to Occupational Radiation Exposure." *Applied Occupational and Environmental Hygiene* (in press).

Nelson, J. M., and R. G. Stevens. 1991. "Enhanced X-Ray Sensitivity from Excess Ferritin Iron." *Cell Proliferation* 24(4):411.

Ogorzalek-Loo, R. R., H. R. Udseth, and R. D. Smith. 1991. "Evidence of Charge Inversion in the Reaction of Singly Charged Anions with Multiply Charged Macroions." *J. Phys. Chem.* 95:6412-6415.

Perkins, R. W., D. E. Robertson, C. W. Thomas, and J. A. Young. 1990. "Comparison of Nuclear Accident and Nuclear Test Debris." In *Proceedings of an Internationl Symposium on Environmental Contamination Following a Major Nuclear Accident*, pp. 111-139. International Atomic Energy Agency, Vienna, Austria.

Robertson, D. E., R. W. Perkins, E. L. Lepel, C. W. Thomas, and R. A. Kiddy. 1992. "Radionuclide Concentrations in Environmental Samples Collected Around Chernobyl During the International Chernobyl Project." PNL-SA-20936, Pacific Northwest Laboratory, Richland, Washington.

Rockwood, A. L., M. Busman, H. R. Udseth, and R. D. Smith. 1991. "Thermally Induced Dissociation of Large Ions from Electrospray Ionization." *Rapid Commun. Mass Spectrom* 5:582-585.

Rockwood, A. L., M. Busman, and R. D. Smith. 1991. "Coulombic Effects in the Dissociation of Large Highly Charged Ions." *Int. J. of Mass Spectrom. Ion Proc.* 111:103-130.

Schmidt-Böcking, H., R. Dörner, J. Ullrich, J. Euler, H. Berg, E. Forberich, S. Lencnas, O. Jagutzki, A. Gensmantel, K. Ullmann, R. D. DuBois, Feng Jiazhen, R. E. Olson, A. Gonzales, and S. Hagmann. 1991. "Multiple Ionization in Ion-Atom Collisions Investigated by Recoil Ion Momentum Spectroscopy." *Lecture Notes in Physics, High-Energy Ion-Atom Collisions*, eds., D. Berenyi and G. Hock, pp. 268-281. Springer Verlag, Berlin, Germany.

Smith, R. D., J. A. Loo, C. G. Edmonds, and H. R. Udseth. 1991. "Combined Capillary Electrophoresis and Electrospray Ionization Mass Spectrometry." In *Analytical Applications of Spectroscopy*, A.M.C. Davies and C. S. Creaser, eds., pp. 149-164. Royal Society of Chemistry.

Smith, R. D., J. A. Loo, and C. G. Edmonds. 1991. "The Analysis of Biomolecules by Electrospray Ionization-Mass Spectrometry and Tandem Mass Spectrometry." Chapter 2 in *Clinical Mass Spectrometry* (in press).

Smith, R. D., J. A. Loo, R. R. Ogorzalek-Loo, M. Busman, and H. R. Udseth. 1991. "Principles and Practice of Electrospray Ionization-Mass Spectrometry for Large Polypeptides and Proteins." *Mass Spectrometry Reviews* (in press).

Smith, R. D., H. R. Udseth, C. J. Barinaga, and C. G. Edmonds. 1991. "Instrumentation for High Performance Capillary Electrophoresis-Mass Spectrometry." *J. of Chromatography*, 559:197-208.

Toburen, L. H. 1991. "Atomic and Molecular Physics in the Gas Phase." In *Proceedings of Physical an Chemical Mechanisms in Molecular Radiation Biology 1990*, Woods Hole, Massachusetts (in press).

Toburen, L. H., and W. E. Wilson. 1991. "Biological Effects of Inner-Shell Ionization." *AIP Conference Proceedings 215*, pp. 878-888. American Institute of Physics, New York, New York.

Winger, B. D., K. J. Light-Wahl, and R. D. Smith. 1991. "Gas Phase Proton Transfer Reactions Involving Multiply Charged Cytochrome c Ions and Water under Thermal Conditions." *J. Amer. Soc. for Mass Spectrom* (in press).

Presentations

Bean, R. M., S. D. Harvey, H. R. Udseth, J. A. Campbell, R. B. Lucke, and B. L. Thomas. 1991. "Analysis of DNA Adducts." Presented at the 46th Northwest Regional ACS Meeting in La Grande, Oregon.

Braby, L. A., and T. L. Morgan. 1991. "Role of DNA Deletion Length in Mutation and Cell Survival." Presented at the Workshop on Biophysical Modeling of Radiation Effects, Padua, Italy. PNL-SA-19425A, Pacific Northwest Laboratory, Richland, Washington.

Braby, L. A., and J. M. Nelson. 1991. "The Effects of Individual Proton Tracks on Cells." Presented at the 9th International Congress of Radiation Research Society, Toronto, Canada. PNL-SA-19201A, Pacific Northwest Laboratory, Richland, Washington.

Braby, L. A., and J. M. Nelson. 1991. "Linear-Quadratic Dose Kinetics or Dose-Dependent Repair/Misrepair." Presented at the Workshop on Biophysical Modeling of Radiation Effects, Padua, Italy. PNL-SA-20040, Pacific Northwest Laboratory, Richland, Washington.

Braby, L. A., and J. M. Nelson. 1991. "Microbeam Studies of the Sensitive Structures Within Living Cells." Presented at the Scamming Microscopy Meeting, Bethesda, Maryland. PNL-SA-19443A, Pacific Northwest Laboratory, Richland, Washington.

Braby, L. A., and J. M. Nelson. 1991. "Single Particle Irradiation of Individual Cells." Presented at the Investigators Meeting on Space Radiation Research held at the NASA Johnson Space Center, Houston, Texas. PNL-SA-19304A, Pacific Northwest Laboratory, Richland, Washington.

Braby, L. A., T. J. Conrol, D. C. Elegy, and L. W. Brackenbush. 1991. "Use of Tissue Equivalent Proportional Counters to Characterize Ra ation Quality on the Space Shuttle." Presented at the New Horizons in Radiation Protection & Shielding Conference to be held April 26-30, 1992 in Pasco, Washington. PNL-SA-19981S, Pacific Northwest Laboratory, Richland, Washington.

DuBois, R. D. 1991. "Ionization in Few Electron Atom-Atom Collisions." (INVITED PAPER) Presented at the Third U.S.-Mexico Cooperative Joint Symposium on Atomic and Molecular Physics, Cuernavaca, Mexico. PNL-SA-19200A, Pacific Northwest Laboratory, Richland, Washington.

DuBois, R. D., S. T. Manson, O. Heil, R. Maier, M. Kuzel, and K.-O. Groeneveld. 1991. "First Born Calculations for Electron Emission Occurring in H° - He Collisions." Presented at the XVII International Confrence on the Physics of Electronic and Atomic Collisions, Brisbane, Australia. PNL-SA-19264A, Pacific Northwest Laboratory, Richland, Washington.

DuBois, R. D., and L. H. Toburen. 1991. "Electron Emission in 100 keV/amu C^{q+} - He Collisions." Presented at the XVII International Conference on the Physics of Electronic and Atomic Collisions, Brisbane, Australia. PNL-SA-19265A, Pacific Northwest Laboratory, Richland, Washington.

DuBois, R. D., O. Heil, R. Maier, M. Kuzel, and K.-O. Groeneveld. 1991. "A Coincidence Study of the Electron Emission Occurring in H° - He Collisions." Presented at the XVII International Conference on the Physics of Electronic and Atomic Collisions, Brisbane, Australia. PNL-SA-19267A, Pacific Northwest Laboratory, Richland, Washington.

Light-Wahl, K. J., J. A. Loo, and R. D. Smith. 1991. "Protein Structural Effects on Electrospray Ionization Mass Spectra and Tandem Mass Spectra." Presented at ASMS of Mass Spectrometry and Allied Topics, Nashville, Tennessee.

Light-Wahl, K. J., J. A. Loo, C. G. Edmonds, and R. D. Smith. 1991. "Hemoglobin Variants as Models for Investigation of Dissociation of Intact Polypeptide Chains by ESI Tandem Mass Spectrometry." Presented at 39th ASMS Conference on Mass Spectrometry and Allied Topics, Nashville, Tennessee.

Loo, J. A., K. J. Light-Wahl, C. G. Edmonds, and R. D. Smith. 1991. "Tandem Mass Spectrometry and MS/MS/MS of Multiply Charged Ions from Large Biomolecules." Presented at ASMS on Mass spectrometry and Allied Topics, Nashville, Tennessee.

Loo, J. A., K. J. Light-Wahl, R. D. Smith, and R. R. Ogorzalek-Loo. 1991. "Protein Structural Effects on Electrospray Ionization Mass Spectra and Tandem Mass Spectra." Presented at ASMS on Mass spectrometry and Allied Topics, Nashville, Tennessee.

Miller, J. H., C. J. Benham, and C. E. Swenberg. 1991. "Mechanisms for the Dependence of Strand Scission on Superhelical Density." Presented at the 9th International Congress of Radiation Research Society, Toronto, Canada. PNL-SA-19159A, Pacific Northwest Laboratory, Richland, Washington.

Miller, J. H., D. L. Frasco, C. E. Swenberg, and A. Rupprecht. 1991. "Energy Transfer Mechanisms in DNA and Their Relation to Deposition in Submicron Volumes." (INVITED PAPER) Presented at the 9th International Congress of Radiation Research Society, Toronto, Canada. PNL-SA-19709A, Pacific Northwest Laboratory, Richland, Washington.

Miller, J. H., J. M. Nelson, E. W. Fleck, and C. J. Benham. 1991. "Effects of Torsional Stress on the Interaction of DNA with Radiation and Chemicals." Presented at the 30th Hanford Life Sciences Symposium, Richland, Washington. PNL-SA-20085A, Pacific Northwest Laboratory, Richland, Washington.

Miller, J. H., D. L. Frasco, M. Ye, C. E. Swenberg, L. S. Myers, Jr., and A. Rupprecht. 1991. "Free-Radical Yields in Proton Irradiation of Oriented DNA: Relationship to Energy Transfer Along DNA Chains." Presented at the NATO Advanced Studies Institute on the Biological Effects and Physics of Solar and Galactic Cosmic Rays, Armacao de Pêra, Algrave, Portugal. PNL-SA-20043A, Pacific Northwest Laboratory, Richland, Washington.

Morgan, T. L., E. W. Fleck, P. J. Lager, and B. F. J. Rossiter. 1991. "X-Ray-Induced Deletions in Tinron Sequences Cause Gene Inactivation." Presented at the 9th International Congress of Radiation Research Society, Toronto, Canada. PNL-SA-19161A, Pacific Northwest Laboratory, Richland, Washington.

Morgan, T. L., L. A. Braby, E. W. Fleck, R. F. Jostes, and F. T. Cross. 1991. "Model of Radiation Mutagenesis." Presented at the 24th Radiological and Chemical Physics Contractors Meeting, New York. PNL-SA-19339A, Pacific Northwest Laboratory, Richland, Washington.

Nelson, J. M., J. H. Miller, M. Ye, and E. W. Fleck. 1991. "Effect of Base Composition on Radiation Strand Scission." Presented at the 9th International Congress of Radiation Research Society, Toronto, Canada. PNL-SA-19155A, Pacific Northwest Laboratory, Richland, Washington.

Nelson, J. M., and R. G. Stevens. 1991. "Enhanced X-Ray Sensitivity from Excess Ferritin Iron." Presented at the 15th Annual Cell Kinetics Society Meeting, Kiawah Island, North Carolina. PNL-SA-19149A, Pacific Northwest Laboratory, Richland, Washington.

Nelson, J. M., and R. G. Stevens. 1991. "Body Iron Stores May Modify Sensitivity to Occupational Radiation Exposure." Presented at the 30th Hanford Life Sciences Symposium, Richland, Washington.

Ogorzlek-Loo, R. R., H. R. Udseth, and R. D. Smith. 1991. "Ion-Ion Reactions of Large Cations and Anions Generated by Electrospray Ionization." Presented at ASMS Conference on Mass Spectrometry and Allied Topics, Nashville, Tennessee.

Rockwood, A. L., M. Busman, H. R. Udseth, and R. D. Smith. 1991. "Thermally Induced Dissociation of Large Ions from Electrospray Ionization." Presented at ASMS on Mass Spectrometry and Allied Topics, Nashville, Tennessee.

Rockwood, A. L., J. A. Loo, H. R. Udseth, C. G. Edmonds, and R. D. Smith. 1991. "Obtaining Structural Information from Electrospray Ionization-Mass Spectrometry at the Large Molecule Limit." Presented at ASMS on Mass Spectrometry and Allied Topics, Nashville, Tennessee.

Smith, R. D. 1991. "Capillary Electrophoresis Electrospray Ionization-Mass Spectrometry of Peptides and Proteins." Presented at 11th International Symposium on HPLC of Proteins, *Peptides, Polynucleotides*, Washington, D.C.

Smith, R. D. 1991. "Development of High Performance ICR." Workshop on High Field ICR, Tallahassee, Florida.

Smith, R. D. 1991. "Tandem Mass Spectrometry of Large Multiply Charged Molecules." Fourth International Symposium on Tandem Mass Spectrometry, Lake Louise, Alberta, Canada.

Smith, R. D., H. R. Udseth, A. L. Rockwood, K. J. Light-Wahl, M. Busman, and C. G. Edmonds. 1991. "Dissociation of Large Molecular Ions from Electrospray Ionization." Presented at Joint Meeting of FACSS XVIII and Pacific Conference, Anaheim, California.

Smith, R. D., A. L. Rockwood, and H. R. Udseth. 1991. Advanced Methods for Structural Characterization of Large Multiply Charged Ions: Obtaining Charge State Determination and Improved Sensitivity." Presented at ASMS on Mass Spectrometry and Allied Topics, Nashville, Tennessee.

Smith, R. D., A. L. Rockwood, J. A. Loo, H. R. Udseth, and C. G. Edmonds. 1991. "Obtaining Structural Information from Electrospray Ionization-Mass Spectrometry at the Large Molecule Limit." Presented at ASMS on Mass Spectrometry and Allied Topics, Nashville, Tennessee.

Smith, R. D., A. L. Rockwood, M. Busman, J. A. Loo, R. R. Ogorzalek-Loo, and H. R. Udseth. 1991. "Activation and Dissociation of Large Multiply Charged Ions." Presented at Ion Activation and Dissociation Symposium, Sanibel Island, Florida.

Smith, R. D., J. A. Loo, C. G. Edmonds, A. L. Rockwood, and H. R. Udseth. 1991. "Electrospray Ionization-Tandem Mass Spectrometry for the Characterization of Large Biomolecules." Presented at 1991 Pittsburgh Conference, Chicago, Illinois.

Smith, R. D., H. R. Udseth, J. A. Loo, and C. G. Edmonds. 1991. "The Analysis of Peptide and Protein Mixtures by Capillary Electrophoresis-Tandem Mass Spectrometry." Presented at 3rd International Symposium on HPCE, San Diego, California.

Smith, R. D., J. A. Loo, C. G. Edmonds, C. J. Barinaga, and H. R. Useth. 1991. "Electrospray Ionization and Tandem Mass Spectrometry of Large Molecules." Presented at Ion Activation and Dissociation Symposium, Sanibel Island, Florida.

Toburen, L. H. 1991. "The Effective Charge of Energetic Ions in Matter." Presented at the 9th International Congress of Radiation Research Society, Toronto, Canada. PNL-SA-19193A, Pacific Northwest Laboratory, Richland, Washington.

Toburen, L. H. 1991. "Fundamental Physical Mechanisms for Use in Radiation 'Signatures'." (INVITED PAPER) Presented at the 24th Radiological and Chemical Physics Contractors Meeting, New York. PNL-SA-19224A, Pacific Northwest Laboratory, Richland, Washington.

Udseth, H. R., J. H. Wahl, C. J. Barinaga, and R. D. Smith. 1991. "Interface Contributions to Peak Broadening in CE-ESI-MS." Presented at 39th ASMS Conference, Nashville, Tennessee.

Wilson, W. E., and H. G. Paretzke. 1991. "A Stochastic Model of Ion Track Structure." Presented at the 9th International Congress of Radiation Research Society, Toronto, Canada. PNL-SA-19160A, Pacific Northwest Laboratory, Richland, Washington.

Author Index

Author Index

Distribution

Distribution

DOMESTIC

W. R. Albers
EH-12, GTN
Department of Energy
Washington, DC 20545

D. Anderson
ENVIROTEST
1108 NE 200th Street
Seattle, WA 98155-1136

Assistant Secretary
Environment, Safety & Health
EH-1, FORS
Department of Energy
Washington, DC 20545

F. Badgley
13749 NE 41st Street
Seattle, WA 98125

R. E. Baker
8904 Roundleaf Way
Gaithersburg, MD 20879-1630

R. W. Barber
EH-131, GTN
Department of Energy
Washington, DC 20545

A. D. Barker
Battelle Columbus Laboratories
505 King Avenue
Columbus, OH 43201

N. F. Barr
ER-72, GTN
Department of Energy
Washington, DC 20545

J. R. Beall
ER-72, GTN
Department of Energy
Washington, DC 20545

E. S. Beckford
Office of Nuclear Regulatory Research
U.S. Nuclear Regulatory Commission
Washington, D.C. 20555

W. R. Bibb
Energy Programs and Support Division
Department of Energy
P.O. Box 2001
Oak Ridge, TN 38731

L. C. Brazley, Jr.
NE-22, GTN
Department of Energy
Washington, DC 20545

D. J. Brenner
Radiological Research Lab
College of Physicians and Surgeons
Columbia University
630 W. 168th Street
New York, NY 10032

G. Burley
Office of Radiation Programs, ANR-458
Environmental Protection Agency
Washington, DC 20460

W. W. Burr, Chairman
Medical & Health Sciences Division
Oak Ridge Associated Universities
P.O. Box 117
Oak Ridge, TN 37830

L. K. Bustad
College of Veterinary Medicine
Washington State University
Pullman, WA 99164-7010

R. J. Catlin, President
Robert J. Catlin Corporation
701 Welch Road, Suite 1119
Palo Alto, CA 94304

A. Chatterjee
Lawrence Berkeley Laboratory
MS 29-100
1 Cyclotron Road
Berkeley, CA 94720

N. Cohen
New York University Medical Center
P.O. Box 817
Tuxedo, NY 10987

Council on Environmental Quality
722 Jackson Place, NW
Washington, DC 20503

Department of Energy
Environment & Health Division
P.O. Box 5400
Albuquerque, NM 87115

Department of Energy
Director, Health Protection Division
P.O. Box 5400
Albuquerque, NM 87115

DOE Office of Scientific and Technical Information (12)

A. P. Duhamel
ER-74, GTN
Department of Energy
Washington, DC 20545

S. J. Farmer
17217 77th Avenue W.
Edmonds, WA 98020

B. H. Fimiani
Battelle, Pacific Northwest Laboratories
Washington Operations
370 L'Enfant Promenade, Suite 900
901 D Street, SW
Washington, DC 20024

M. E. Frazier
ER-75, GTN
Department of Energy
Washington, DC 20545

W. R. Garrett
Oak Ridge National Laboratory
P.O. Box 2008
Oak Ridge, TN 37831

T. F. Gesell
Idaho Operations Office
Department of Energy
785 DOE Place
Idaho Falls, ID 83402-4149

R. D. Gilmore, President
Environmental Health Sciences, Inc.
Nine Lake Bellevue Building
Suite 104
Bellevue, WA 98005

G. Goldstein
ER-74, GTN
Department of Energy
Washington, DC 20545

G. H. Groenewold
Energy and Mineral Research Center
University of North Dakota
Box 8123, University Station
Grand Forks, ND 58202

E. J. Hall
Radiological Research Laboratory
Columbia University
630 West 168th Street
New York, NY 10032

J. W. Healy
51 Grand Canyon Drive
White Rock, NM 87544

R. F. Hirsch
ER-75, GTN
Department of Energy
Washington, DC 20545

R. O. Hunter, Jr.
ER-1, FORS
Department of Energy
1000 Independence Avenue, SW
Washington, DC 20545

F. Hutchinson
Department of Molecular Biophysics & Biochemistry
Yale University
260 Whitney Avenue
P.O. Box 6666
New Haven, CT 06511

M. Inokuti
Argonne National Laboratory
9700 South Cass Avenue
Argonne, IL 60439

H. Ishikawa, General Manager
Nuclear Safety Research Association
P.O. Box 1307
Falls Church, VA 22041

A. W. Johnson
Vice President for Academic Affairs
San Diego State University
San Diego, CA 92182

J. F. Johnson
Kenworth Truck Co.
P.O. Box 1000
Kirkland, WA 98083

L. J. Johnson
Idaho National Engineering Lab
IRC MS 2203
P.O. Box 1625
Idaho Falls, ID 83415

G. Y. Jordy, Director
ER-30, GTN
Department of Energy
Washington, DC 20545

B. J. Kelman
P. O. Box 3015
Menlo Park, CA 94025

G. A. Kolstad
ER-15, GTN
Department of Energy
Washington, DC 20545

R. T. Kratzke
NP-40
Department of Energy
Germantown, MD 20545

Librarian
Brookhaven National Laboratory
Research Library, Reference
Upton, Long Island, NY 11973

Librarian
Colorado State University
Documents Department--The Libraries
Ft. Collins, CO 80523

Librarian
Electric Power Research Institute
3412 Hillview Avenue
P.O. Box 10412
Palo Alto, CA 94303

Librarian
Health Sciences Library, SB-55
University of Washington
Seattle, WA 98195

Librarian
Los Alamos National Laboratory
Report Library, MS P364
P.O. Box 1663
Los Alamos, NM 87545

Librarian
Oregon Regional Primate
Research Center
505 NW 185th Avenue
Beaverton, OR 97006

Librarian
Washington State University
Pullman, WA 99164-6510

Library
Serials Department
(#80-170187)
University of Chicago
1100 East 57th Street
Chicago, IL 60637

J. N. Maddox
ER-73, GTN
Department of Energy
Washington, DC 20545

J. R. Maher
ER-65, GTN
Department of Energy
Washington, DC 20545

C. R. Mandelbaum
ER-32, GTN
Department of Energy
Washington, DC 20545

S. Marks
8024 47th Place West
Mukilteo, WA 98275

H. M. McCammon
ER-75, GTN
Department of Energy
Washington, DC 20545

C. B. Meinhold
Radiological Sciences Division
Bldg. 703M
Brookhaven National
Laboratory
Upton, Long Island, NY 11973

M. L. Mendelsohn
Biomedical and Environmental
Research Program
Lawrence Livermore National
Laboratory, L-452
University of California
P.O. Box 5507
Livermore, CA 94550

C. Miller
P.O. Box 180
Watermill, NY 11976

N. S. Nelson
Office of Radiation Programs,
ANR-461
Environmental Protection
Agency
401 M Street, SW
Washington, DC 20460

W. R. Ney, Executive Director
National Council on Radiation
Protection and Measurements
7910 Woodmont Avenue
Suite 1016
Washington, DC 20014

Nuclear Regulatory
Commission
Advisory Committee on Reactor
Safeguards
Washington, DC 20555

M. J. O'Brien
Radiation Safety Office, GS-05
University of Washington
Seattle, WA 98195

R. G. Rader
ER-33, GTN
Department of Energy
Washington, DC 20545

D. P. Rall, Director
National Institutes of
Environmental Health
Sciences
P.O. Box 12233
Research Triangle Park,
NC 27709

L. A. Rancitelli
Battelle Memorial Institute
505 King Avenue
Columbus, OH 43201-2693

J. Rasey
Division of Radiation Oncology
University of Washington
Medical School
Seattle, WA 98195

C. R. Richmond
Oak Ridge National Laboratory
4500N, MS-62523
P.O. Box 2008
Oak Ridge, TN 37831-6253

J. S. Robertson
ER-73, GTN
Department of Energy
Washington, DC 20545

S. L. Rose
ER-73, GTN
Department of Energy
Washington, DC 20545

R. D. Rosen, Tech. Librarian
Environmental Measurements
Laboratory
Department of Energy
376 Hudson Street
New York, NY 10014

L. Sagan
Electric Power Research
Institute
3412 Hillview Avenue
P.O. Box 10412
Palo Alto, CA 94304

R. A. Scarano
Mill Licensing Section
Nuclear Regulatory
Commission
Washington, DC 20545

M. Schulman
ER-70, GTN
Department of Energy
Washington, DC 20545

R. Shikiar
Battelle - Seattle
4000 NE 41st Street
Seattle, WA 98105

W. K. Sinclair, President
National Council on Radiation Protection
7910 Woodmont Avenue
Suite 1016
Bethesda, MD 20814

J. N. Stannard
University of California
17441 Plaza Animado #132
San Diego, CA 92128

E. T. Still
Kerr-McGee Corporation
P.O. Box 25861
Oklahoma City, OK 73125

J. Stroman
Library
Department of Energy/NIPER
P.O. Box 2128
Bartlesville, OK 74005

Technical Information Service
Savannah River Laboratory
Room 773A
E. I. duPont de Nemours & Company
Aiken, SC 29801

R. G. Thomas
ANL, ER-203
9700 S. Cass Avenue
Argonne IL 60439

P. W. Todd
Department of Chemistry
University of Colorado
Boulder, CO 80303

E. J. Vallario
15228 Red Clover Drive
Rockville, MD 20853

M. N. Varma
ER-74
Department of Energy
Washington, DC 20545

G. J. Vodapivc
DOE - Schenectady Naval Reactors Office
P.O. Box 1069
Schenectady, NY 12301

G. L. Voelz
Los Alamos National Laboratory
MS-K404
P.O. Box 1663
Los Alamos, NM 87545

B. W. Wachholz
Radiation Effects Branch
National Cancer Institute
EPN, Room 530
8000 Rockville Pike
Bethesda, MD 20892

R. A. Walters
Assistant to the Associate Director
Los Alamos National Laboratory
MS-A114
P.O. Box 1663
Los Alamos, NM 87545

W. W. Weyzen
Electric Power Research Institute
3412 Hillview Avenue
P.O. Box 10412
Palo Alto, CA 94303

W. E. Wilson, Associate Director
Nuclear Radiation Center
Washington State University
Pullman, WA 99164

F. J. Wobber
Department of Energy
14 Goshen Court
Gaithersburg, MD 20879-4403

R. W. Wood
PTRD, OHER
ER-74, GTN
Department of Energy
Washington, DC 20545

D. Woodall, Manager
Physics Group
EG&G Idaho, INEL
P.O. Box 1625
Idaho Falls, ID 83415

Zhu Zhixian
Laboratory for Energy-Related Health Research
University of California
Davis, CA 95616

FOREIGN

G. E. Adams, Director
Medical Research Council
Radiobiology Unit
Harwell, Didcot
Oxon OX11 ORD
ENGLAND

D. C. Aumann
Institut für Physikalische Chemie
Universität Bonn
Abt. Nuklearchemie
Wegelerstrasse 12
5300 Bonn 1
GERMANY

M. R. Balakrishnan, Head
Library & Information Services
Bhabda Atomic Research Centre
Bombay - 400 085
INDIA

G. W. Barendsen
Laboratory for Radiobiology
AMC, FO 212
Meibergdreef 9
1105 AZ Amsterdam
THE NETHERLANDS

A. M. Beau, Librarian
Département de Protection Sanitaire
Commissariat á l'Énergie Atomique
BP No. 6
F-92265 Fontenay-aux-Roses
FRANCE

G. Bengtsson, Director-General
Statens Stralskyddsinstitut
Box 60204
S-104 01 Stockholm
SWEDEN

D. J. Beninson
Gerencía de Protección Radiológica y Seguridad
Comisión Nacional de Energía Atómica
Avenida del Libertador 8250
2° Piso Of. 2330
1429 Buenos Aires
ARGENTINA

J. Booz
KFA Jülich Institut für Medezin
Kernsforschungsanlage Jülich
Postfach 1913
D-5170 Jülich
GERMANY

M. J. Bulman, Librarian
Medical Research Council
Radiobiology Unit
Harwell, Didcot
Oxon OX11 ORD
ENGLAND

Cao Shu-Yuan, Deputy Head
Laboratory of Radiation Medicine
North China Institute of Radiation Protection
P.O. Box 120
Tai-yuan, Shan-Xi
THE PEOPLE'S REPUBLIC OF CHINA

M. Carpentier
Commission of the European Communities
200 rue de la Loi
J-70 6/16
B-1049 Brussels
BELGIUM

Chen Xing-An
Laboratory of Industrial Hygiene
Ministry of Public Health
2 Xinkang Street
Deshengmenwai, Beijing
THE PEOPLE'S REPUBLIC OF CHINA

R. Clarke
National Radiological Protection Board
Harwell, Didcot
Oxon OX11 ORQ
ENGLAND

Commission of the European Communities
DG XII - Library SDM8 R1
200 rue de la Loi
B-1049 Brussels
BELGIUM

Deng Zhicheng
North China Institute of Radiation Protection
Tai-yuan, Shan-Xi
THE PEOPLE'S REPUBLIC OF CHINA

Director
Commissariat á l'Énergie Atomique
Centre d'Etudes Nucléaires
Fontenay-aux-Roses (Seine)
FRANCE

Director
Commonwealth Scientific and Industrial Research Organization
Aspendal, Victoria
AUSTRALIA

Director
Laboratorio di Radiobiologia Animale
Centro di Studi Nucleari Della Casaccia
Comitate Nazionale per l'Energia Nucleare
Casella Postale 2400
I-00100 Roma
ITALY

D. Djuric
Institute of Occupational and Radiological Health
11000 Beograd
Deligradoka 29
YUGOSLAVIA

L. Feinendegen, Director
Institut für Medezin
Kernsforschungsanlage Jülich
Postfach 1913
D-5170 Jülich
GERMANY

A. Geertsema
Sasol Technology (Pty), Ltd.
P.O. Box 1
Sasolburg 9570
REPUBLIC OF SOUTH AFRICA

G. B. Gerber
Radiobiology Department
Commission of the European Communities
200 rue de la Loi
B-1049 Brussels
BELGIUM

J. A. B. Gibson
Radiation Dosimetry Department
AEA Environment & Energy
Harwell Laboratory
Didcot
Oxon OX11 ORA
ENGLAND

D. Goodhead
Medical Research Council
Radiobiology Unit
Harwell, Didcot
Oxon OX11 ORD
ENGLAND

A. R. Gopal-Ayengar
73-Mysore Colony
Mahul Road, Chembur
Bombay-400 074
INDIA

G. F. Gualdrini
ENEA
8 Viale Ercolani
I-40138 Bologna
ITALY

J. L. Head
Department of Nuclear Science & Technology
Royal Naval College Greenwich
London SE109NN
ENGLAND

T. Jaakkola
University of Helsinki
Department of Radiochemistry
Unioninkatu 35, 00170
Helsinki 17
FINLAND

Jiang Shengjie, Standing Vice President
Chinese Nuclear Society
P.O. Box 2125
Beijing
THE PEOPLE'S REPUBLIC OF CHINA

K. E. Lennart Johansson
Radiofysiska Inst.
Regionsjukhuset
S-901-82 Umeå
SWEDEN

A. M. Kellerer
Institut für Medizin Strahlenkunde
Universität Würzburg
Versbacher Strasse 5
D-8700 Würzburg
GERMANY

H.-J. Klimisch
BASF Aktiengesellschaft
Abteilung Toxikologie, Z470
D-6700 Ludwigshafen
GERMANY

A. Kövér
Nuclear Ressearch Institute of Hungary
Hungarian Academy of Science
P.O. Box 51
H-4001 Debrecen
HUNGARY

G. H. Kraft
c/o GSI Postbox 110541
Planck Str.
D-6100 Darmstadt
GERMANY

T. Kumatori
National Institute of Radiological Sciences
9-1, Anagawa-4-chome
Chiba-shi 260
JAPAN

H. P. Leenmouts
National Institute of Public Health & Environmental Hygiene
P.O. Box 1
NL-3720 BA Bilthoven
THE NETHERLANDS

Li De-Ping
Professor and Director of North China Institute of Radiation Protection, NMI
Tai-yuan, Shan-Xi
THE PEOPLE'S REPUBLIC OF CHINA

Librarian
Centre d'Etudes
Nucléaires de Saclay
P.O. Box 2, Saclay
Fig-sur-Yvette (S&O)
FRANCE

Librarian
CSIRO
314 Albert Street
P.O. Box 89
East Melbourne, Victoria
AUSTRALIA

Librarian
HCS/EHE
World Health Organization
CH-1211 Geneva 27
SWITZERLAND

Librarian
Kernforschungzentrum Karlsruhe
Institut für Strahlenbiologie
Postfach 3640
D-75 Karlsruhe 1
GERMANY

Librarian
Max-Planck-Institut für Biophysics
Forstkasstrasse
D-6000 Frankfurt/Main
GERMANY

Librarian
Ministry of Agriculture, Fisheries & Food
Fisheries Laboratory
Lowestoft, Suffolk NR33 OHT
ENGLAND

Librarian
National Institute of Radiological Sciences
9-1, Anagawa-4-chome
Chiba-shi 260
JAPAN

Librarian
Supervising Scientist for the Alligator Rivers Region
Level 23, Bondi Junction Plaza
P.O. Box 387
Bondi Junction NSW 2022
AUSTRALIA

Library
Atomic Energy Commission of Canada, Ltd.
Whiteshell Nuclear Research Establishment
Pinawa, Manitoba ROE 1L0
CANADA

Library
Department of Meteorology
University of Stockholm
Arrhenius Laboratory
S-10691 Stockholm
SWEDEN

Library
Risø National Laboratory
DK-4000 Roskilde
DENMARK

Ma Fubang, Director
Chief Engineer
Institute of Atomic Energy
P.O. Box 275
Beijing
THE PEOPLE'S REPUBLIC OF CHINA

A. M. Marko
9 Huron Street
Deep River, Ontario KOJ 1PO
CANADA

H. Matsudaira, Director-General
National Institute of Radiological Sciences
9-1, Anagawa-4-chome
Chiba-shi 260
JAPAN

R.G.C. McElroy
Atomic Energy Commission of Canada, Ltd.
Dosimetric Research Branch
Chalk River, Ontario K0J 1J0
CANADA

J. C. Nénot, Deputy Director
Département de Protection
Centre d' Etudes Nucléaires
BP No. 6
F-92260 Fontenay-aux-Roses
FRANCE

R. V. Osborne
Atomic Energy of Canada Ltd.
Chalk River Nuclear Laboratories
Chalk River, Ontario KOJ1JO
CANADA

H. G. Paretzke
GSF Institut für Strahlenschutz
Ingolstadter Landstrasse 1
D-8042 Neuherberg
GERMANY

O. Pavlovski
Institute of Biophysics
Ministry of Public Health
Givopisnaya 46
Moscow D-182
RUSSIA

V. Prodi
Department of Physics
University of Bologna
Via Irnerio 46
I-40126 Bologna
ITALY

Reports Librarian
Harwell Laboratory, Bldg. 465
UKAEA
Harwell, Didcot
Oxon OX11 ORB
ENGLAND

P. J. A. Rombout
Inhalation Toxicology Department
National Institute of Public Health and Environmental Protection
P.O. Box 1
NL-3720 BA Bilthoven
THE NETHERLANDS

M. Rzekiecki
Commissariat à l'Énergic Atomique
Centre d'Etudes Nucleaires de Cadarache
BP No. 13-St. Paul
Les Durance
FRANCE

H. Smith
International Commission on Radiological Protection
P.O. Box 35
Didcot
Oxon OX11 ORJ
ENGLAND

J. W. Stather
National Radiological Protection Board
Building 383
Chilton, Didcot
Oxon OX11 ORQ
ENGLAND

Sun Shi-quan, Head
Radiation-Medicine Department
North China Institute of Radiation Protection, MNI
P.O. Box 120
Tai-yuan, Shan-Xi
THE PEOPLE'S REPUBLIC OF CHINA

J. W. Thiessen
Radiation Effects Research Foundation
5-2 Hijiyama Park
Minami-Ku
Hiroshima 732
JAPAN

D. Van As
Atomic Energy Corporation
P.O. Box 582
Pretoria 0001
REPUBLIC OF SOUTH AFRICA

D. W. Van Bekkum
TNO Institute of Applied Radiobiology and Immunology
ISI Lange Kleiweg
P.O. Box 5815
2280 HV RIJSWIJK
THE NETHERLANDS

Vienna International Centre Library
Gifts and Exchange
P.O. Box 100
A-1400 Vienna
AUSTRIA

M. Waligorski
Institute of Nuclear Physics
Radzikowskiego 152
31-342 Urakow
POLAND

Wang Hengde
North China Institute of Radiation Protection
P.O. Box 120
Tai-yuan, Shan-Xi
THE PEOPLE'S REPUBLIC OF CHINA

Wang Renzhi
Institute of Radiation Medicine
11# Tai Ping Road
Beijing
THE PEOPLE'S REPUBLIC OF CHINA

Wang Ruifa, Associate Director
Laboratory of Industrial Hygiene
Ministry of Public Health
2 Xinkang Street
P.O. Box 8018
Deshengmenwai, Beijing
100088
THE PEOPLE'S REPUBLIC OF CHINA

Wei Lü-Xin
Laboratory of Industrial Hygiene
Ministry of Public Health
2 Xinkang Street
Deshengmenwai, Beijing
100088
THE PEOPLE'S REPUBLIC OF CHINA

B. C. Winkler, Director Licensing
Raad Op Atomic
Atoomkrag Energy Board
Privaatsk X 256
Pretoria 0001
REPUBLIC OF SOUTH AFRICA

Wu De-Chang
Institute of Radiation Medicine
27# Tai Ping Road
Beijing
THE PEOPLE'S REPUBLIC OF CHINA

Meng Zi-Quiang
Department of Environmental Science
Shanxi University
Tai-Yuan, Shan-Xi
THE PEOPLE'S REPUBLIC OF CHINA

ONSITE

DOE Richland Operations Office (3)

P. W. Kruger, A5-90
E. C. Norman, A5-10
R. D. Freeberg, A5-55

Tri-Cities University Center

H. Gover, Librarian, H2-52

Hanford Environmental Health (2)

L. J. Maas, B6-61
M. J. Swint, H1-02

Westinghouse Hanford Co.

D. E. Simpson, B3-51

Pacific Northwest Laboratory (117)

W. J. Apley, P8-34
S. T. Autrey, K2-10
R. W. Baalman (5), K1-50
W. J. Bair, K1-50
C. A. Baldwin (10), P7-58
N. E. Ballou, P7-07
R. M. Bean, P8-08
L. A. Braby, P8-47
B. A. Bushaw, K3-58
B. D. Cannon, K3-58
F. Carr, Jr., K7-53
T. D. Chikalla, P7-75
T. T. Claudson, K6-23
D. W. Dragnich , K1-46
R. D. DuBois, P8-47
C. G. Edmonds, P8-19
C. E. Elderkin, K6-11

J. W. Falco, K6-78
D. R. Fisher, K3-53
J. S. Fruchter, K6-81
G. K. Gerke, K6-91
M. E. Geusic, K2-57
W. A. Glass, K4-13
R. H. Gray, K1-33
R. Harty, K3-55
L. A. Holmes, E3-08
J. R. Houston, A3-60
A. C. James, K3-51
J. R. Johnson, K3-53
M. L. Knotek, K1-48
W. W. Laity, K2-50
E. A. Lepel, P8-08
J. A. Mahaffey, P7-82
N. F. Metting, P8-47
J. H. Miller, P8-47
T. L. Morgan, P8-47
J. T. Munley, K3-58
J. M. Nelson, P8-47
J. F. Park, P7-52
R. C. Pedersen, P8-10
R. W. Perkins, P7-35
D. E. Robertson, P8-01
G. F. Schiefelbein, P8-38
L. C. Schmid, K1-34
B. D. Shipp, K1-73
R. D. Smith, P8-19
D. L. Springer, P7-56
G. M. Stokes, K1-74
J. A. Stottlemyre, K6-75
T. S. Tenforde (15), K1-50
B. L. Thomas, P7-72
L. H. Toburen (15), P8-47
R. J. Traub, K3-57
H. R. Udseth, P8-19
B. E. Vaughan, K1-66
T. J. Whitaker, K2-10
R. E. Wildung, P7-54
W. R. Wiley, K1-46
J. R. Williams, K7-22
L. D. Williams, K1-41
W. E. Wilson, P8-47
N. A. Wogman, P7-35
J. D. Zimbrick, P7-50
Health Physics Department Library
Life Sciences Library (2)
Publishing Coordination
Technical Report Files (5)

☆ U.S. GOVERNMENT PRINTING OFFICE 1992—693-932

END

DATE
FILMED
8/7/92